الجمهورية الجزائرية الديمقراطية الشعبية
PEOPLE'S DEMOCRATIC REPUBLIC OF ALGERIA
وزارة التعليم العالي والبحث العلمي
MINISTRY OF HIGHER EDUCATION AND SCIENTIFIC RESEARCH

Univerity of 20 August 1955 - SKIKDA -
Faculty of Technology
Departement of Civil Engeneering
Réf:D012122009D

جامعة 20 أوت 1955 ـ سكيكدة ـ
كلية التكنولوجيا
قسم الهندسة المدنية

THESIS

Presented to obtain

Doctoral Diploma

Option: Structures and Soils

Presented by :

Haroune BENMALEK

Theme

Crack analysis in composite materials

Defended publicly at: 07.07.2022
Discerned by jury members:

Rachid DJEBIEN	Lecturer C.A	University of 20 August 1955-Skikda	President
Salah BOUZIANE	Professor	University of 20 August 1955-Skikda	Supervisor
Hamoudi BOUZERD	Professor	University of 20 August 1955-Skikda	Co-Supervisor
Mohamed BOURADA	Professor	University of Djillali liabes-Sidi bel abbes	Examiner
Cherait YACINE	Professor	University of 8 mai 1945 - Guelma	Examiner

Academic Year : 2021 - 2022

Acknowledgments

THANKS TO ALLAH FIRST AND FOREMOST
THANKS TO MY PARENTS AND MY FAMILY FOR
UNCONDITIONAL LOVE SUPPORT AND PRAYERS THAT HAVE
CARRIED AND SUSTAINED ME ON THIS JOURNEY.

I WOULD LIKE TO THANK MY SUPERVISOR THE PROFESSOR
SALAH BOUZIANE AND CO-SUPERVISOR THE PROFESSOR HAMOUDI BOUZERD
FOR THEIR ASSISTANCE AND GUIDANCE
THROUGHOUT THE PROCESS OF RESEARCH.

MY SEPCIAL HONOR IS ADDRESSED TO THE LECTURER CLASS A RACHID
DJEBIENE, THE PROFESSOR MOHAMED BOURADA AND THE PROFESSOR YACINE
CHERAIT FOR ACCEPTING TO BE PART OF THE SCIENTIFIC EXAMINATION
COMMITTEE.

MY THANKS SHOULD GO TO THE UNIVERSITY 20 AOUT 1955 OF SKIKDA.
THE UNIVERSITY DJILLALI LIABES OF SIDI BEL ABBES.
LABORATORY OF CIVIL ENGINEERING AND HYDRAULICS,
UNIVERSITY OF MAY 8, 1945, GUELMA, ALGERIA.
LABORATORY OF MATERIALS AND HYDROLOGY, UNIVERSITY OF SIDI BEL ABBES,
SIDI BEL ABBES, ALGERIA.

Abstract

A mixed finite element is presented with an isoparametric formulation in the natural plane (ξ, η).This element extended for the analysis of the bending functionally graded beams under static loads. The Parameters of beams like Young's modulus and Poisson's ratio are changing through the thickness direction as a power-law distribution. The results obtained by the present mixed finite element are presented and compared with analytical and numerical solutions obtained in the literature.
The present element is also proposed to analyze kinking crack in functionally graded materials. Quasi-static crack propagation under mode 1, and the mixed-mode is performed for the homogenous and functionally graded plate under uniform axial tension. The results obtained by the present mixed finite element presented and compared with previous experimental and numerical obtained by finite element software in the literature. Where the present element proven a good results with the fewer elements and lower computational effort.

Keywords: Mixed finite elements, composite materials, functionally graded materials, FGM beam, FGM plat, crack, kinking.

الملخص

يتم تقديم عنصر متهي مختلط بصيغة متساوية في المستوى الطبيعي (ξ, η). امتد هذا العنصر لتحليل انحناء المواد المتدرجة وظيفيًا تحت الأحمال الثابتة. تتغير المعاملات الخاصة للعوارض مثل معامل يونج ونسبة بواسون في اتجاه السُمك وفق القانون الاسي. يتم عرض النتائج التي تم الحصول عليها بواسطة العنصر المحدد المختلط الحالي ومقارنتها بالحلول التحليلية والرقمية التي تم الحصول عليها في النتايج السابقة.

يُقترح أيضًا العنصر الحالي لتحليل توسع شق ملتوي في المواد المتدرجة وظيفيًا و المواد المتجانسة تحت الاحمال الثابتة في الوضع 1 و الوضع المختلط تحت التوتر المحوري المنتظم. تم عرض النتائج التي تم الحصول عليها بواسطة العنصر المحدد المختلط الحالي ومقارنتها مع التجارب السابقة والرقمية التي تم الحصول عليها بواسطة برنامج العناصر المتهية. حيث اثبت العنصرالحالي نتايج جيدة باقل عدد للعناصر واقل مجهود حسابي.

كلمات مفتاحية:

عناصر متهية مختلطة، مواد مركبة، مواد متدرجة وظيفيًا، عارضة متدرجة وظيفيا، شريحة متدرجة وظيفيا، شق، شق مائل.

Contents

List of Figures

List of Tables

List of symbols

A^e	The element area.
E	The Young modulus.
E_m	The Young modulus of metal.
E_c	The Young modulus of ceramic.
$E(x)$	The Young modulus.
E_{tip}, ν_{tip}	The Young modulus and Poisson ration at the crack tip, respectively.
e	The thickness of the element.
$f(z)$	The shear stress function.
$f_{ij}^I(\theta)\, f_{ij}^{II}(\theta)\, f_{ij}^{III}(\theta)$	The angular function for (i = 1.2.3) mode 1,2 and 3 respectively.
G	The energy release rate.
$g(x)$	Pure power-law function of x.
$g_{ij}^I(\theta)\, g_{ij}^{II}(\theta)\, g_{ij}^{III}(\theta)$	The angular function.
g_i^1, g_i^{11}	The angular functions for mode 1 and 2.
K_T	The stress concentration factor.
K	The stress intensity factor.
$K_I K_{II} K_{III}$	The stress intensity factors for mode 1, 2, and3 respectively.
K_I^{aux}, k_I^{aux}	The auxiliary stress intensity factors for modes 1 and 2.
k	The power-law index.
L_σ	The part of the contour where the stresses are imposed.
n	The nonhomogeneous constant.
n_1	The first component of the unit outward the normal to Γ .
n_t	The total number of elements in the discretized structure.
n_f	The number of elements concerned by the disturbance Δa due to the inclined extension of the crack.
η	The order used in the model.
H	The thickness of graded material.
h_t	The thickness of the coating.
u	The displacement of any point of the beam in x directions.
μ	The shear modulus.
μ_{tip}	The shear modulus at the crack tip.
$\mu_0(x_2)$	The arbitrary function of x_2.

u_1, u_2	The relative displacements.
u_2	The displacements relative to the crack tip at locations (i_{-1}) and (i_{-2}) in the x_2 direction.
r	The distance from the crack tip along the x_1 direction.
u_k, v_k, w_k	The components of the displacements of the layer k in the directions x, y, and z, respectively.
u_0, v_0, w_0	The components of the field of displacement on the mean. plane of the plate ($z = 0$).
ν	The Poisson ration.
ν_m	The Poisson ration of metal.
ν_c	The Poisson ration of ceramic.
W	The width of FGM.
W_{ext}	The extern energy.
W_{elas}	The elastic energy.
W_{kin}	The kinematic energy.
W_{rup}	The rupture energy.
W_{pot}	The potential energy.
W_ε	The strain energy.
w_d	The strain energy density.
w	The displacement.
$\bar{w}$	The non dimensional displacement.
w_i, w_j	The coefficients of weight.
$w_b(x)$	The bending components for the transverse displacement.
$w_s(x)$	The shear components for the transverse displacement.
Δa	The characteristic length associated with the crack-tip elements.
β	The material constant.
β_E	The nonhomogeneity parameters for Young modulus variation.
β_ν	The nonhomogeneity parameters for Poisson ration variation.
γ_E	The nonhomogeneity parameters for Young modulus variation.
γ_ν	The nonhomogeneity parameters for Poisson ration variation.
γ_x, γ_y	The transverse shear strain measured on the mean plane.
λ	The energy required to create the surface.
σ_{12}, σ_{22}	The shear and the normale stress ahead of the crack tip.
$\sigma_{ij} n_j = s_i$	The components of tractions along Γ.
σ_{x0}	The non-singular stress.
ϕ	The rotation of cross-section.
$\phi_i^k(z)$	Lagrange interpolation functions (1D) continuous according to the thickness coordinates.
ξ_i, η_j	The coordinates of the integration points.
Γ	The contour enclosing the crack tip.
ds	The infinitesimal length element along the contour Γ.
θ	The kink angle.
$C_{i,j}$	The coefficients depending on θ, for smaller kink angle for $(i, j = 1, 2)$.

$\{\bar{T}^e\}$	The imposed traction of L_σ.
$\{\tau_c\}$	Stresses on the contours of the element.
$\{\tau_i\}$	Stresses inside of the finite element.
$\{f^e\}$	The volume forces vector.
$\{F_u^e\}$	The vector of displacements.
$\{F_\sigma^e\}$	The vector of stresses.
$\{\sigma\}$	The vector of stresses for the finite element.
$\{\varepsilon\}$	The vector of deformations for the finite element.
$\{u\}$	The displacement field.
$\{u\}_i$	The column vector containing the nodal values of element i.
$[M]$	The shape functions matrix (linear in ξ, linear in η) of stresses.
$[N]$	The shape functions matrix (linear in ξ, linear in η) of displacements.
$[I]$	The unit matrix.
$[J]$	The Jacobian matrix.
$[P_n]$	The nodal matrix.
$[K_e]$	The elementary stiffness-flexibility matrix.
$[K]_i$	The elementary matrix of element.
$[S]$	The matrix of flexibility.
$[S(z)]$	The compliance matrix.
$[\Gamma]$	Transformation matrix of the degree of freedom.

Chapter 1

General introduction

1.1 Introduction

The homogeneous materials failed, the industry needs advanced materials able to stand the high stress results under different loading. The Japanese researchers devloped new thin composite material ables to decrease the high thermal stress and eliminate the sharp interface. The new materials are considered as an advanced materials composed of two materials and more. The interface between materials is replaced by graded material, where the proprieties of the two materials vary smoothly.
Functionally graded materials (FGM) are materials made of several layers containing different components such as ceramics and metals. They are advanced composites exhibiting macroscopically inhomogeneous characteristics. In 1987, the Japanese researchers initiated a large-scale project, this latter aims to develop structures materials used as a thermal barrier in aerospace programs.
The walls of spacecraft constitute materials work at surface temperatures of 1800 ° C as it is a temperature gradient of 1300 ° C. At that time, no industrial material product resists such thermo-mechanical stresses. Three characteristics considered for the design of such materials:

- The surface layer of the material resists thermal and high-temperature oxidation.
- Toughness is related to the low-temperature side.
- The relaxation affected the thermal stress along with the material.

The FGM proposed to develop a new composite that has the advantage of the both properties of ceramics and metals.
The microstructural phases of FGM have different functions, and the FGM achieves multistructural status by variation of their properties. The gradually varying the volume fraction of one constituent of the material, their material properties present a smooth and continuous passage from one surface to another, thus eliminating interface problems and the attenuating the stress concentrations. The ceramic constituent of the functional gradient material can withstand high-temperature environments due to their better thermal resistance characteristics. On the other side, the metallic ensures better mechanical performance and reduces the possibility of a rupture and damage (see figure 1-1).

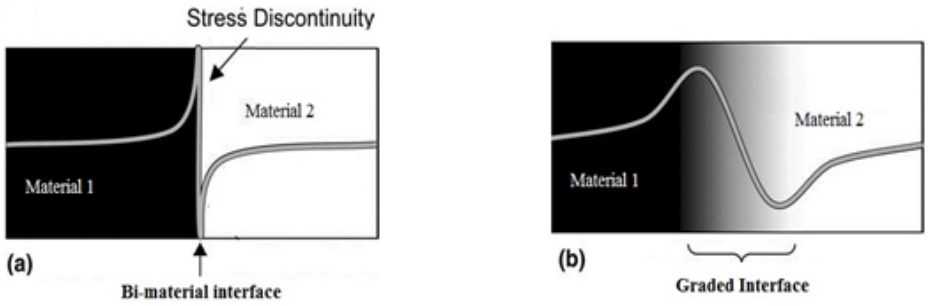

Figure 1.1: (a) The high stress in the sharp interface in bi-material. (b) Graded region to eliminate the interface (FGMs)[1].

In the first period (1987-1989), the researchers had succeeded in fabricating small experimental pieces (1-10 mm thick and 30 mm in diameter) that could withstand maximum temperatures of 2000K (surface temperature), where the temperature gradient of 1000K. In the second period (1990-1991), the aim was to produce parts with larger sizes and more complex shapes, unlike those are fabricated before. Ten years later, the FGM applications extended to other applications: optics, sensor technology, biomechanical (see figure 1-2).

Figure 1.2: Field application of FGMs .

From 1992 until our days, the researches in FGMs know a high published year after year in many fields (see figure 1-3), so FGM has become an essential material for researches (see figure 1-4).
The new analysis is about crack analysis which is different from the classical one, which refers to analysis materials with not considering the small deflect as results of manufacturing or displacements but only stress analysis and defining the critical stress region. The recent in this analysis is crack analysis which considers the presence of a defect in the material

with different crack orientations and lengths. The experimental test includes the fracture toughness test, which is the ability of a material to resist the propagation of a crack, and it is opposite to fragility. So in this research, an analysis of the bending and crack behavior of FGMs is presented.

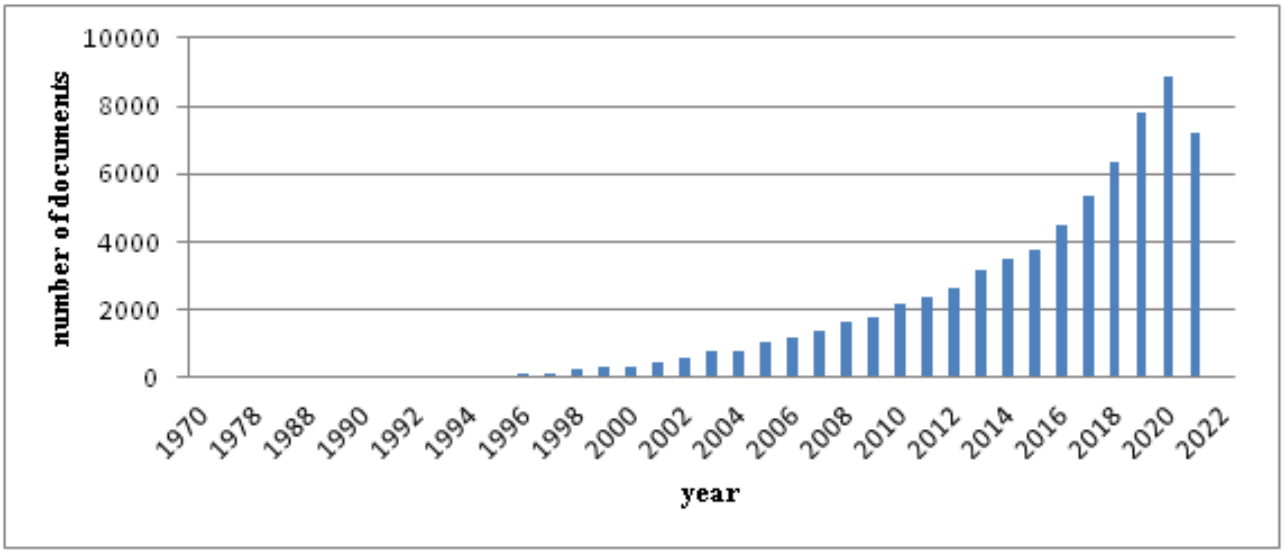

Figure 1.3: Number of documents includes FGMs in Scopus data bases.

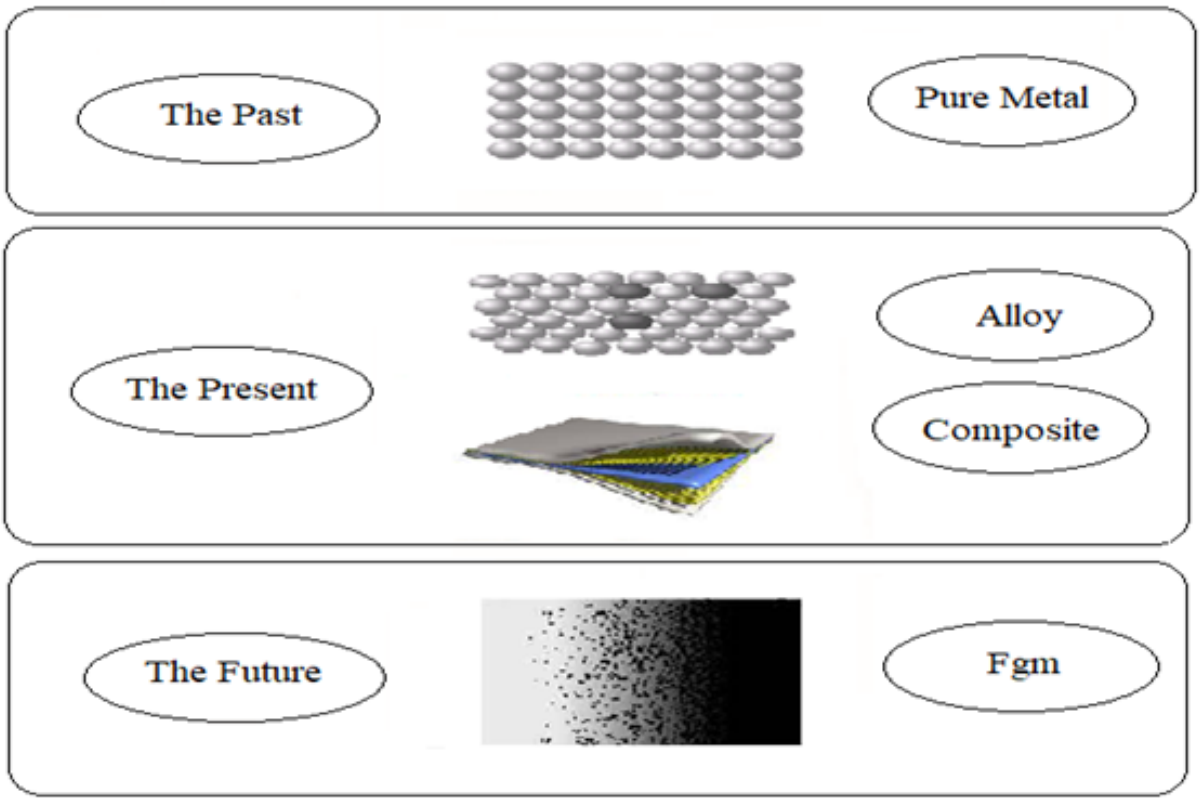

Figure 1.4: Engineering materials devolvement.

1.2 Problem statement

The composite materials have a complex fracture interface. This interfacial material fails and delaminates because of the stress concentration in their interface and the stress outcome of thermal, static, and dynamic loading. The interface is replaced by a graded region constituted by a variation of two materials properties to avoid the stress concentration. Investigating the bending behavior under static loads with different boundary conditions is necessary.
The crack behavior of the gradient materials has been treated through the conception of fracture mechanics, which involves the interface crack. The crack modeling in the graded region is related to the complex geometry of these composite materials. On the other hand, the experiment tests are not available for all cases. So a numerical model implanted in a software program is more suitable to treat the failure of FGMs in different cases to avoid the experimental test.

1.3 Objective of study

The study aims to develop and use the mixed finite element RMQ7 (Reissener Modified Quadrilateral) developed by Bouzerd [2] and reformulated by Bouziane [3]. This latter introduced the isoparametric form, which represented the kinking and curves crack to model, compute and evaluate the energy release. This research aims to model and analyze the bending behavior of FGM under static loads. The study also extended the mixed element for crack analysis in FGMs includes a straight and kinking crack.

1.4 Scoop

The bending behavior of FGM under static loads is investigated using a special mixed finite element. The crack behavior and the affection on the crack prediction and propagation cross the graded region are presented.
The problem of the crack in FGMs under mode1 and mixed mode is investigated in the case curved or kinking crack. This issue is treated with a special mixed finite element.

1.5 Importance of study

The FGMs are valuable materials in the industry fields after the failure of the homogenous and composite materials. The need to analyze the crack in these materials is required to define their bending behaviors under static loads and their safety conditions such as maximum stress and crack length before the break-up. Evaluating the damage inspection intervals is necessary to construct a better design and obtain the maintenance plan to avoid disasters. Using such numerical simulation is low cost and more effort time than experiments.

1.6 Thesis organization

The study consists of six chapters:
The first chapter is a general introduction to this work. In this part, the problem statement, the aime of the study, the importance of the study, and the thesis organization are presented.
The second chapter is reserved for definition the development, manufacture, fields of application and properties variation of FGM. The comparison between FGMs and traditional

composite materials is presented in this section.
In the third chapter, a general overview of different theoretical models of beams and plates is presented.
In the fourth chapter, a theoretical crack in FGMs, the analytical, and the numerical analysis of the crack problem is discussed.
The fifth chapter is devoted to the presentation of the formulation of the mixed finite element that used to analyze the FGMs after the above two chapters indicate and clarify the bending and crack problem in FGMs.
The sixth chapter is reserved for studying the application examples to validate the technique proposed in this work. These examples deal with the analysis of functionally graded beam bending and kinking crack problems analysis in FGMs under static loads. A general conclusion is presented for the current research and the proposal for future study.

Chapter 2

Literature review

2.1 Introduction

Functionally graded materials (FGMs) are a new class of composite material created by discontinuously or continuously varying the volume fractions in the thickness direction. Recently this type of material attracted the attention of many researchers because of the advantages of decreasing the disparity in material properties and reducing thermal stresses. The research and publication activity in FGMs increased over the past few years. The researchers define property gradient materials as a particular compound material for which the volume fraction varies continuously through the thickness.
The mechanical properties between adjacent layers in multilayers produce high stresses at the interfaces. These high interfacial stresses can lead to cracks at the interface region known as delamination. Moreover, other fracture mechanisms result from an unexpected change in the mechanical and thermal properties of the layers. FGM microstructure was designed to optimize the performance of structural by the distribution of corresponding properties. These property distributions are assembled into the products, it ensuring multiple functions such as bonds between particles. The product will be tough enough on the inside to resist breaking and protect from corrosion on the outside.

2.2 Processing methods for FGM

In this section a bibliographic study presents processing methods which are used for the fabrication of FGMs.

2.2.1 Deposition based methods

The deposition based methods are precious methods for manufacturing thin FGM as a discontinuous or continuous graded layer. The vapor deposition methods, electrophoretic deposition, and thermal spray methods produce FGM for coating applications. The gradient properties were manufactured in FGM in one or more directions [4].
The deposition-based method fabricated the characterization of functionally graded coatings bonded to substrate stainless steel material. The vacuum chamber deposits two materials on a substrate where the composition of the deposited mixture gradually changes from FGM YSZ (Ni-yttria-stabilized zirconia) to stainless steel, along the growth coating direction as a linear composition profile [4].

2.2.1.1 Vapor deposition techniques

The vapor deposition method manufactured a thin graded layer. The technique divides into chemical and physical desposition techniques.

- **Chemical vapor deposition techniques**

  The chemical vapor deposition fabricates the layer by transferred the gas into the sample. The chemical reaction during the transport or on the sample surface takes place. The layer build-up by the parts of the redacted material, which stay at the surface (see figure 2-1).

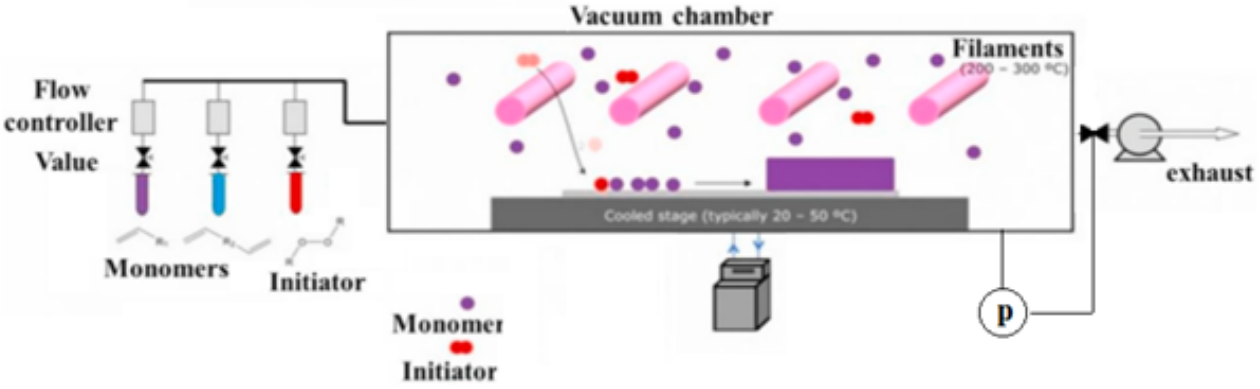

Figure 2.1: Chemical vapor disposition [5].

kawase et al.[6] prepared a compositionally gradient layer with a continuous composition distribution. They also changed the reactant mixture composition gradually from propane to dimethyldichlorosilane by the chemical vapor deposition method. The graded material resists under quick cooling tests (1000 to 0°C). Chemical vapor deposition technique was used to coat Tungsten on a W/Cu FGM. The coated-tungsten tile was brazed on the CuCrZr heat sink with a cooling channel [7].

- **Physical vapor deposition techniques**

  Physical vapor deposition (PVD) is a coating process that uses an evaporative condenser of film material on a substrate to deposit thin films. This process contains various types such as evaporative deposition, electron beam physical vapor deposition, cathode arc deposition, ion plating, sputtering, and enhanced sputtering. In the physical vapor deposition, the material is transported from a condensed state to a vapor stage and returns to a thin condensed film stage (see figure 2-2).

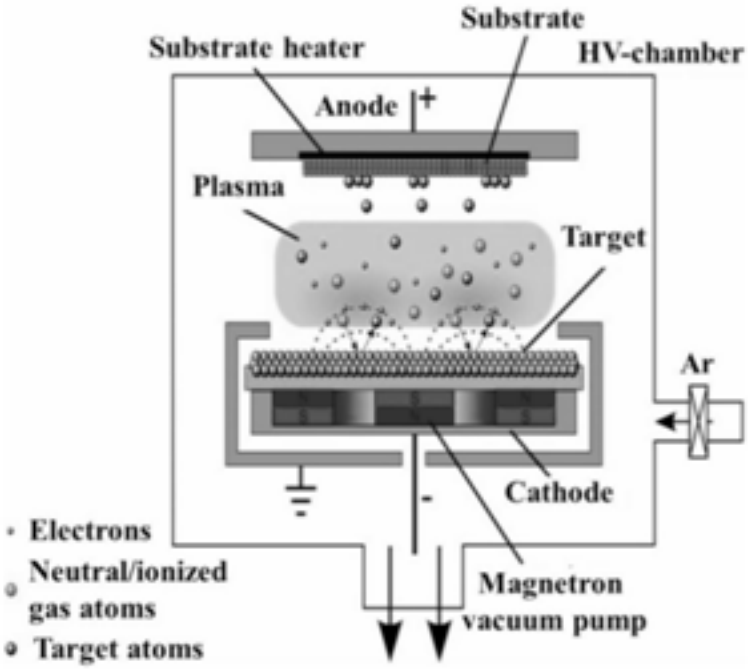

Figure 2.2: PVD techniques [8].

The PVD techniques used the heat or the bombardment with ions (sputtering) to evaporate the solid coating material with introduced reactive gas. It creates a composition with the metal vapor. The technique deposited the thin film on the substrate. A comprehensive review of the information and knowledge related to physical vapor deposition and their industry uses was detailed [9].

Abegunde et al.[10] presented a review of deposition techniques based on chemical and physical vapor deposition techniques and their application region for surface coating.

2.2.1.2 Thermal spray method

The thermal spray method used a heat source to liquefy the raw materials for coating. The process sprayed the raw materials into a base material by treating gases at the end. The molten material (liquid) is still pushed until it solidifies and forms a solid layer (see figure 2-3).

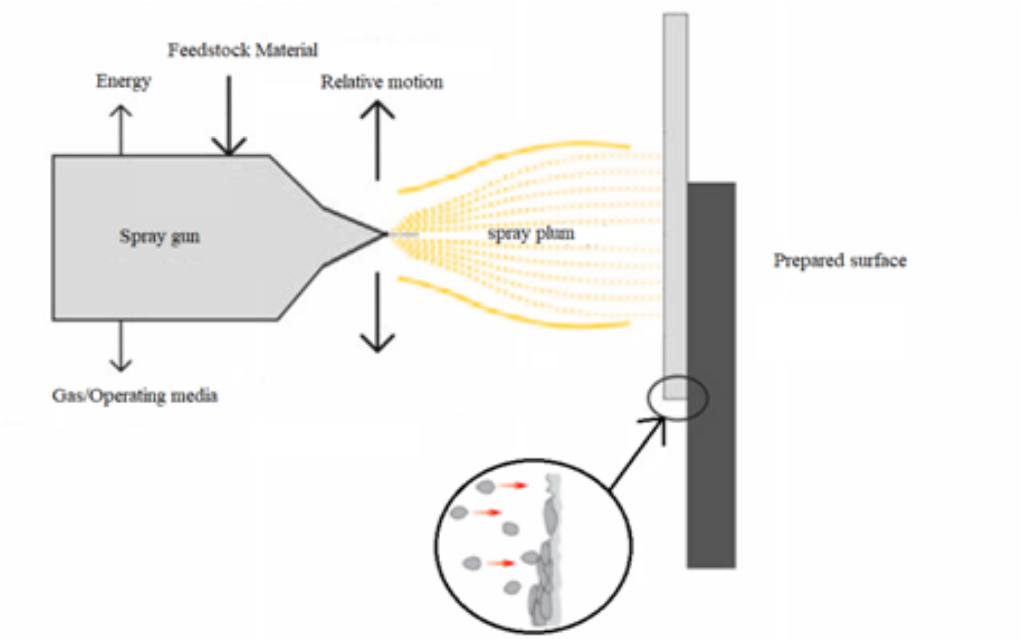

Figure 2.3: Thermal spray coating [11].

The vacuum plasma spraying fabricated functionally graded Ni-yttria-stabilized zirconia (YSZ) coatings. The graded coating changes in the coating direction. This latter is employed as a thermal barrier in aerospace industries [12].

2.2.1.3 Electrodeposition method

The electrophoretic deposition (EPD) method has been used in the production of FGMs. This method is a simple method for producing graded materials based on electrophoresis principles (see figure 2-4).

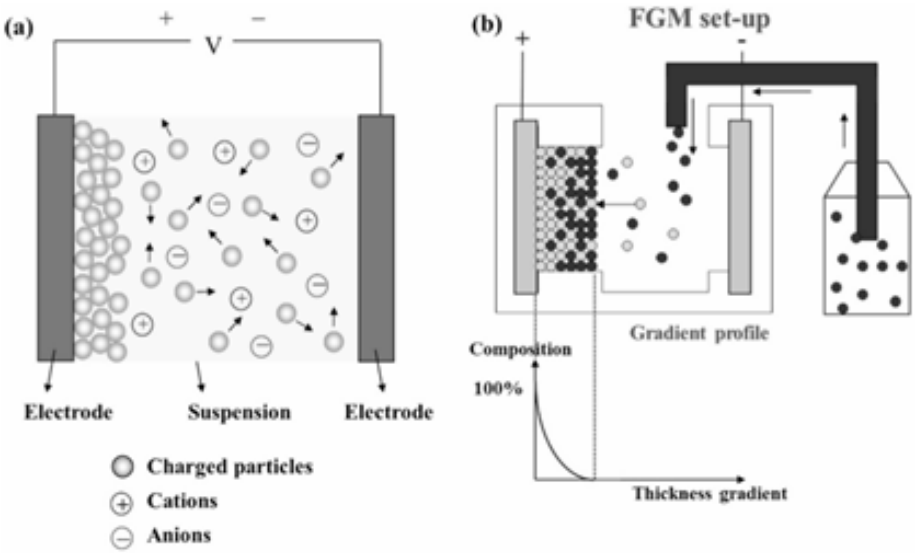

Figure 2.4: (a) Schematic diagram of EPD process and (b) Concept of EPD process for produced FGM [13].

Electrophoretic deposition is applied electric field to a suspension of a powder in a liquid. The powder particles move under the effect of the electric field. Regularly the powder

particles also deposit at one of the electrodes. The form of the electrode determines the deposit form. Electrophoretic deposition is compatible with shaping layered microstructures (laminates). The manner varies continually between two or more suspensions.
High hardness and high toughness combined in one component as graded WC-Co by depositing from a powder suspension when the other one is added continuously during the process [13]. The advance of coating techniques and methods was recently reviewed [11].

2.2.2 Solid-state methods

Solid-state methods are hopeful methods of the production of FGM materials.

2.2.2.1 Additive manufacturing method

Additive manufacturing is an approach to producing metallic FGMs, which widely studied in the recent years. The additive manufacturing process fabricated metallic materials.
Yan et al. [14] presented an overview of the advances in metallic FGMs produced by laser metal deposition (LMD) .

The modeling, processing, microstructures, and mechanical properties of FGMs produced via additive manufacturing are discussed [15].

2.2.2.2 Powder metallurgy method

The powder metallurgy methods manufactured FGM (see figure 2-5). The basic principles of FGM structure, properties, and their applications are discussed [16]. The manufacturing of aluminum-steel FGMs formed by the powder metallurgy process was presented [17].

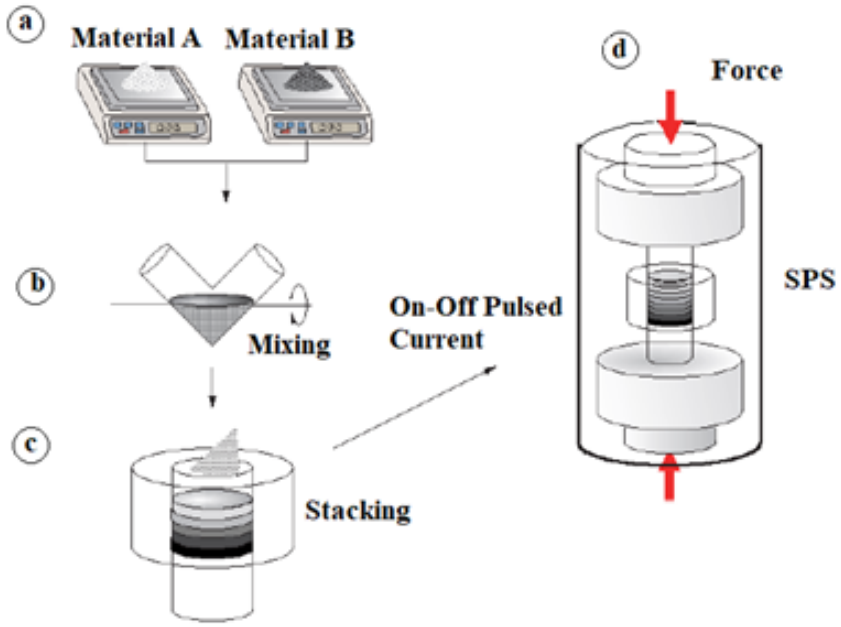

Figure 2.5: The production process of the FGMs by powder metallurgy method [18].

2.2.3 Liquid state methods

The liquid state divides into many producing processes of gradient properties, such as centrifugal force, slip casting, tape casting, and infiltration process.

Centrifugal casting is an advanced casting branch commonly used in the metallurgical industry. The centrifugal force makes the material stronger. The design and the fabrication of a low-cost horizontal and vertical centrifugal casting machine illustrated the effect of horizontal and vertical centrifugal casting parameters [19].

2.2.3.1 Centrifugal force methods

Centrifugal casting is a potential solidification processing technique. The method is used for producing almost symmetric in shape cast components with improved properties. Centrifugal casting has been considered the cost-effective technique for producing functionally graded metal matrix composites. Rajan et al.[20] presented an overview of centrifugal processing techniques in functionally graded aluminum alloys and composites. The centrifugal solid-particle method and centrifugal mixed-powder fabricated FGMs [21].
Centrifugal in-situ techniques produced a gradient Fe-TiC composite via a combination of in situ reaction. Cast iron and Ferrotitanium melted with a high-frequency induction furnace coupled with centrifugal equipment [22]. In addition, there exist other methods like the centrifugal slurry method and the centrifugal pressurization method detailed in [18].

2.2.3.2 Slip casting methods

The slip casting used a liquid matrix with fine grain sizes to suspense ceramic particles. The surface is shaded capillary into a porous mold, where the matrix is drained from the slip. The walls of the mold stay in a layer of clay slip. The left-over fluid is drained out of the mold after the thickness is attained. When the mold is dry, the cast will be removed away. The benefit of this process is the capability to fabricate complex shapes and continuously graded materials.
Centrifugal slip casting technique was used for producing FGM from the Al2O3–Cu–Ni system[23]. FGMs (metal-ceramic) were fabricated by using the slip casting method (the sealing cap) [24].

2.2.3.3 Tap casting methods

Thin FGMs produced by tape casting with a high up of modern ceramics. Tape casting is a suitable technique to fabricate ceramic tapes. This technique is applied to process dense substrates for electronic applications. Tape casting makes it possible to change the thickness of the product. A comprehensive review of new strategies and accomplishments to produce porous ceramic materials by tape casting was presented [25]. Tape casting technique fabricated functionally graded ceramic tapes side-by-side [26].

2.2.3.4 Infiltration methods

The liquid state process of fabricating the FGMs like an infiltration, which soaks in a molten matrix space that fills the space between ceramic particles, holds preformed ceramic particles.
Graded silicon carbide (SiC) is made by changing the concentration of the inorganic salt mixture and using Aluminum as the binder. The microstructure analysis shows the graded distribution of SiC particles. All the melt has infiltrated throughout the performance to produce FGMs [27]. The process infiltrated the pressure-less sintering with molten copper (Cu) to fabricate the FGM (Cu copper /W Tungsten) [28].

2.3 FGM types

The concept of FGM was to eliminate the sharp interface that existed in the traditional composite material and replace it with a progressively varying interface, the changing in this region of the interface called the graded region. The gradual region has led to the progress of different types of FGMs. The FGM produced include porosity gradient, microstructure gradient, and the chemical composition gradient. Each of these types of FGMs is described bravely in the following sections.

2.3.1 Gradient of the microstructure in FGMs

The microstructural of FGM changes gradually. The FGM microstructure was designed to fabricate material with different microstructures. This latter changes gradually to obtain the required properties of the material [29]. In some cases, the FGM could be made of the same material but with different microstructures like bamboo tress [30].

2.3.2 Gradient of the porosity in FGMs

Porosity is a morphological property independent of the material. Others defined it as a percentage of voids in solid [31]. The porosity of this material changes with the variation of the spatial position. The schematic diagram of the typical porosity gradient of a FGM is shown in figures 2-6.

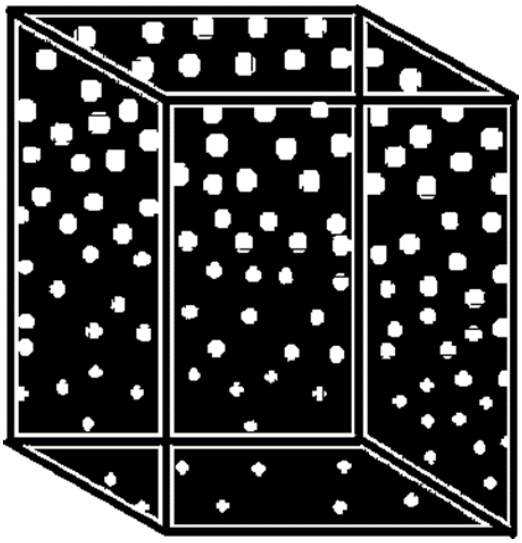

Figure 2.6: Porosity gradient of a FGM.

The porosity gradient of a FGM can be divided into a porosity density gradient or a pore size gradient. In the gradient, the porosity density is produced depending on the spatial position through the volume of the material. While the porosity size is fabricated depending on the varying pore sizes, the pore shape, or both [29]. In addition, there is a natural porosity gradient in bones [32].

2.3.3 Gradient of the chemical composition in FGMs

The graded chemical composition varies depending on the spatial position in the FGM. The variation could be in the form of a single-phase or a multi-phase material [33].

The graded single-phase is produced when the compound consists of a single-phase due to the solubility of chemical elements from one to the other [29] (see figure 2-7).

Figure 2.7: Chemical composition samples for the Ti/Nb and Ti6Al4V/Mo couples [34].

Most FGMs with a multi-phase chemical composition are commonly used and designed [29].

2.4 Application of FGMs

The FGMs have high potential in sensitive applications where the working conditions are strict, including the heat shields of spacecraft, tube heat exchangers, biomedical implants, and plasma coatings in fusion reactors. Numerous combinations of normal mismatched functions created modern materials for chemical plants, aeronautics, and nuclear reactors.

2.4.1 Civil engineering

Graded concrete elements adjust the interior composition of structural components with structural performance and specific thermal requirements. The properties change continuously of the material depending on its porosity, strength, or stiffness. The gradual change of concrete components allows the continuous alteration of concrete properties in all spatial dimensions. The porosity influences the structural and thermal insulation characteristics (see figure 2-8) [35].

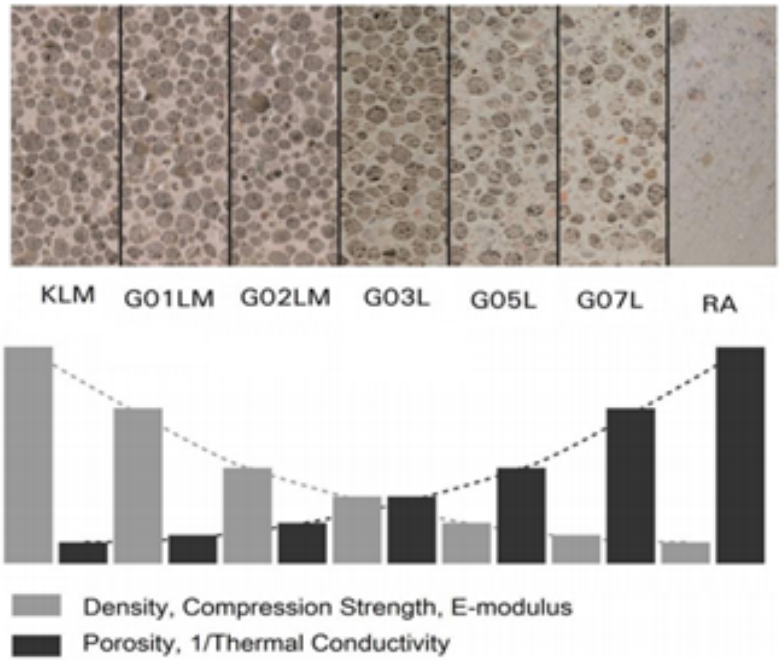

Figure 2.8: Porosity and density characteristics of hardened concrete [35].

The graded characteristic of concrete affects sections in positive bending only and does not affect in a negative moment, the decrease rate and the ultimate moment capacity [36]. The gravitational approach (see figure 2-9), which has proven excellent in artificially creating a graded concrete specimen, is developed [37].

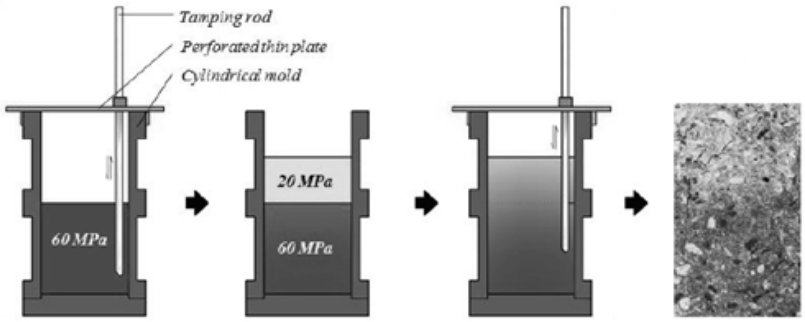

Figure 2.9: The gravitational approach for functionally graded concrete production[37].

2.4.2 Aeronautics

The FGM concept was invented from the research field at materials properties, including the requirements such as thermal conductivity and thermal barrier property in a material. At present, it can produce lightweight, durable, and hard materials which are applicable to a large type of fields such as structural materials, energy conversion equipment, and others. FGM will be an indispensable technology for space station construction. FGM is also applicable to the outer wall of space planes and rocket engine parts [38].

2.4.3 Biomaterials

FGM enhances the biocompatibility of the medicinal components. While the uniform structure failed to achieve the strength of bonding, corrosion, and abrasion resistance. FGMs in the present moment are widely used in prosthetic devices and bones and joints replace because it has high hardness, strength, and a long lifetime [8]. A new approach used gradient material manufacturing to improve the load transfer to the bone [39].

2.4.4 Energy

Energy conversion devices used FGM. The concept of FGMs with a graded thermal is used in various energy systems, such as running a single material at very high temperatures or low temperatures as in the thermal power generators, solar power components, energy conversion devices capacitors, electrodes, and sensors [40].

2.5 The materials distribution

The materials with gradient properties are produced by changing the composition of materials continuously with non-uniform microstructures and spatially graduated macro-properties. The FGM is characterized by the variation of volume fractions of one phase or more. Most researchers use the power function, the exponential function, or the sigmoid function in the objective to describe material distribution [41].

2.5.1 Power-law form (rule of the mixture)

Power-law is a mathematical function used to approximate mechanical and thermal properties in composite materials by the relative amounts of the constitutes and their individual properties.
The Japanese researchers used the power law to illustrate the volume fraction of the other phase, which is graded in the first phase in thickness direction [42],[43],[44],[45] (see figure 2-10).
Recently thickness variation model was used on FGM with cross-section by refined Timoshenko beam theory and Euler-Bernoulli beam theory [46].

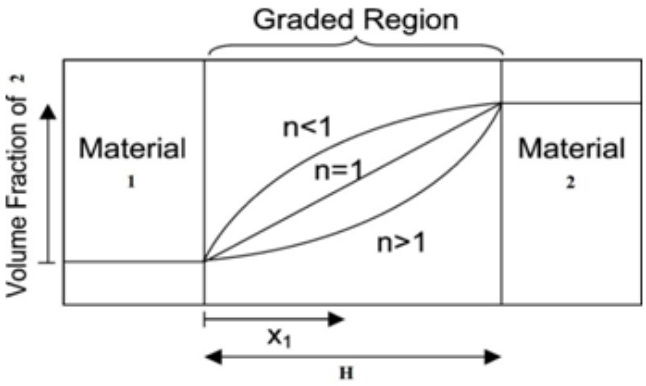

Figure 2.10: The power law describes the volume fraction distribution in FGMs[1].

$$\begin{aligned} E(x) &= g(x)E_m + (1-g(x))E_c \\ \nu(x) &= g(x)\nu_m + (1-g(x))\nu_c \end{aligned} \tag{2.1}$$

If $g(H) = 1$, that require $g(0) = 0$, then the material at the FGM surface is pure ceramics, and at the bottom is pure metal. In this case, $g(x)$ is a pure power-law function of x.

$$g(x) = \left(\frac{x}{H}\right)^n \tag{2.2}$$

Where:

n the nonhomogeneity parameter of FGM between zero and infinity.

H the thickness of graded material.

In the infinty cases. $E(x)$ would approach E_m for n going to 0, and $E(x)$ would approach E_c for n going to infinity.

The value of $n = 1$. 0 corresponds to the linear variation of $E(x)$, for n between zero and one, the FGM is metal-rich, for n between one and the infinity is ceramic-rich.

2.5.2 Exponential form

This form was the vast model applied to model the continuous changing in FGM [47],[48],[49] [50],[51]. The exponential form (see figure 2-11) is defined by:

$$\begin{aligned} E(x) &= E_0 e^{nx} \\ \mu(x) &= \mu_0 e^{nx} \end{aligned} \tag{2.3}$$

Where:

E and μ are the value of the Young modulus and the shear modulus varies along the X direction.

E_0 and μ_0 are the value of the Young and shear modulus at $X = 0$.

n is a nonhomogeneous constant.

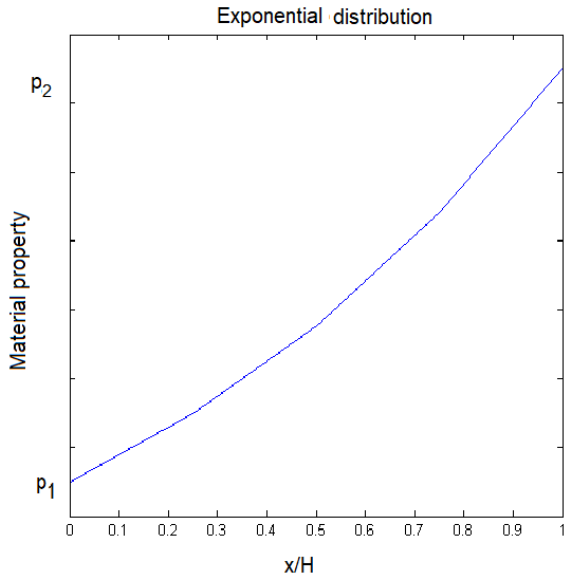

Figure 2.11: Exponential material property in the graded region.

2.5.3 Sigmoid form

The material properties of the FGM change continuously in the thickness direction (x-axis) only. The Young's modulus and Poisson ratio are functions only of x. The volume fraction

of the FGM coating–substrate system was described using two power-law functions. The functions guarantee the distribution of the stresses along with all the interfaces [52]. The two power-law functions are defined by:

$$\begin{aligned} g_1(x) &= \frac{1}{2}\left(\frac{x}{ht/2}\right)^n; \qquad 0 \le x \le ht/2 \\ g_2(x) &= 1-\frac{1}{2}\left(\frac{ht-x}{ht/2}\right)^n; \qquad ht/2 \le x \le ht \end{aligned} \tag{2.4}$$

where n is a material parameter, and ht is the thickness of the coating, using the law of mixtures, Young's modulus of the S-FGM beam can be calculated by:

$$\begin{aligned} E(x) &= g_1(x)E_m + (1-g_1(x))E_c; \qquad 0 \le x \le ht/2 \\ E(x) &= g_2(x)E_m + (1-g_2(x))E_c; \qquad ht/2 \le x \le ht \end{aligned} \tag{2.5}$$

Figure 2-12 represents the sigmoid distributions, and this FGM beam is called (S-FGM beam).

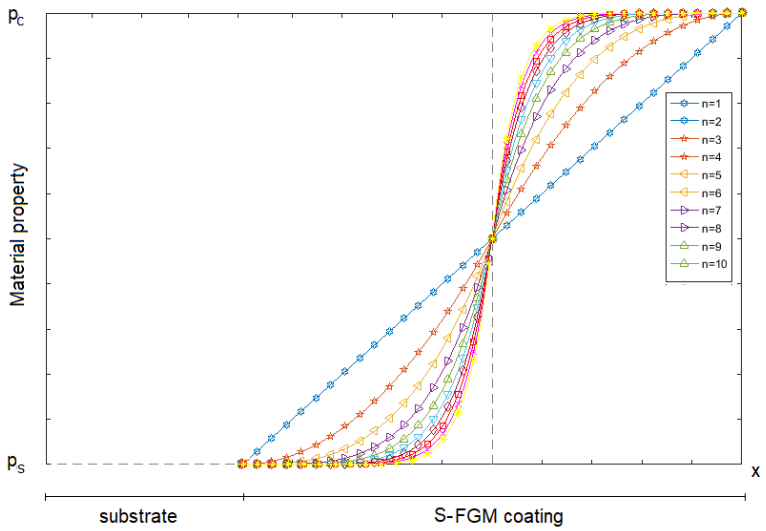

Figure 2.12: Volume fraction variation through-thickness (S-FGM).

2.6 Comparison of FGMs and traditional composite materials

FGMs are materials made of several layers containing different components such as ceramics and metals. They are composites exhibiting macroscopically inhomogeneous characteristics. The material properties change continuously in the composition. The microstructure of the material distinguishes FGMs from conventional composite materials (see figure 2-13). This difference is the gradient parameter that characterizes the material properties of FGMs.

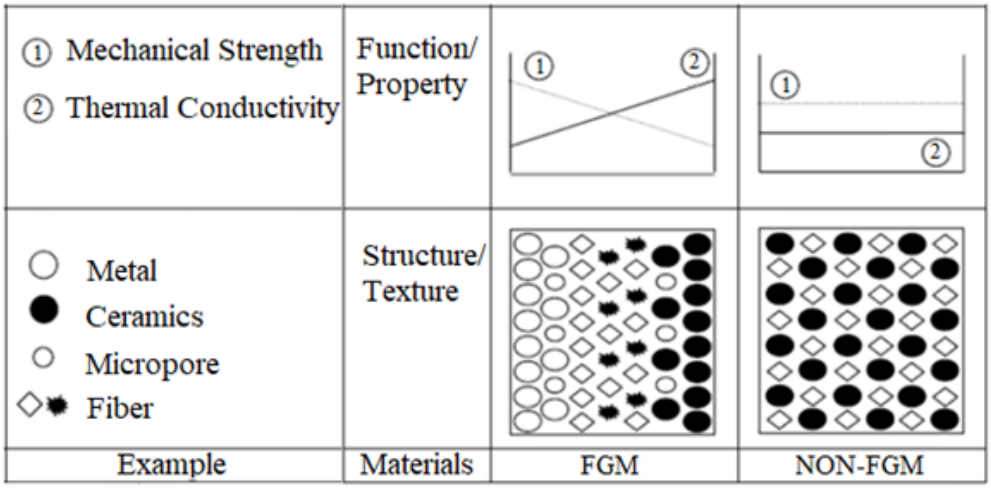

Figure 2.13: Characteristics of FGM and composite materials [53].

A simple model illustrating the differences between materials with gradient properties and conventional materials (see figure 2-14) was established by Uchidat [54]. The compound plane material has a plane characteristic, and the connected material has a boundary on the interface of two materials. FGMs have exceptional characteristics which differ from those of compound and bonded planar materials.
Therefore, FGMs create a center of attention because of their application in industrial fields since they have a twin property of the two mixed raw materials. The component distribution is continuously graduated. For example, an FGM with a ceramic-metal component has thermal conductivity and metallic strength on the metal side, and high temperature resistivity with non-oxidation on the ceramic side.

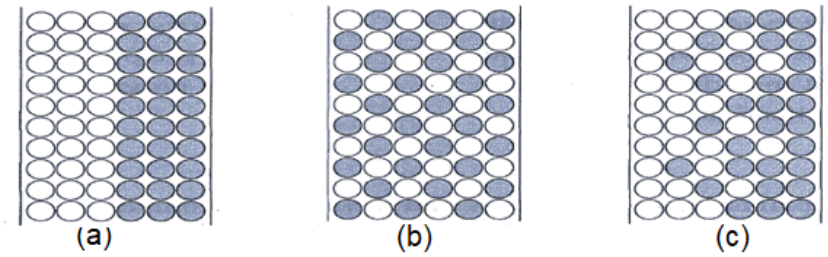

Figure 2.14: The component distribution of materials: Connected material (a), Compound plane material (b), Property gradient material (c)[54].

2.7 Conclusion

In this chapter, the development, manufacture, application areas, progress, and properties variation of the FGMs are outlined. An illustration is presented to clarify the difference between FGMs and traditional composite materials.

Chapter 3

Bending theories in the FGMs

3.1 Introduction

The composite material analysis is more complex than homogeneous structure materials because of their basic mechanical properties. Numerous theories simplified the complexity of these materials in engineering structures. In this chapter, a bibliographical review of different types of models and approaches used for composite materials. In addition, the bending theories applicable to functionally graded structures are presented.

3.2 Displacement based beam theories

The deformation kinematics of the beam was represented by using theories such; the classical beam theory (CBT), the first-order shear deformation theory (FSDT), and the higher-order shear deformation theories (HSDTs). CBT neglects the effect of the transverse shear deformation where FSDT and HSDTs considered the influence of transverse shear deformation. The analytical solution by this theories and the numerical solution by the finite element method were presented.

3.2.1 Classical beam theory(CBT)

The classical beam theory, developed by Bernoulli-Euler, this theory is the uncomplicated beam theory. It is also known as the Euler–Bernoulli beam theory. The CBT assumes that the plane section perpendicular to the neutral layer before bending remains plane and perpendicular to the neutral layer after bending (see figure 3-1).

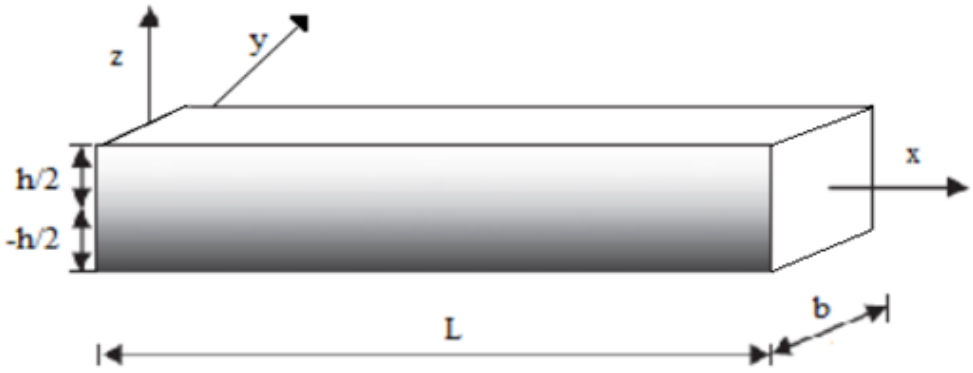

Figure 3.1: The classical beam theory.

The normal transverse and transverse shear deformation were neglected in these assumptions. The displacement field of the classical beam theory written as CBT:

$$\begin{aligned} u(x,z) &= u_0(x) - z\frac{dw_0}{dx} \\ w(x) &= w_0(x) \end{aligned} \tag{3.1}$$

Where:

u and w: The displacement in x and z directions, respectively.

$u_0$and w_0: The neutral axis displacement in x and z directions, respectively.

3.2.2 First-order shear deformation theory (FSDT)

The First-order shear deformation theory, recently known as the Timoshenko-Ehrenfest beam theory [55], predicts constant transverse shear stress through the thickness. FSDT assumes that the plane sections perpendicular to the neutral layer before bending remain plane but not necessarily perpendicular to the neutral layer after bending. The FSDT requires the problem to depend on the shear correction factor, where the influence of transverse shear deformation should consider it. Displacement fields of Timoshenko beam theory written as FSDT :

$$\begin{aligned} u(x,z) &= u_0(x) - z\phi(x) \\ w(x) &= w_0(x) \end{aligned} \tag{3.2}$$

Where:

ϕ: The rotation of cross-section.

3.2.3 Higher order shear deformation theories (HSDTs)

The limitations of CBT and FSDT led to the development of HSDTs.HSDTs use polynomial or non-polynomial shape functions to account the effect of transverse shear deformation and to get the realistic variation of transverse shear stress across the thickness of the beam. Unified displacement fields of several HSDTs which consider the effect of transverse shear deformation and neglect the influence of normal transverse deformation written as:

The first higher shear deformation theory:

$$\begin{aligned} u(x,z) &= u_0(x) - z\frac{dw_0}{dx} + f(z)\phi(x) \\ w(x) &= w_0(x) \end{aligned} \tag{3.3}$$

Or the second higher shear deformation theory:

$$\begin{aligned} u(x,z) &= u_0(x) - z\left[\frac{dw_b(x)}{dx} - \frac{dw_s(x)}{dx}\right] + f(z)\frac{dw_s(x)}{dx} \\ w(x) &= dw_b(x) + dw_s(x) \end{aligned} \tag{3.4}$$

Where:

$f(z)$: The shear stress function.

w_b: The shear components for the transverse displacement.

w_s: The bending components for the transverse displacement.

3.2.4 Analytical solutions for FGM beams

Daouadji et al. [56] used the partial differential equation to solve the plane stress problem of a cantilever functionally graded beam subjected to a linearly distributed load. Zhong and Yu [57] analyzed cantilever functionally graded beam variations with arbitrary material properties subjected to different loads. They presented a general two-dimensional solution by using the Airy stress function. Chu et al. [58] developed a two-dimensional elasticity solution of FGMs under tension and bending. The elasticity solution is based on the Airy stress function method and strain compatibility equation. Xu et al. [59] studied the stress and displacement distributions of simply-supported functionally graded beams at two ends. They obtained the two-dimensional elasticity solution for the problem by considering the Young's modulus change over the thickness as exponential-law and constant Poisson's ratio. Huang et al. [60] presented a semi-analytical solution for the anisotropic functionally graded beams under the arbitrary load, the solution based on the sub-layer approximation. The material parameters changed in the thickness direction. Yang et al. [61] developed a general two-dimensional solution for a bilayer functionally graded cantilever beam with concentrated loads at the free end. The functionally graded beam problem was treated as a non-homogeneous plane stress problem and proposed the solution for the functionally graded sandwich beams problem.
Nguyen et al. [62] analyzed rectangular functionally graded beams axially loaded under static and free vibration by the first-order shear deformation beam theory. The solution was obtained using the Navier solution technique. The influence of the power-law index, material contrast, and Poisson's ratio on the displacements, natural frequencies, buckling loads, and load–frequency curves were investigated.
Benatta et al. [63] used higher-order shear deformation theory for short functionally graded symmetric beams bending under a three-point test. The virtual work principle was utilized to obtain the governing equations. Benatta et al. [64] studied the static response of simply-supported functionally graded hybrid beam by the higher-order shear deformation beam theory under the transverse uniform load. Sallai et al. [65] used various shear deformation theories to analyze the simply-supported sigmoid FGM beam bending subjected to a uniformly distributed transverse loading using shear deformation theories. Thai and Vo [66] developed higher-order shear deformation beam theories for bending and free vibration of graded beams. The influences of the power-law index and shear deformation in graded materials bending and free vibration responses are studied.
Hadji et al.[67] developed a new higher-order shear deformation model for static and free vibration analysis of functionally graded beams. Hamilton's principle was used to derive the equations of motion. The Navier solution was used to obtain stresses, displacements, and frequencies for different material properties. Atmane et al. [68] presented an efficient hyperbolic beam theory for bending, free vibration, and buckling analysis of FGM porous beams resting on a two-parameter elastic foundation using Hamilton's principle and Navier technique.
Li et al. [69] used load equivalence and mathematical similarity of the governing equations, bending solutions homogenous Euler– Bernoulli beams into FGM Timoshenko beams solution by the same geometry, loading, and end stresses. Akbas [70] used the Euler-Bernoulli beam theory and Timoshenko beam theory to investigate free vibration and static bending analysis of simply-supported functionally graded beams resting on the Winkler foundation. Generic N-order estimation based on Carrera's unified formulation was supposed for the unknown variables displacement over the beam cross-section. A Navier type, closed-form solution based Euler-Bernoulli's and Timoshenko's, were obtained for the linear static analysis of functionally graded beams under bending and torsional loadings [71].
Li [72] presented a new unified approach for analyzing static and dynamic behaviors of

functionally graded beams by two theories (The Rayleigh and Euler–Bernoulli beam theories) which were reduced from the Timoshenko beam theory. The method can apply to layered Timoshenko beams. Li et al. [73] presented bending solutions of functionally graded beams based on the Levinson beam theory. The deflection, the rotational angle, the bending moment, and the shear force of FGM Levinson beam were expressed in terms of the deflection of homogenous Euler-Bernoulli beams, with the same geometry, loading, and boundary conditions.

3.2.5 Numerical solutions by the finite element methods for FGMs beams

Static analysis of cantilevered and simply-supported beams using a new mixed finite element based on higher-order shear deformation theory was studied [74]. Ziou [75] developed a finite element with three degrees of freedom per node, based on the Euler-Bernoulli beam theory (CBT) and the Timoshenko beam theory (TBT). This element was used to analyze the bending, vibration FGMs beams. Guenfoud [76] developed a new finite element for bending the functionally graded beam and coque. In addition, a new shear function based on the higher-order shear deformation theory was used in the same analysis.
Vo et al. [77] developed a two-noded Hermite-cubic element based on a refined shear deformation theory. The finite element was used to analyze static and vibration analysis of functionally graded beams with simply-supported, cantilever-free, and clamped-clamped boundary conditions.
Kapuria et al.[78] used a finite element model based on a third-order zigzag theory to analyze the layered functionally graded beams. This latter accurately models the mechanics of layered functionally graded beams.
Jing et al. [79] used a combination approach based on the cell-center finite volume method and the Timoshenko beam theory to analyze static and free vibration of functionally graded beams one dimensional. Carrera's unified formulation was employed for the static analysis of functionally graded beams. The governing is derived and solved by the finite element Method [80].
Aldousari [81] used Euler–Bernoulli theory and modeled the bending of a functionally graded beam subjected to a uniform distributed load. The power function, symmetric power function, and sigmoid function describe the distribution of material properties through the beam thickness. The virtual work and the weak form derive the element stiffness matrices and force vectors using the finite element method, the power index exponent, and the elasticity ratio effect on the static deflection and stress distribution.
Akbaş [70] employed Euler-Bernoulli beam theory and Timoshenko beam theory to study free vibration and static bending analysis of functionally graded beams resting on the Winkler foundation. The material properties change in the thickness direction according to power-law distributions. The foundation parameter and the material properties distribution affect the response of the static and vibration of the functionally graded beam.
Recently, Rahmani et al.[82] analyzed bending of functionally graded and porous functionally graded beams based on various beam theories. The results were proved numerically by the finite element method. The material properties change through the thickness direction as power-law volume fraction. They also investigated the effects of the power-law index, porosity exponent, and different boundary conditions on bending.

3.3 Displacement based plate theories

3.3.1 Classical plates theory (CPT)

The classical plates theory (CPT) is based on the assumptions of Kirchhoff-Love, which assumed that the straight lines remain straight and perpendicular to the midplane after deformation (see figure 3-2).
This theory is considered to be the simplest model of the equivalent single layer (ESL) theories. The classical plates theory is suitable only for thin plates like thin functionally graded plates/shells. The deflection generated by the shear deformation remains negligible compared to the deflection obtained by the plate curvature, where the shear and normal deformation effects are neglected. The field of displacement is written as follows:

$$\begin{aligned} u(x,y,z) &= u_0(x,y) - z\frac{dw_0}{dx} \\ v(x,y,z) &= v_0(x,y) - z\frac{dw_0}{dy} \\ w(x,y,z) &= w_0(x,y) \end{aligned} \tag{3.5}$$

Where:
(u_0, v_0, w_0) are the components of the field of displacement on the mean plane of the plate $(z = 0)$.

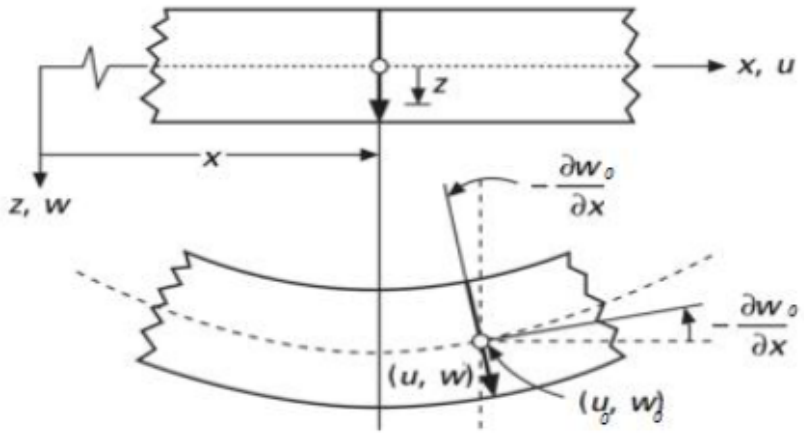

Figure 3.2: The classical plate displacement [83].

Ma and Wang [84] used CPT to analyze bending and the thermal post-buckling behaviors of functionally circular plates. Damanpack [85] used the boundary element method of the neutral surface. In addition, they used the CPT model for analyzing the bending behavior of functionally graded plates.

3.3.2 First order shear deformation theory (FSDT)

Mindlin [86] developed the first-order shear deformation theory (FSDT). Mindlin's approach [86] assumed that the displacement field in the plane through the thickness is linear. The theory accounts for the shear deformation effect by a linear variation of in-plane displacements through the thickness. The shear correction factor is necessary in this case, it relating to the loading, boundary conditions, and geometric parameters (see figure3-3).

The displacement field of the first-order shear strain theory is given by:

$$\begin{aligned} u(x,y,z) &= u_0(x,y) + f(z)\phi_x(x,y) \\ v(x,y,z) &= v_0(x,y) + f(z)\phi_y(x,y) \\ w(x,y,z) &= w_0(x,y) \end{aligned} \tag{3.6}$$

where:
(u_0, v_0, w_0) are the membrane displacements and (ϕ_x, ϕ_y) the rotations around the x and y axes, respectively given by:

$$\phi_x = \frac{dw_0}{dx}, \quad \phi_y = \frac{dw_0}{dy} \tag{3.7}$$

And

$$f(z) = z \tag{3.8}$$

$f(z)$: The shear stress function.

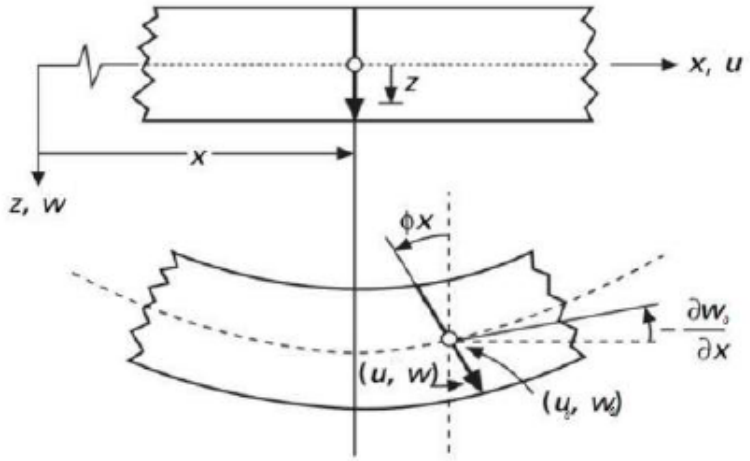

Figure 3.3: The first shear deformation theory displacement [83].

Della and Venini [87] used the FSDT and a variational hierarchic family of finite element formulation to study the bending of functionally graded plates under thermal and mechanical loadings.
Ardestani et al. [88] analyzed eccentrically and concentrically graded hardened plates bending under transverse loadings. The kernel particle method and FSDT were employed. Reddy et al. [89] analyzed functionally graded circular and annular plate bending and stretching analysis using the FSDT.

3.3.3 High order shear deformation theory (HSDT)

Generally, the shear correction factor in the FSDT and TSDT is not easy to obtain. Several theories of high order were developed by Reddy [90], [91] and Taj et al [92] to avoid the employ of the shear correction factor (see figure 3-4).
Generally, these theories describe the displacement field by using a Taylor series expansion across the thickness of the width and can be written as:

$$u(x,y,z) = u_0(x,y) + z\phi_a(x,y) + z^2\phi_a^2(x,y) + \ldots + z^\eta\phi_a^\eta(x,y) \tag{3.9}$$

Where:
η: The order used in the model.

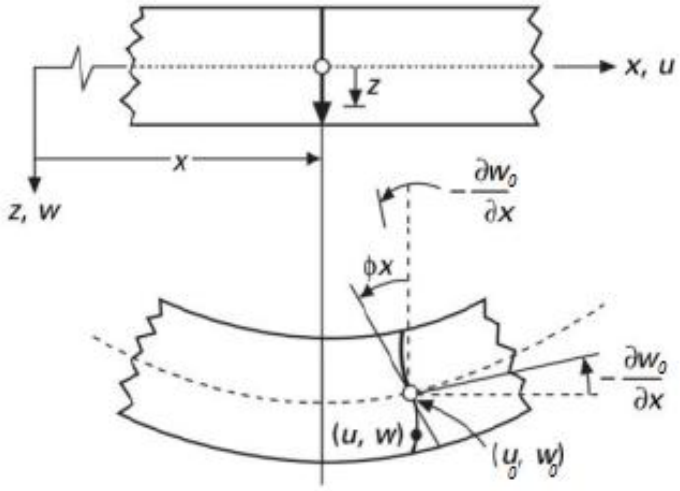

Figure 3.4: The higher shear deformation theory displacement[83].

According to Mallikarjuna and Kant [93], [94], the development of these high order theories is based on this hypothesis:
-The displacements are small compared to the thickness of the plate.
-The transverse sections, initially plane and normal to the mean plane, do not remain necessarily plane after deformation.
-The axial strain in the transverse direction is not negligible.
-The normal stress in the transverse direction generally not negligible.

The field of displacements which used in most high order theories (HSDT) and based on Mindlin theory [86] written in the following form:

$$\begin{aligned} u(x,y,z) &= u_0(x,y) - z\frac{dw_0(x,y)}{dx} + f(z)\gamma_x(x,y) \\ v(x,y,z) &= v_0(x,y) - z\frac{dw_0(x,y)}{dx} + f(z)\gamma_y(x,y) \\ w(x,y,z) &= w_0(x,y) \end{aligned} \tag{3.10}$$

with

$$\begin{aligned} \gamma_x &= \frac{dw_0}{dx} + \phi_x \\ \gamma_y &= \frac{dw_0}{dy} + \phi_y \end{aligned} \tag{3.11}$$

Where:
(u_0, v_0, w_0) : The membrane displacements.
(ϕ_x, ϕ_y) : The rotations around the x and y axes, respectively.
(γ_x, γ_y) : The transverse shear strain measured on the mean plane.
Reddy [95] analyzed functionally graded plates under thermo-mechanical loading by developing a general HSDT in addition to Von Karman geometric nonlinearity. There is a possibility to deduce the others theory (CPT, FSDT, TSDT, and HSDT) with free traction in the top and the bottom surfaces directly from the developed general HSDT.

Kant et al. [96] used HSDT for static bending and free vibration responses of plates with functional properties. Jha et al. [97] [98] used HSDT to study the static bending of functionally graded plates. Meksi et al. [99] presented a new shear deformation plate theory for bending, buckling, and free vibration responses of FGM sandwich plates.

3.3.3.1 Third shear deformation theory (TSDT)

Reddy [90] developed the third shear deformation theory (TSDT) for laminated composite plates by introducing the effect of transverse shear deformation. The results proved and satisfied the zero-traction boundary conditions on the top and the bottom of plate surfaces. Reddy proposed the shear stress function as follow:

$$f(z) = z\left(1 - \frac{4}{3h^2}z^2\right) \tag{3.12}$$

The analytical and the finite element formulations based on the TSDT were solved by Reddy [91]. The formulations were used for the thermo-mechanical coupling, time dependency, and Von Karman-type geometric nonlinearity. A finite isoparametric element content nine-node with seven degrees of freedom per node was developed by Gulshan Taj et al. [92]. The finite element formulation is based on the TSDT. They used it for the bending analysis of functionally graded plates under thermo-mechanical loadings.
Tran et al. [100] used TSDT and isogeometric analysis (IGA) for bending, buckling, and free vibration of plates with functionally graded proprieties. Jari et al. [101] use the TSDT and IGA to study the linear and non-linear buckling and free vibration of functionally graded plates under mechanical and thermal loadings. Oktem et al. [102] used the TSDT and boundary-discontinuous generalized double Fourier series approach to analyze simply supported plates with functional properties, and also obtained the analytical solutions for bending analysis of doubly-curved shells. The other theories based on the development of the shear stress function are addressed in table 3-1.

The theory	The shear stress function
The Sinus shear deformation plate theory (SSDT) [103]	$f(z) = \frac{h}{\pi}\sin(\frac{\pi z}{h})$
The exponential shear deformation plate theory (ESDPT) [104]	$f(z) = ze^{-2(z/h)}$
The hyperbolic shear deformation plate theory (HSDPT) developed by [105]	$f(z) = \frac{\cosh(\pi/2)}{[\cosh(\pi/2)-1]} - \frac{(h/\pi)\sinh\left(\frac{\pi}{h}z\right)}{[\cosh(\pi/2)-1]^z}$

Table 3.1: The shear stress function.

3.3.4 Numerical solutions by the finite element method for FGM plates

Martínez-Pañeda [106] modeled the functionally graded properties in finite elements by employing two formulations, point-based integration and a nodal-based variation via temperature dependence. The FGM plate is under uniform displacement perpendicular to the material gradient direction and uniform traction perpendicular and parallel to the material gradient direction. The element-based formulations [106] were proposed for fracture analysis of FGM in future research.
The Kirchhoff-Love theory and the isoparametric mixed finite element concept have been used by Orakdöğen et al. [107] to study the coupling effect of extension and the bending of FGM plate under transverse loading. The material properties vary continuously throughout the thickness direction according to sigmoid distribution in the functionally graded plates. They proved that the influence of membrane extension-bending is better than others in some simply supported FGM plates.

The unified formulation (UF) and Reissner's mixed variational theorem were used by Brischetto and Carrera [108] for plates with functionally graded properties under a transverse mechanical load investigation.
The material properties change continuously in the thickness direction according to thickness functions as Legendre's polynomials. Van Long et al.[109] used a new eight-unknown shear deformation theory and finite element for bending and the free vibration of functionally graded plates analysis. The finite element with four nodes was employed. The graded properties vary continuously in the thickness direction as power-law distribution. They also performed a parametric study to investigate the effect of the power-law index and the thickness ratio on the behavior plate bending.
Recently, Tran et al.[110] used an edge-based smoothed finite element method associated with the mixed interpolation of tensorial components technique for the three-node triangular element to analyze static bending and free vibration of functionally graded porous variable-thickness plates.

3.4 Discrete layer and layer-wise approach (local approximation)

Layer-wise models assume separate displacement fields to each material layer rather than global kinematics. The model provides a correct kinematic representation of deformation in the discrete layers and describes the accuracy of stresses at the folds.
In this approach, each layer is treated individually by imposing the continuity conditions in displacements or stresses on the interfaces. The first and the higher-order theories were tested for each substructure. The theory development was based on the layer-wise approach proposed by Reddy [111], who defined the thinner layer-by-layer approximation of the fields of displacement along with the thickness of a multilayer (see figure 3-5). This model represented the displacements as a linear combination of the materials by coordinates functions in the plane or thickness. The corresponding displacement field in the k^{th} layer was written as follows:

$$\begin{aligned} u(x,y,z) &= \sum_{i=1}^{n} u_i^k(x,y)\phi_i^k(z) \\ v(x,y,z) &= \sum_{i=1}^{n} v_i^k(x,y)\phi_i^k(z) \\ w(x,y,z) &= \sum_{i=1}^{n} w_i^k(x,y)\phi_i^k(z) \end{aligned} \tag{3.13}$$

where :
u^k, v^k, w^k : The components of the displacements of the layer k in the directions x, y, and z, respectively.
$\phi_i^k(z)$: Lagrange interpolation functions (1D) continuous according to the thickness coordinates.

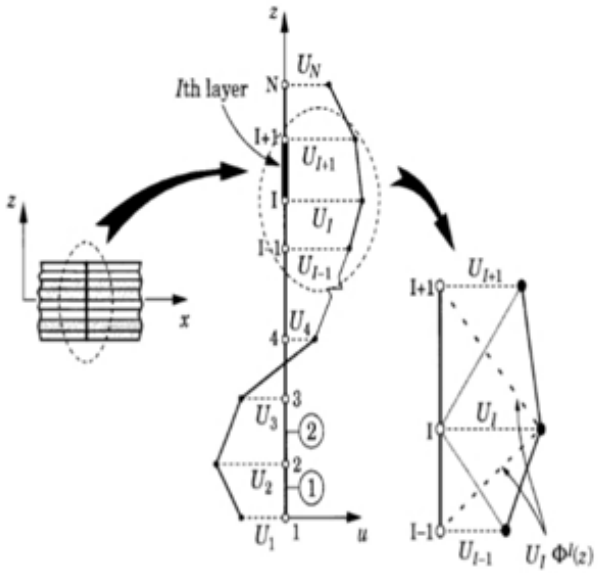

Figure 3.5: Displacements and linear approximation functions used in the Laye-rwise theory[83].

A general finite element formulation based on the layer-wise theory was developed for a functionally graded plate with piezoelectric layers under static loads modeling [112]. The intermediate functionally graded layer was made of many anisotropic sub-layers. The non-linear distribution of electric potential in thick piezoelectric layers was obtained.
Carrera et al. [113] used the equivalent single layer and layer-wise approaches to investigate the static response problem of multilayered plates and shells embedding graded material layers. Carrera's unified formulation (CUF) was employed to obtain a refined model based on Reissner's mixed variational theorem. The CUF described the continuous variation in the thickness direction for the embedded FGM layers.

3.4.1 Zig-zag theories

The zig-zag theories involve taking a movement pattern (or stress) in each layer, and the compatibility conditions and equilibrium interface are used to reduce the number of unknown variables [114]. The number of kinematic variables is dependent on the number of layers as in the equivalent single layer approach (ESL). Figure 3-6(a) shows the geometry and notations of a three-layered laminate used in zig-zag theories, and figure 3-6 (b) shows a generic zigzag function in terms of interfacial axial displacements.

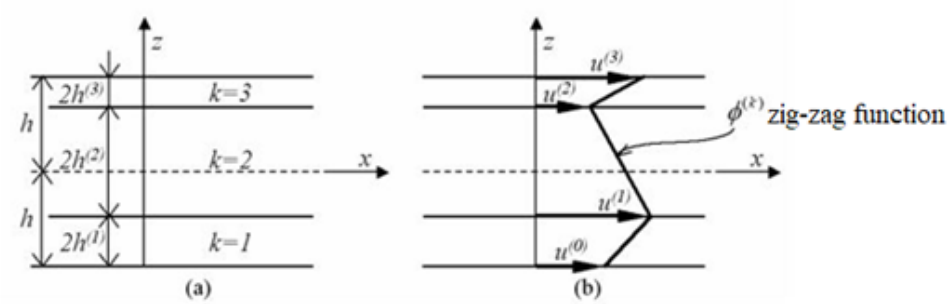

Figure 3.6: Geometry and notations of a generic zigzag function used in zig-zag theories [115].

Tessler et al. [115] proposed higher-order zig-zag theory to calculate transverse shear stresses from constitutive equations. This theory presents the variation of the piecewise shear stresses, which vanish in the upper and lower surfaces as a parabolic variation. Di Sciuva and Sorrenti [116] presented a refined zig-zag theory (eRZT) in conjunction with the Ritz method to bending analysis of functionally graded sandwich plates (carbon nanotube-reinforced) under bi-sinusoidal and uniform transverse pressure. The eRZT predicts the response for static more accurately than FSDT and TSDT.
Dorduncu [117] presented a novel non-local model for stress and displacement prediction analysis of a graded sandwich plates core with the refined zig-zag theory (RZT) without shear correction factors. The material graded properties treating by using mixing rules and change through the thickness. The interfacial stresses can be avoided by grading the material properties of the core through the thickness direction. A review of theories and modeling of FGMs was presented [118][119].

3.5 Conclusion

In this chapter, the layered approach or the single-layer equivalent approach for beams and plates are presented. classical beam theory (CBT), first-order shear deformation beam theory (FSDBT), and high-order shear deformation beam theory (HSDBT) are detailed. The classical plate theory (CPT) of Love-Kirchhoff used for the study of thin plates, the first-order shear theory (FSDT), and the high order theories (HSDT) also presented. The discrete layer, layer-wise approach, and zig-zag theories are presented for the multilayered structure. These theories are developed in order to study displacements and stresses in plates and beams where HSDT gives realistic displacement and stresses unlike other theories.

Chapter 4

Fracture theories in the FGMs

4.1 Introduction

Fracture mechanics is the best available design technology for developing the failure criterion with the local discontinuity of material. The purpose of fracture mechanics is to study macroscale cracks by fracture mechanism to understand the mechanical process that produced a notch. The microcracks propagated at the microscopic scale, and it started from existing microcracks or other modes of failure, such as creep. The fracture mechanics are also used in the design and dimensioning of materials after a damage analysis. This analysis predicts a damaged band in the material by evaluating the residual life of a cracked structure.
Fracture mechanics divides into the brittle fracture (Linear-elastic fracture mechanics), in the absence of significant plastic deformation and ductile fracture (Elastic-plastic fracture mechanics), in the presence of non-negligible plastic strain.
In this chapter, the notion of fracture mechanics and the fracture criteria used in functionally graded materials (FGMs) are presented, and also the techniques to evaluate the fracture parameters as stress intensity factors (SIF's) or the energy release rate (G).

4.2 Cracks and notches

The crack is new internal borders in the structure presented by local discontinuity. The crack has lips and cracks front, where the lips of crack are surfaces that form the new border of a crack. The lips are connected by a curve called the crack front. This curve is open for an emerging crack (see figure 4-1.a) and closed for an internal crack (see figure 4-1.b). In 2D analysis, the lips are straight segments in the simplest case and curves in the complex case.

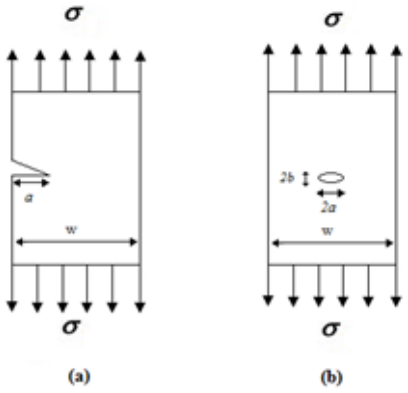

Figure 4.1: Crack and notche.

4.3 Propagation mode

The lips of the crack displacement of crack propagation associated with the three modes (see Figure 4.2):
Mode 1: Opening mode.
Mode 2: Plane sliding mode.
Mode 3: Anti-plane sliding mode.

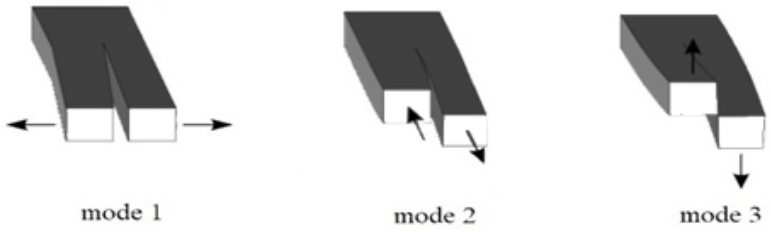

Figure 4.2: Failure mode.

4.4 Cracked elastic medium

In a cracked elastic medium, the region close to the crack tip divides into three zones:
1- The crack tip front zone: is the direct vicinity of the crack tip. Studying this zone is very complex in the far fields as the stresses tend towards infinity at the crack tip. This zone was considered a punctual from a mechanical point of view.
2- The singular zone: in this zone, the stress field présents a singularity $r^{-1/2}$, where r is the singularity of order –1/2. The singular zone characterizes by obtained the solution in pure elasticity.
3- The far fields zone: is the external zone of the region close to the crack tip, which connects the singular zone with the boundary conditions of loading and displacement.

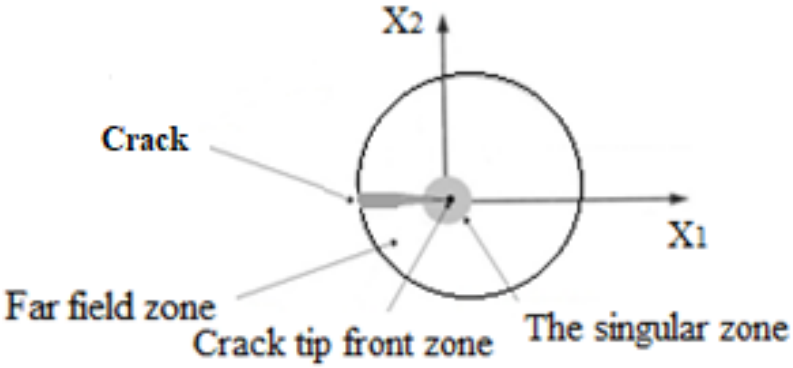

Figure 4.3: Mechanical field zones in cracked medium.

4.5 Stress concentration factor

By considers a defect of the elliptical form of length 2a and the radius at the bottom of notch l (see figure 4.4).

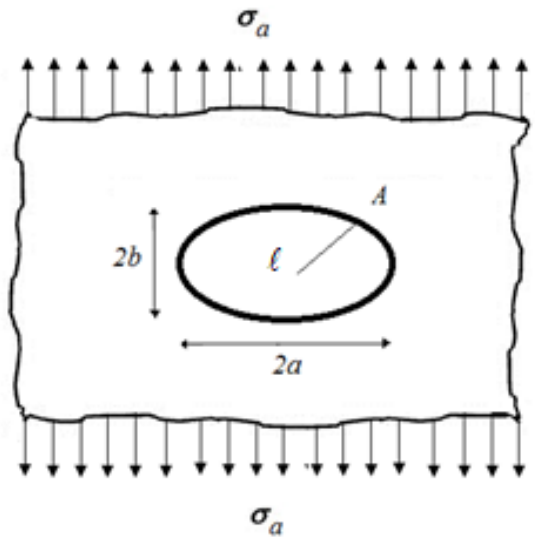

Figure 4.4: The stress concentration.

The local stress at the end A is written :

$$\sigma_L(A) = \sigma_a\left(1 + \frac{2a}{b}\right) = \sigma_a\left(1 + 2\sqrt{\frac{a}{l}}\right) \tag{4.1}$$

In the case concerning a very smaller notch, $l \ll a$ the local stress and the stress concentration factor were written as:

$$\begin{aligned} \sigma_L(A) &\approx 2\sigma_a\sqrt{\frac{a}{l}} \\ \kappa_T &= 2\sqrt{\frac{a}{l}} \end{aligned} \tag{4.2}$$

Where:

κ_T: The stress concentration factor.

The stress concentration factor can become very large for sharp notches such as cracks.

The important thing is to distinguish between the stress concentration factor κ_T, which only gives local information at the very tip of the notch, and the stress intensity factor κ, which describes the whole of the spatial singularity of the stress field.

κ_T has no dimensions, it is not the same for K which related by the square root of a length, namely:

$$[K] = SIF's \qquad Mpa\sqrt{m}$$

4.6 Stress intensity factors

Irwin [120] presented the stress intensity factors corresponded to particular kinematics of the crack movements (see figure 4-5). In the frame of linear fracture mechanics, the stresses and strains in the vicinity of a crack admit an asymptotic development whose singular term is written as:

$$\sigma_{ij} = \frac{K_I}{\sqrt{2\pi r}} f_{ij}^{I}(\theta) + \frac{K_{II}}{\sqrt{2\pi r}} f_{ij}^{II}(\theta) + \frac{K_{III}}{\sqrt{2\pi r}} f_{ij}^{III}(\theta) \qquad \text{for}\,(i,j=1,3) \tag{4.3}$$

Where:

$f_{ij}^{I}(\theta)\, f_{ij}^{II}(\theta)\, f_{ij}^{III}(\theta)$:The angular function for the mode 1, 2 and 3 respectively, which depends on the variable θ.

K_I, K_{II}, K_{III} :The stress intensity factors for mode 1, 2, and 3, respectively.

$SIFs$ independent of, r et θ, and depend only on the geometry of the crack and the boundary conditions.

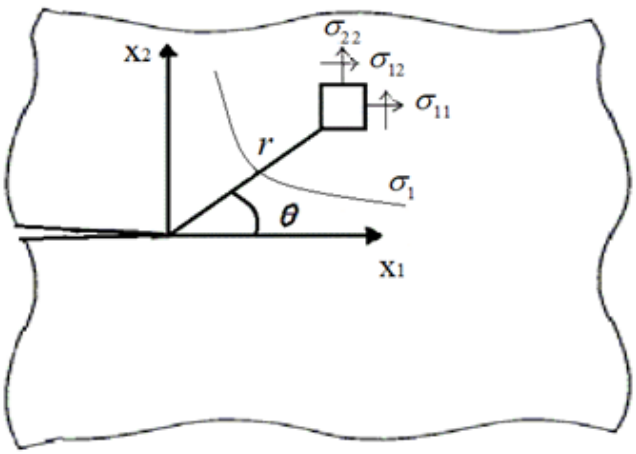

Figure 4.5: The stresses in the vicinity of a crack.

The relation (4-3) shows that the singularity $r^{-1/2}$ when the components u_i of displacement in the crack tip $r^{-1/2}$ tending towards zero. The displacement expression in the vicinity

of the crack tip is written:

$$u_i = \frac{K_I}{\mu}\sqrt{\frac{r}{2\pi}}g_{ij}^{I}(\theta) + \frac{K_{II}}{\mu}\sqrt{\frac{r}{2\pi}}g_{ij}^{II}(\theta) + \frac{K_{III}}{\mu}\sqrt{\frac{r}{2\pi}}g_{ij}^{III}(\theta) \qquad \text{for } (i,j=1,3) \tag{4.4}$$

Where:
$g_i^I(\theta), g_i^{II}(\theta), g_i^{III}(\theta)$: The angular function for modes 1,2 and3.
The angular function does not control the stress distribution and it depends only on the crack length and the loading mode.

4.7 Fracture mechanics approaches

Fracture mechanics studied the fields of displacements, strains, and stresses in the vicinity of a crack by two approaches: A local approach studied the stress and strain fields in the vicinity of the crack front. The global approach is studying the global behavior of the cracked structure on the energetic level.

4.7.1 Local approach

The local approach is used in fracture mechanics to models the damage. It specifies fracture mechanics parameters using local stress and strain fields at the tip of the crack. The approach introduced the notion of stress intensity factors. This approach obtained the fields at the crack tip. The field is strongly disturbed by the singularity created by the crack point.

4.7.1.1 Solution of Muskhelishvili

Muskhelishvili [121] studied an infinite panel containing a crack of length $2a$ according to the axis x_1, and applied a uniform traction according to the axis x_2. (Figure 4.6 a). There exists an exact analytical solution of this problem, on the axis $x_2 = 0$, by supposing a state of plane stresses:
If $x_1 > a$

$$\sigma_{11} = \sigma_{22} - \sigma_\infty \qquad \sigma_{22} = \frac{\sigma_\infty}{\sqrt{\left(1 - \left(\frac{a}{x_1}\right)^2\right)}} \tag{4.5}$$

$$\varepsilon_{22} = \left(\frac{\sigma_\infty}{E}\right)\left(\nu + \frac{1-\nu}{\sqrt{\left(1 - \left(\frac{a}{x_1}\right)^2\right)}}\right) \tag{4.6}$$

If $0 \le x_1 \le a$

$$[u_2] = 2u_2 = \left(\frac{4a\sigma_\infty}{E}\right)\sqrt{\left(1 - \left(\frac{a}{x_1}\right)^2\right)} \tag{4.7}$$

The displacement formula u_2 (on the boundary of the crack) represented the lips opening by an ellipse.

The change of variable $X_1 = a + r$ shows a singularity in the the vicinity of the crack tip a in $r^{1/2}$ when r tends towards 0.

$$\sigma_{22} \propto a\sigma_\infty\sqrt{\left(\frac{a}{2r}\right)} \tag{4.8}$$

4.7.1.2 Asymptotic solution of Westergaard

Westergaard [122] introduced the Airy function and verified the equilibrium equations of the solution bi-harmonic equations $\Delta\Delta\psi = 0$. Then the Airy $\psi(x,y)$ function is the stress function.

The method of complex function obtains the asymptotic solution in the vicinity of the crack tip.

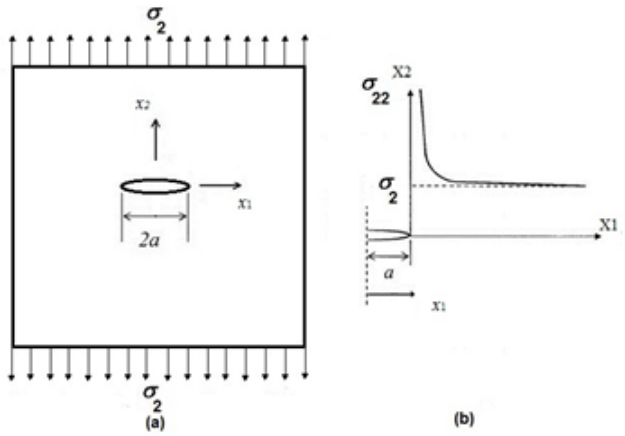

Figure 4.6: The stresses distribution ahead of the vicinity of a crack.

Irwins [120] showed that the first term of the limited expansion is the same, except for a multiplicative factor, for all the problems corresponding to a given opening mode. The stress of a linear crack in a plane medium related to mode 1 is perpendicular to its axis, where the stress intensity factor in mode 1 is:

$$K_I = \lim_{r\to 0}\left(\sigma_{22}\sqrt{2\pi r}\right) \tag{4.9}$$

4.7.2 Global approach

The dissipation energy is the value between the energy state of a system before and after cracking [123]. This energy can be linked to surface energy, and this was an intrinsic characteristic of the material.

4.7.2.1 The energy release rate

Irwins [120] defined the energy release rate G, which reflects the balance of the energies intervening during the increase of cracks (The elastic energy restored during the crack propagation. While the energy dissipated during the creation of new surfaces). The energy release rate is related to a variation of the potential energy stored in the structure compared to an increase in the crack. The energy balance for a cracked solid after an increase ∂S is written:

$$\partial W_{ext} = \partial W_{elas} + \partial W_{kin} + \partial W_{rup} \quad \text{and} \quad \partial W_{rup} = 2\lambda\partial s \tag{4.10}$$

Where:

W_{ext} : The extern energy.
W_{elas} : The elastic energy.
W_{kin} : The kinematic energy.
W_{rup} : The rupture energy.

Starting from a state of equilibrium ($W_{kin} = 0$), the energy release rate and the balance

become respectively:

$$G = \frac{\partial}{\partial s}(W_{ext} - W_{elas}) = \frac{\partial W_{pot}}{\partial s} \tag{4.11}$$

$$(G - 2\lambda)\,\partial s = \partial W_{kin} \tag{4.12}$$

Where:

W_{pot} is the potential energy.
$\partial s = b.\Delta a$
λ is the energy required to create the surface.
G is a quantity independent of the geometry of the material and characteristic of the stability of the propagation of a crack.

If $G = 2\lambda$: The crack propagates while maintaining the equilibrium.
If $G < 2\lambda$: The crack cannot extend.
If $G > 2\lambda$: The crack will be unstable.
G is a negative value since W_{pot} decreases with the increase of s.
For a two-dimensional cracked medium with thickness b, G is written from the relation (4-11) as:

$$G = \frac{1}{b}.\frac{\partial W_{pot}}{\Delta a} \tag{4.13}$$

Where Δa is the increased crack length
For a unit thickness:

$$G = \frac{\partial W_{pot}}{\Delta a} \tag{4.14}$$

4.8 Fracture mechanics in FGMs

The FGMs developed to be one of the successful advanced composite materials entered in essential fields. The researcher's trying to understand the damage in these materials. Fracture mechanics theories and experimental tests provide technical support for design and manufacturing. They study the effect of external loads and geometry of material and the crack tip and its location with different boundary conditions. Remarkable theories are based on the principle of continuum solid mechanics and thermodynamics to determine the criterion for fracture initiation and propagation, the influence of material graded on stress distribution in the crack tip in FGM studied in various studies [124], [125], [126], [127], [128], [129].
The singularity and the angular distribution of stress and displacement field in the crack tip is like in homogenous materials [48],[51],[130],[131],[132],[133]. So this applied computational fractures on FGM as homogenous. The finite element is utilized without any modification by treating it as homogenous materials crack problems.

4.9 FGMs crack tip field

FGMs are new advanced materials with properties (E, ν) change with spatial position.
Williams [134] proposed the eigenfunction expansion technique, which investigated the nature of near-tip fields in a cracked material.
Eischen [135] use the eigenfunction expansion technique to investigate asymptotic crack-tip fields in graded materials. He has also shown that the material property variation is not affected by the stress field angular functions, which are associated with the first two terms ($r^{-1/2}$ and r^0), but on the other hand, the nonhomogeneity parameter affection related by the higher-order terms ($r^{1/2}$ and higher). Eischen [135] proposed that (E, ν) are piecewise continuously. He also showed that nonhomogenous and homogeneous materials have the

same crack-tip elastic fields.
Jin and Noda [136] accurate the studies in the paper [135]. For further studies extended to 3D, anisotropic, and for elastic-plastic FGM problem ([135], [136], [137]). Jin and Noda [136] give asymptotic crack-tip stress and displacement fields in FGMs as follow:

$$\begin{aligned}\sigma_{11} &= \frac{K_I}{\sqrt{2\pi r}} f_{11}^{I}(\theta) + \frac{K_{II}}{\sqrt{2\pi r}} f_{11}^{II}(\theta) + \sigma_{x0} + ... \\ \sigma_{22} &= \frac{K_I}{\sqrt{2\pi r}} f_{22}^{I}(\theta) + \frac{K_{II}}{\sqrt{2\pi r}} f_{22}^{II}(\theta) + ... \\ \sigma_{12} &= \frac{K_I}{\sqrt{2\pi r}} f_{12}^{I}(\theta) + \frac{K_{II}}{\sqrt{2\pi r}} f_{12}^{II}(\theta) + ...\end{aligned} \tag{4.15}$$

Where:
K_I, K_{II} : The stress intensity factors in mode 1 and 2.
$f_{ij}^{I}(\theta)$ and $f_{ij}^{II}(\theta)$ for $(i, j = 1, 2)$: The angular function for mode 1 and 2.
σ_{x0}: The non-singular stress.
The near-tip displacement is written:

$$u_i = \frac{K_I}{\mu_{tip}} \sqrt{\frac{r}{2\pi}} g_i^{I}(\theta) + \frac{K_{II}}{\mu_{tip}} \sqrt{\frac{r}{2\pi}} g_i^{II}(\theta) + ... \qquad \text{for}(i = 1, 2) \tag{4.16}$$

Where:
μ_{tip}: The shear modulus.
$g_i^{I}(\theta)$, $g_i^{II}(\theta)$: The angular function for mode 1, 2.
F. Erdogan [48] used a singular part of the crack-tip stresses in a graded material given in the equation (4-15) under plane stress conditions.
The crack-tip energy release rate G is related to the stress intensity factors by the relation below:

$$\begin{aligned}G &= \frac{1}{E_{tip}}(k_I^2 - k_{II}^2) \qquad \text{in plane-stress condition} \\ G &= \frac{(1 - \nu_{tip}^2)}{E_{tip}}(k_I^2 - k_{II}^2) \qquad \text{in plane–strain conditions}\end{aligned} \tag{4.17}$$

Where:
E_{tip} and ν_{tip} : The Young modulus and poisson ration at the crack tip, respectively.

4.9.1 Auxiliary fields

Kim and Paulino [138] used the auxiliary fields (displacements, stresses, and strains) to evaluate mixed-mode SIFs, these fields based on the interaction integral methods. They also developed fields for homogeneous materials and used an incompatible formulation which accounts for the mismatch displacement between graded materials and the homogeneous.

4.9.1.1 Auxiliary fields for SIFs

For evaluating mixed-mode SIFs Kim and Paulino [138] used the auxiliary displacement and stress fields of asymptotic fields of crack-tip [134] with the properties of material simplified at the location of crack-tip ([135],[136]).

$$\sigma_{ij} = \frac{K_I^{aux}}{\sqrt{2\pi r}} f_{ij}^{I}(\theta) + \frac{K_{II}^{aux}}{\sqrt{2\pi r}} f_{ij}^{II}(\theta) + ... \qquad \text{for}(i, j = 1, 2). \tag{4.18}$$

$$u_i = \frac{K_I^{aux}}{\mu_{tip}}\sqrt{\frac{r}{2\pi}}g_i^I(\theta) + \frac{K_{II}^{aux}}{\mu_{tip}}\sqrt{\frac{r}{2\pi}}g_i^{II}(\theta) + \ldots \qquad \text{for}(i = 1, 2). \tag{4.19}$$

Where:

μ_{tip}: The shear modulus at the crack tip.
K_I^{aux}, K_{II}^{aux}: The auxiliary stress intensity factors for modes 1 and 2.
g_i^I, g_i^{II}: The angular functions for mode 1 and 2.

4.9.2 Displacement correlation technique

The displacement correlation technique (DCT) represents one of the simplest methods to evaluate SIFs. It correlates the numerical results for displacement at specific locations on the crack with available analytical solutions. The crack opening displacement (COD) for quarter-point singular element, at $x = -r$, is given by Shih et al. [139] and used by Kim and Paulino [137](See figure 4-7), can be written as:

$$COD(-r) = (4u_{2,i-1} - u_{2,i-2})\sqrt{\frac{r}{\Delta a}} \tag{4.20}$$

Where:

u_2 : The displacements relative to the crack tip at locations (i_{-1}) and (i_{-2}) in the x_2 direction.
r : The distance from the crack tip along the x_1 direction.
Δa : The characteristic length associated with the crack-tip elements.

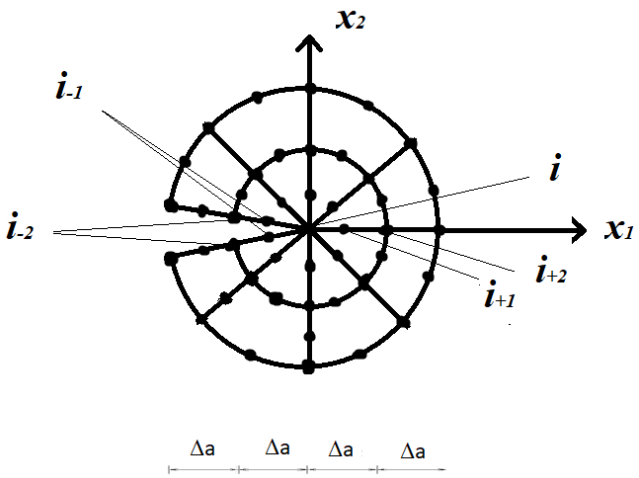

Figure 4.7: Crack tip rosette of singular quarter-point [137].

The material properties were considered at the crack-tip location. Thus, consistent with the equation (4-16), the analytical expression for equation (4-19) without introducing the higher-order terms, can be written as:

$$COD(-r) = k_1\left(\frac{k+1}{\mu}\right)_{tip}\sqrt{\frac{r}{\Delta\pi}} \tag{4.21}$$

$$\begin{aligned} k_I &= \sqrt{\frac{2\pi}{\Delta a}}\left[4\left(\frac{\mu}{k+1}\right)_{tip}u_{2,i-1} - \left(\frac{\mu}{k+1}\right)_{tip}u_{2,i-2}\right] \\ k_{II} &= \sqrt{\frac{2\pi}{\Delta a}}\left[4\left(\frac{\mu}{k+1}\right)_{tip}u_{1,i-1} - \left(\frac{\mu}{k+1}\right)_{tip}u_{1,i-2}\right] \end{aligned} \tag{4.22}$$

Note that for mode 2, the COD was replaced by CSD (crack sliding displacements).
Where:

$\mu = \mu(X)$ and $k = k(X)$ are the material properties in the crack tip location for SIFs expressions.

4.9.3 Modified crack closure

Rybicki and Kanninen [140] employed Irwin's [120] virtual crack-closure method and proposed the modified crack-closure integral method. They obtained the energy release rates for modes 1 and 2. The displacements behind the crack tip and the stresses ahead of the crack tip are used by utilizing only a one-step finite element analysis, without local homogeneity around the crack tip, which is a suitable method for FGMs.

The energy release rate is predictable with a virtual crack extension technique. Irwin [120] give the expression for G_I (mode 1) and G_{II} (mode 2) as:

$$\begin{aligned} G_I &= \lim_{\partial a \to 0} \frac{2}{\partial a} \int_{x_1=0}^{x_1=\partial a} \frac{1}{2} \sigma_{22}(r = x_1, \theta = 0, a) u_2(r = \partial a - x_1, \theta = \pi, a + \partial a) \partial x_1 \\ G_{II} &= \lim_{\partial a \to 0} \frac{2}{\partial a} \int_{x_1=0}^{x_1=\partial a} \frac{1}{2} \sigma_{12}(r = x_1, \theta = 0, a) u_1(r = \partial a - x_1, \theta = \pi, a + \partial a) \partial x_1 \end{aligned} \tag{4.23}$$

Where

σ_{12} and σ_{22}: The shear and the normale stress ahead of the crack tip.

u_1 and u_2: The relative displacements.

The energy release rates related to the stress intensity factors as following

$$\begin{aligned} G_I &= \left(\frac{k+1}{8\mu}\right)_{tip} k_I^2 \\ G_{II} &= \left(\frac{k+1}{8\mu}\right)_{tip} k_{II}^2 \end{aligned} \tag{4.24}$$

Raju [141] has shown that the values of G for mode 1, and 2 are expressed in terms of the equivalent nodal forces and the relative nodal displacements employing it in singular quarter-point elements around the crack tip [137] (see figure 4-8).

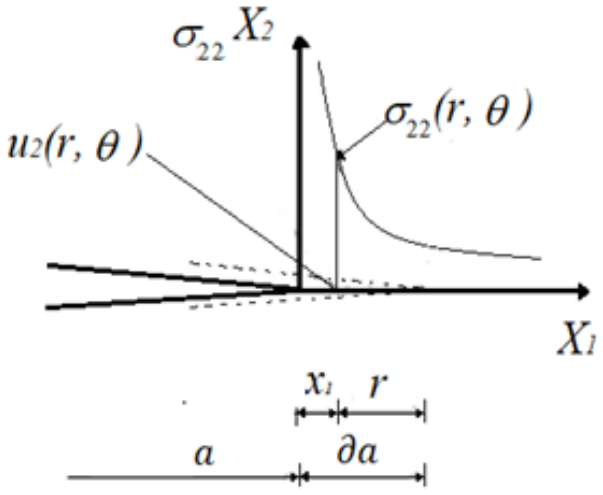

Figure 4.8: Virtual crack extension and normal crack distribution [137].

4.9.4 J-integral

The J-integral is also called the path of the independent integral [142]. J-integral is widely used in predicting fracture of materials (see figure 4-9).

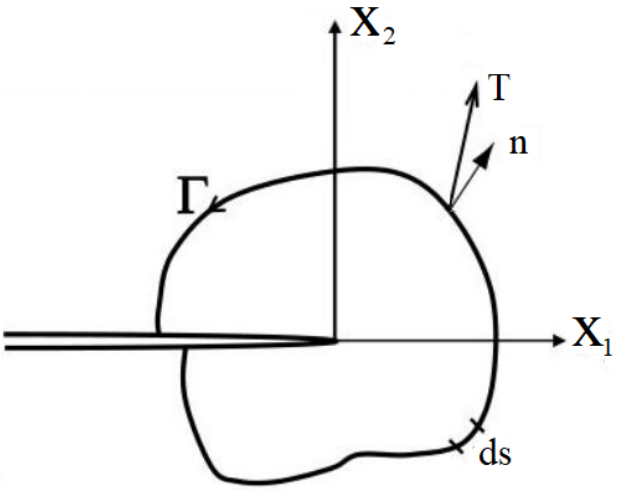

Figure 4.9: J-integral path.

The J-integral extended of nonhomogeneous elastic materials by Honein and Herrmann [143], when Young's modulus is parallel to the crack direction, the shear modulus change exponentially in the direction of x_1 (see equation (4-25)). Poisson's ratio is independent of x_1 .

$$\mu(x_1, x_2) = \mu_0(x_2) exp(\beta x_1) \tag{4.25}$$

Where:

β: The material constant.

$\mu_0(x_2)$: The arbitrary function of x_2.

The path-independent integral for this nonhomogeneous material proposed by Honein and Herrmann [143] and used by Kim and Paulino [137] in FGM is as follow:

$$J = \int_{\Gamma} \left[\left(w_d n_1 - \sigma_{ij} n_j \frac{\partial u_i}{\partial x_1} \right) - \frac{\beta}{2} \sigma_{ij} n_j u_j \right] ds \tag{4.26}$$

Where:

Γ: The contour enclosing the crack tip.

n_1: The first component of the unit outward the normal to Γ.

$\sigma_{ij} n_j = s_i$: The tractions components along Γ.

ds: The infinitesimal length element along Γ.

w_d: The strain energy density.

Honein and Herrmann [143] written relation between the independent J-integral and stress intensity factors k as :

$$\begin{aligned} J &= \frac{1}{E_{tip}} (k_I^2 - k_{II}^2) \qquad \text{in plane-stress condition} \\ J &= \frac{(1 - \nu_{tip}^2)}{E_{tip}} (k_I^2 - k_{II}^2) \qquad \text{in plane–strain conditions} \end{aligned} \tag{4.27}$$

Where:

E_{tip} and ν_{tip}: The Young modulus and poisson ration at the crack tip.

4.9.5 Maximum strain energy release rate

Hussain et al.[144] analyzed a branch and straight crack at an arbitrary angle, they proposed that crack propagate in the direction where there is a maximum strain energy release, and they give the energy release rate as a function of angle which used by Kim and Paulino [138] in FGM and given as follow:

$$G(\theta) = \frac{4}{E_{tip}}\left(\frac{1}{3+\cos^2\theta}\right)^2 - \left(\frac{1-\pi/\theta}{1+\pi/\theta}\right)^{\frac{\pi}{\theta}} (1+\cos^2\theta)k_2^2 + 8\sin\theta\cos\theta k_1 k_2 + (9-5\cos^2\theta)k_2^2 \quad (4.28)$$

The initiation angle obtained from these conditions

$$\frac{\partial G(\theta)}{\partial(\theta)} = 0,\ \frac{\partial^2 G(\theta)}{\partial^2(\theta)} \Rightarrow \theta = \theta_0 \quad (4.29)$$

The crack initiation angle determined by the condition

$$G(\theta_0) = G_c(x) \quad (4.30)$$

4.9.6 The maximum circumferential stress

Kim and Paulino [138] give the asymptotic stress fields for cracked linear elastic FGMs as follow:

$$\begin{aligned}
\sigma_{rr} &= \frac{1}{\sqrt{2\pi r}}\cos\frac{\theta}{2}\left[k_I\left(1+\sin^2\frac{\theta}{2}\right)+\frac{3}{2}k_{II}\left(\sin\theta-2\tan^2\frac{\theta}{2}\right)\right] \\
\sigma_{\theta\theta} &= \frac{1}{\sqrt{2\pi r}}\cos\frac{\theta}{2}\left[k_I\cos^2\frac{\theta}{2}-\frac{3}{2}k_{II}\sin\theta\right] \\
\sigma_{r\theta} &= \frac{1}{2\sqrt{2\pi r}}\cos\frac{\theta}{2}\left[k_I\sin\theta+k_{II}(3\sin\theta-1)\right]
\end{aligned} \quad (4.31)$$

The maximum circumferential stress theory was proposed by Erdogan and Sih [145]. The mentioned theory used by Kim and Paulino [138]. The kink angle is relative to the original crack line.
The initiation angle obtained from these conditions

$$\frac{\partial \sigma_{\theta\theta}}{\partial(\theta)} = 0,\ \frac{\partial^2 \sigma_{\theta\theta}}{\partial^2(\theta)} \Rightarrow \theta = \theta_0 \quad (4.32)$$

$$k_I\sin\theta - k_{II}(3cos\theta - 1) = 0 \quad (4.33)$$

The crack initiation angle determined by the condition

$$\cos\frac{\theta_0}{2}\left[k_I\cos\frac{\theta_0}{2}-\frac{3}{2}k_{II}\sin\theta_0\right] = k_{ic}(x) \quad (4.34)$$

4.10 Crack modeling in FGM

Modeling and optimizing the graded properties was studied to analyze thermal stress intensity factors in FGM. The analytical model with arbitrary distributed properties was used to solve the crack parallel to the gradient direction [146]. The finite element method is used for computing stress fields near the crack tip in FGM under thermal loading [130]. FEM is used to analyze crack with the arbitrary variable for structure reliably calculation[147]. FEM modeling using the virtual crack extension was used to compute SIFs and energy release rate directly from exiting cracks, the graded variation modeled by determining the

stiffness and the energy across each element [148]. A dummy thermal loads technique was proposed to model FGM using the finite element code ANSYS APDL [149]. The previous code was used to model the continuous variation of the graded properties at each finite element.
The stress intensity factors were evaluated as a function at each increment of crack extension [150],[151], and also for thermal loading conditions by using the displacement-based method, which termed to the generalized displacement correlation[152], and by using a modified displacement extrapolation technique method [153]. K_{IImin} criterion would provide a strong prediction robust for crack growth direction. In addition, the finite element formulation and the simulation of the graded material are done by modeling the continuity of material properties as the continuity of displacement function. The integral of Gauss's points were obtained using the isoparametric transformation technique to confirm the mathematical solution. The model is proposed for further studies as 3D problem FEM computation[154].
A new formulation of a finite element using interpolation function and exponential material properties gradient, this element solves the unformed displacement loading problem perpendicular to the graded region [155]. The finite element analysis of graded cellar structure shows that increasing the density flow increases the effective elastic modulus [156]. The performance of high order elements is better than the conventional homogenous element in the same case when they have the same shape function [157]. The material force method evaluates J-integral in FGM [49]. A numerical model capable to estimate the kinking angle crack in FGM [158]. The boundary element methods are used to model and analyze crack growth[131].

4.11 Crack investigation in FGM by the finite element method

Crack behavior was investigated in orthotropic FGM by a generalized finite element developed to compute SIFs. The finite element formulation is based on the displacement correlation technique and the modified crack closer integral [159]. The numerical results are accurate to the analytical solution results of Erdogan [48].
The virtual crack closer technique by one step was used to compute the energy release rate for kinking cracks [160]. The mentioned technique evaluated kinking crack angle by a function of SIFs under the mixed-mode problem. Where the finite element method and displacement extrapolation technique based on strain energy density theory [161]. The same mentioned technique evaluated SIFs and the energy release rate. In this case, the material properties were modeled by a linear function of temperature distribution which was implanted into the software by setting thermal expansion to zero [162].
The finite element formulation coupled with thermoelasticity theory. SIFs and T stress were evaluated for orthotropic FGM crack problems under static and dynamic thermal loads. The numerical results proved a small influence of thermal graduation on the SIFs and T stress [163]. The FEM analyzed the crack problem by the modified crack closer integral. The energy release rate and SIFs were evaluated in the double cantilever beam test [140].
The FEM was also used for simulating crack behavior under static and dynamic loading. SIFs and the energy release rate evaluated by local flexibility formulation in Timoshenko beam with functionally graded properties. The study proved that the effect of crack depth on the natural frequency, the natural frequency decrease as the crack depth and slenderness are increased [44], for SIFs evaluation around the crack tip in functionally graded /micro-discontinuous interface [164], for crack simulation and SIFs evaluation of the interface crack problem in bi-material FGM coating bonded to the homogenous substrate [165], and for dynamic fracture analysis of the sandwich structure. The experimental data of crack histories

were used [166].
A computational investigation of cracked FGM and SIFs evaluation by different approach like J-integral, modified crack closer, displacement correlation technique, theses approaches coupled to finite element formulation for elastic FGM under mixed-mode [137]. J-integral contour is evaluated in FGM using the material force [49]. The FEM used the node release technique to analyze the transient crack problem in FGM [167].
The virtual crack closure technique was proposed to analyze FGM fracture by using a graded finite element. The computational simulation solved the linear quasi-static thermoelastic problem in the plane strain state by the FEM [43]. The graded quadrilateral element in isoparametric form was used in the weak path test for FGM [168]. Quasi-static crack behavior in gradient material was investigated under mixed loading. In this case, the finite element is coupled with the generalized maximum tangential stress criterion. The numerical results were proved by the experimental digital image correlation technique [169].
The displacement correlation technique analyzed crack in orthotropic FGM coating under thermal loads. The influence of parameter geometry, boundary condition, and nonhomogeneous parameters on SIFs was discussed [170]. The clamped displacement discontinuous technique used a numerical model by FEM to evaluate SIFs for a kinking crack problem in anisotropic FGM [171]. A new finite element with singularity formulation based on the Westergard stress function was presented to analyze the crack problem in isotropic FGM [172]. The graded finite element analyzed the dynamic crack problem by a 2D virtual crack closer technique. The element used the subroutine ONAT and UEL through Abacus software [173].

4.12 Kinking crack

The kinked crack is the crack that propagates in a new direction from the old one (see figure 4-10). The crack growth occurs in a path that provides the maximum energy release rate or the crack propagation direction related to maximum circumferential stress values. The theories were used to predict the kink angle.
Gu and Asaro [174] proposed the small crack kinking model of Cotterell and Rice [175] for FGMs. Cotterell and Rice [175] used the first-order approximation and obtained these coefficients.

$$\begin{aligned} C_{11} &= \frac{1}{4}\left(3\cos\theta+\cos\frac{3\theta}{2}\right) \\ C_{12} &= -\frac{3}{4}\left(\sin\frac{\theta}{2}+\sin\frac{3\theta}{2}\right) \\ C_{21} &= \frac{1}{4}\left(\sin\frac{\theta}{2}+\sin\frac{3\theta}{2}\right) \\ C_{22} &= \frac{1}{4}\left(\cos\theta+\cos\frac{3\theta}{2}\right) \end{aligned} \tag{4.35}$$

The SIFs at the kinked crack tip was expressed as :

$$\begin{aligned} k_I^* &= C_{11}(\theta)k_I + C_{12}(\theta)k_{II} \\ k_{II}^* &= C_{21}(\theta)k_I + C_{22}(\theta)k_{II} \end{aligned} \tag{4.36}$$

where:
k_I^* and k_{II}^*: The SIFs at the kinked crack tip.
K_I and K_{II} : The SIFs at the main crack tip.

θ: The kink angle.

C_{ij} for $(i, j = 1, 2)$: The coefficients depending on θ, for smaller kink angle.

Gu and Asaro [174] used a local homogeneous core near the main crack tip (characterized by the near-tip fields) to model kinking crack for small-kink conditions in the four-points bending fracture test. They employed Cotterell and Rice's [175] expression for kink crack, and they showed the affection of graded material on the kink angle. T. L. Becker et al. [176] used finite element methods to study a finite kinked crack by evaluating the SIFs at the tip of small-kink angle, the SIFs on the kinked angle is linked to the original crack SIFs.

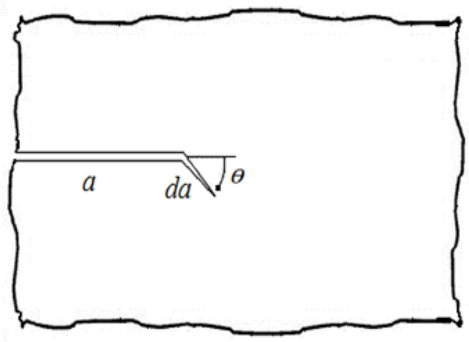

Figure 4.10: kink crack-tip.

A numerical solution for kinked and slightly curved crack in mode 1 proves that crack stability depends on tensile stress [175], the vanish mode 2 , the maximum energy release rate criterion, and disturbed dislocation technique based on the integrated solution were used in case of under combined loading [177]. The using of Irwin-Williams expression test to get the solution form of SIF's under non-symmetric loading [178]. There is little effect on the material gradient in FGM with a crack, but the length and thickness of the surface crack affect the direction of the kinked crack. This crack will propagate in a direction where there is a maximum energy release rate [179]. The crack propagation relates to the competition of the direction force, the energy release rate, the toughness of FGM, and the same energy release rate in bi-material and FGM fracture [180]. Prediction kinking crack in FGM by applicable a maximum tangential stress criterion with setting large length scale was presented [158].

A solution that tasted the crack behavior and toughness in FGM proves that material gradient effect to the kinking crack direction [174]. The theory of complex potentials (complex functions and complex variables) was used to study the effect of the in-plane tensile stress on crack stability. The angle form, the initial angle of crack growth, and tensile stress affect the SIFs at the tip of kinking crack. The results prove that positive tensile stress makes the initial crack angle extended as kinking crack. The negative tensile stress will push the crack to grow straight due to the mode 2 type loading [180]. The crack propagates straight just for a short distance before kinking, and it will be followed by a curved direction [181].

Kinking crack in linear elastic FGM was investigated, the FEM evaluated T stress with the energy release maximum and the vanish mode 2 ($k_{II} = 0$)criterion [176].

The virtual crack closer technique proposed to compute strain energy release in kinking interface crack problem [160], a kinked crack in CU-W graded material under mechanical and thermal loads was invistegated, the graded material with crack analyzed by numerical and proved by experiments [182], the virtual crack closure technique used by the FEM to investigate kinking crack in tri-material under the mixed-mode [183].

4.13 Analytic and numerical solutions for the crack problem in FGMs

Several analytic solutions were proposed for crack problem analysis in FGM, such as the edge crack problem of the graded layer under mode 1. The gradient material effect to stress distribution and SIFs, the solution was generalized for the 3D surface crack problem in FGM plat using the application of the line spring model [124]. The criterion proposed for interface kinking crack in the bi-material crack problem using T stress with the energy condition and maximum tension before failure. The SIFs were assumed as a function of the length to predict kinking crack [184]. A generalized method (refers to the force balance) and isostrain condition were proposed to evaluate SIFs in the crack tip in FGM. The solution coupled by FEM with different crack lengths in distinct regions on FGM, the FEM simulation has the same analytic solution results and proved that SIFs affected by changing the modulus of layer, the SIFs equation evaluate the toughness of FGM [185].
Another solution for analyzing the crack problem in FGM, the Kirchhoff's-classical plat theory obtained by the Galerkin methods, where the equation of motion defining the vibrations in FGM plate with arbitrary center crack oriented, and the crack angle increase by raising the level of frequency parameter [42].
a TSSR (tangential stress concept by Scharmm and Richard) concepts was proposed to predict kinking crack growth under mode 1 in 2D and 3D crack problem in FGM [186]. Ritz approximation, natural frequency response surface method, and frequency contour were obtained using the genetic algorithm optimization technique. The cracked Timoshenko beam with graded properties was studied, the non-destructive vibration and hybrid method were employed to detect a crack in FGM [187].
Timoshenko beam with graded properties was analyzed by wave method. Waves reflection was used to locate the discontinuity. SIFs and energy release rate were evaluated by the equation of motion, the first principle of Hamilton, and local flexibility [44]. The crack analysis in the graded Timoshenko beam was done using a natural surface approach with non-linear free vibration clamped-clamped and clamped-free to get the crack location. The crack depth affects on the natural frequencies [188]. A developed method was proposed to locate the crack location, the situation simulated by the FE model [189].
The investigation of the interface crack problem between FGM coating bonded to a homogenous substrate was studied [190], the energy release rates and SIF's were evaluated under thermal loading. The interface crack problem in bi-material consists of functionally graded and homogenous material was studied[191]. Where the maximum density circumferential and the minimum strain energy density were used to evaluate SIFs. The geometer and non-homogeneous parameters influence on SIFs. The determined optimal crack configuration showed a minimal interface crack failure with minimum values of SIFS at the crack interface .
Fracture toughness and kinking crack in graded material were analyzed by the Weiball statistics under mixed-mode [192]. The weight function, SIFS, and residual stress in graded thermal barrier coating (TBC) were evaluated by the finite element method, the influence of parameter geometer, thermal release rate, and the interface toughness to avoid delimitation [193]. The cracked cylinder-shell with gradient properties subject to thermal loads was studied [194]. The problem is approximated as a graded plate with a crack on the elastic foundation.
An analytical approach was proposed to investigate delamination failure in FGM. The energy release rate and SIFs were evaluated for FGM beam cross-section and behind the crack in strain and stress state [195], the approach used for the 2D crack problem, the influence of the graded material, and crack location on delamination were discussed [196].

4.13.1 Dynamic crack

Many numerical types of research investigated the dynamic crack problem in FGM, the numerical solution based on Fourier transform solved by singular integral equation [197]. The preceding solution is used for FGM coating-substrate system [198]. The numerical solution also solved the problem by using the batto-chebcheve method, in interface crack in FGM under anti-plan [199], in weak/macro-discontinuous interface[200], in bi-FGM weak-discontinuous interface [201], under anti plan shear [202], and by using asymptotic analysis [186]. The numerical solution combined the finite element method [166] with using the virtual crack closure technique [173] and by using a cohesive zone mode [203].
Recent study included a transient dynamic for FGM coating problem [204], for more farther studies in the field [205],[206],[207],[208],[209].

4.13.2 Transient crack

Numerical solution based on Fourier transform solved by the singular integral equation was used to investigate the transient crack problem in FGM [210], for anti plan weak/interfacial discontinuous transient interface [211], for the dynamic transient crack problem [212], and by using a generalized pattern differential equation into Laplace equation and the isochromatic stress under mode 1 and 2 [213],[214].

4.13.3 Fatigue crack

Cyclic fatigue came inspectorate structure failure because the loading repeated with sub-critical values flowed by material degradation and crack propagation, which is difficult to predict in many situations. The fatigue crack problem was studied in graded material due to thermal fatigue as TBC system [215],[216].
The reducing stress result from cyclic heat-cool thermal loading and the graded material influence on the crack path [179],[217],[218]. The reducing stress also influences fracture strength and fatigue resistance in FGM [219]. The problem was solved numerically as elastic-plastic fatigue crack initiation [220], a fatigue life analysis was proposed for different situations using the extended finite element of the Galerkin method (EFGM) to investigate the crack in bi-layered plat under thermo-mechanical [221]. In addition to the EFGM, the extended finite element (XFEM) was used in FGM [222] because the simplest and effectiveness of new element criterion prove that the spatial location of the crack is important for fatigue life analysis in FGM.

4.13.4 Thermal crack

Various analytical and numerical methods have been studied to simulate thermal crack of FGMs. The collinear crack in graded material interface subject to thermal shock was solved using a singular integral equation [223].The Fourier transform was introduced in the edge crack problem [224]. The thermal intensity factors were investigated in FGM [225], for stress relaxation at the vicinity of edge crack [226], under two dimensions thermal loading by using the thermal coefficient expansion [227].
The transient thermal stress of edge crack in the stripe of FGM was solved by a multi-layered model [228] and asymptotic analysis [229].
Recently, the weight function was used for mode 1, the integral equation was used to develop Fredholm integral equation in the Laplace field to compute SIFs. The finite element results present a high accuracy than the different finite element methods [230].

Analytical solutions for the thermoelastic problem and optimization technique are suitable for graded material [231]. Ax symmetric study was proposed for the nonhomogeneous infinite body with a penny shaped crack under thermal loading [232]. The previous study was used for transient thermal stress problems in a nonhomogeneous plat with temperature-dependent on material proprieties [233]. The thermal shock and transient thermal in cracked FGM interface problems were studied respectively in [234],[235].
The finite element method was applied to handle graded materials with two cracks [236] and with edge crack cases [237]. The FEM coupled with the domain interaction integral in plastic elastic behavior of cracked FGM [238], for investigation of the singularity field in the crack tip of cracked FGM under elastic and plastic condition [239], the analytical and the numerical solution were combined to solve thermal shock crack problem [128].
The experimental investigation of edge crack interface in bi-material FGM coating bonded to a homogenous substrate under thermal loading [240].
The recent investigation included the interaction of two crack inclines arbitrarily to nonhomogenous half plan boundary under cyclic heating-cooling thermal solved by integral equation and the maximum circumferential stress criterion [241]. The integral equation and generalized differential quadratic method were used for the thermal crack analysis in orthotropic FGM [242], fatigue crack studied by using XFEM [243], for 3D linear elastic fracture [244]. The 3D curved crack in FGM was analyzed by FEM coupled with an integral equation [245]. Analysis crack in FGM under thermo-viscoelastic mode [215]. The modeling of 2D thermoelasticity crack in graded material was studied by the numerical manifold method [246]. A mathematical model was proposed for the pre-existing crack problem in FGM under thermal loading [247], an effective numerical technique coupled with isogeometric analysis to investigate internal defects in FGM plats[248].

4.14 Experimental studies

The investigation of mixed-mode fracture in FGM using the digital image correlation and T stress criterion. The experiment based poly-based FGM manufacturing by selective ultraviolet irradiation of poly. The maximum energy and the generalized maximum hop stress criterion were used to predict crack in the homogenous material. The criterion also extended for the graded materials with a kinked crack, where the k=0 criterion has satisfying results in the case of finite crack extension in FGM [181]. The experimental test using isochromatic contours was used to analyze the displacement around the crack-tip fields in graded materials. The results prove that the nonhomogeneous parameter affects on the singularity in FGM [249]. Experimental test accurate the TSSR concept depends on stress result from different loading in the different region of contours in 2D and 3D crack problem in FGM [186]. The experimental investigation by the optical interferometer, the high-speed plot growth and the data analysis from crack histories were used [166].

4.15 Conclusion

In the chapter above, crack and notch were defined, and their propagation mode was presented. There are two approaches to solving failure problems local and global approach. A literature review of the crack problem in FGM with different kind of crack was presented. The techniques to investigate the crack-tip field in FGM were presented with considering kinked crack.

Chapter 5

Special mixed finite element for the FGMs

5.1 Introduction

Mixed finite elements are based on the principle of displacements and stresses fields simultaneously. Many formulations developed and aimed to model heterogeneous materials exhibiting cracking. Reissner [250] implemented a mixed formulation and represented the kinematics sizes (displacements) and the static quantities (stresses). This formulation subsequently served as a basis for many other kinds of research. However, Reissner's elements present a high degree of freedom. This disadvantage made computation heavy and considerably longer.
Courtade [251] imployed the mixed formulation of Reissner into rectangular four-node finite element. Aivazadeh et al. [252] formulated the mixed interface elements rectangular from the Reissner element by applying the relocation procedure of degrees of freedom, the removal technique from the behavior law materials, and kept only the sizes displacements. Verchery [253] developed mixed elements from Reissner's formulation. The stresses and displacements appear simultaneously unknown. Habib [254] developed a mixed finite element formulation of interfaces axisymmetric applicable to bonded assemblies of tubes in composite materials. Sarhan-Bajbouj [255] developed a family of mixed elements to study the interfaces in bi-materials. Bouzerd [2] developed a mixed finite element able to represent the coherent and the cracked interface. The new genre basis on the mixed principle of Reissner, and by using of Verchery technique [253] to displace some unknowns static towards the inside or on one side of the element, then use static condensation of unknowns internal to the element, and called it Reissner Modified Quadrilateral element with seven nodes (RMQ-7). Bouchemella et al.[256] extended the use of this element to orthotropic homogeneous materials and bi-material in the coherent or cracked interfaces. Boufelloussa [257] made its extension for the cases of cracked interfaces in anisotropic media.
Bouziane [258] used the mixed finite element RMQ-7 for the crack analysis in anisotropic bi-materials interface. Bouziane et al. [3] formulated the mixed finite element RMQ-7 in the isoparametric form [259]. The mixed finite element RMQ-7 guarantees the continuity of displacement and stress vectors through the interface between two materials in the laminated composite analysis. Boulares [260] used the isoparametric mixed finite element RMQ-7 to study kinking crack in homogenous material. Mouats [261] used RMQ-7 to study materials composites fracture in the mode 2.
Djoudi [262] used RMQ-7 to study interlaminar fracture in multilayered composite materials. Remmach [263] used RMQ-7 to study kinking crack in linear, elastic, and anisotropic homogenous material. Bouziane et al. [264] used mixed finite element RMQ-7 to analyze sandwich beams. Then formulated the interface mixed element to study the interface crack

problem in sandwich material [265].
In this work, an extended use of this element in a bending and crack analysis using functionally graded material (FGM) has been accomplished, where the material properties of the FGM change according to different distribution. The graded material modelled as several homogenous layers every one contained several constant homogenous element. The material property located at the centre of the element.

5.2 Formulation of special mixed finite element

The RMQ-7 is a quadrilateral element that has seven nodes and fourteen degrees of freedom. The three sides of the quadrilateral element are compatible with the classical one. In each corner of the quadrilateral element, there is a displacement node. While the fourth side, in addition to the two displacements nodes (node 1, node 2), there is a median node (node 5), and also two stress intermediate nodes located in the middle between the node 1 and 5, and 5 and 2. Respectively (as nodes 6 and 7). The two nodes compute the components the stress along with the interface. The continuous displacement and stress vectors are taken into consideration at this particular side, which will be replaced along with the interface.
In the cracked structures cases, the median node is related to the crack point. The two static nodes on the two sides make it possible to satisfy the essential requirements like the free edge condition on the cracked lips and the continuity condition into the interface.
The Reissner mixed formulation used the nodal variables of all displacements and stresses to construct the interface mixed element. Anywhere the Reissner element is excess nodal variables.
The formulation imposes a strong continuity at the interface level. The stress σ_{11} appears along with the variables considered in the Reissner functional eliminated in the formulation of the interface element because it doesn't appear along with the interface stresses (keeping just the normal stress σ_{22} and shear stress σ_{12}).
The advantage is to have elements with a few numbers degrees of freedom as possible. In the other hand using the Reissner functional formulates the elements with a very high number of degrees of freedom.

5.2.1 Construction stages of the RMQ-7 element

Bouziane et al. [3] configured the interface RMQ-7 element in the natural plane coordinate (ξ, η) by three steps. The first one is the Reissner mixed finite element formulation (see figure 5-1) by adding a medium displacement node on the bottom side. The result is a mixed finite element with five nodes with 22 degrees of freedom called RMQ-5 (see figure 5-2). The second one is the delocalization of some variables within the RMQ-5, adding unknown nodal static displacement of the corners. The result of the delocalization is a mixed RMQ-11 element with 11 nodes and 22 degrees of freedom (figure 5-3). The third one is a static condensation of the unknown internal variables of RMQ-11. This procedure condensed the elementary matrix, which enabled to obtain the present element only with seven nodes and two degrees of freedom by node (see figure 5-4).

5.2.1.1 Reissner mixed finite element

The mixed finite element of Reissner is a four-node element with five degrees of freedom (all displacements and all the stresses) by node (figure 5-1). This element was formulated by using the Reissner variational principle [250].

By posing for an element:

$$\{\varepsilon^e\} = [L_2]\{u^e\} \quad \text{on} \quad A^e \tag{5.1}$$

$$\{u^e\} = \{\bar{u}^e\} \quad \text{on} \quad L_u \tag{5.2}$$

The Reissner functional is

$$R(\{\sigma\},\{u\}) = \frac{e}{2}\int_A \begin{Bmatrix}\sigma\\ u\end{Bmatrix}^t \begin{bmatrix}-[S] & [L_2]\\ [L_1] & [0]\end{bmatrix}\begin{Bmatrix}\sigma\\ u\end{Bmatrix} dS - e\int_{L_\sigma}\{\bar{T}\}^t\{u\}dL_\sigma - e\int_A\{f\}^t\{u\}dS - e\int_{L_u}\{T\}^t(\{u\}-\{\bar{u}\})dL_u \tag{5.3}$$

The Reissner functional can be written as:

$$R(\{\sigma\},\{u\}) = \frac{e}{2}\int_{A^e} \begin{Bmatrix}\{\sigma\}\\ \{\varepsilon\}\end{Bmatrix}^t \begin{bmatrix}-[S] & [I]\\ [I] & [0]\end{bmatrix}\begin{Bmatrix}\{\sigma\}\\ \{\varepsilon\}\end{Bmatrix} dA^e - e\int_{L_\sigma}\{\bar{T}^e\}^t\{u^e\}dL_\sigma - e\int_A\{f^e\}^t\{u^e\}dA^e \tag{5.4}$$

Where:

$[I]$: The unit matrix.
$[S]$: The matrix of flexibility.
A^e : The elementary area.
e : The thickness of the element (assumed constant).
L_σ : The part of finite element contour where the forces $\{\bar{T}^e\}$ are imposed.
$\{\sigma\}$: The vector of stresses for the finite element.
$\{\varepsilon\}$: The vector of deformations for the finite element.
$\{u\}$: The displacement field.
$\{f^e\}$: The volume forces vector.

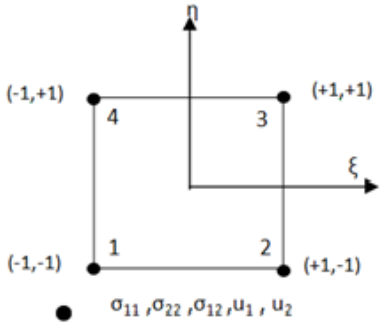

Figure 5.1: The Reissner element.

The stress field at any point is expressed:

$$\{\sigma\} = [M]\{\tau\} \tag{5.5}$$

Where:

$[M]$: The shape functions matrix (linear in ξ, linear in η).

with

$\{\sigma\}^t = \{\sigma_{11}, \sigma_{22}\sigma_{12}\}$
$\{\tau\}^t = \{\sigma^1_{11}, \sigma^1_{22}\sigma^1_{12}, \sigma^2_{11}, \sigma^2_{22}\sigma^2_{12}, \sigma^3_{11}, \sigma^3_{22}\sigma^3_{12}, \sigma^4_{11}, \sigma^4_{22}\sigma^4_{12}\}$

$$[M] = \begin{bmatrix} M_1 & 0 & 0 & M_2 & 0 & 0 & M_3 & 0 & 0 & M_4 & 0 & 0 \\ 0 & M_1 & 0 & 0 & M_2 & 0 & 0 & M_3 & 0 & 0 & M_4 & 0 \\ 0 & 0 & M_1 & 0 & 0 & M_2 & 0 & 0 & M_3 & 0 & 0 & M_4 \end{bmatrix} \tag{5.6}$$

The shape functions are given by G.Dhatt and G. Touzot [266]:

$$\begin{aligned} M_1 &= \frac{1}{4}(1-\xi)(1-\eta) \quad ; \quad M_2 = \frac{1}{4}(1+\xi)(1-\eta) \\ M_3 &= \frac{1}{4}(1+\xi)(1+\eta) \quad ; \quad M_4 = \frac{1}{4}(1-\xi)(1+\eta) \end{aligned} \tag{5.7}$$

The field of displacement is written:

$$\{u\} = [N]\{q\} \tag{5.8}$$

Where:

$[N]$: The shape function matrix (linear in ξ, linear in η) of displacements.
with

$\{u\}^t = \{u_1, u_2\}$
$\{q\}^t = \{u_1^1, u_2^1, u_1^2, u_2^2, u_1^3, u_2^3, u_1^4, u_2^4\}$

$$[M] = \begin{bmatrix} N_1 & 0 & N_2 & 0 & N_3 & 0 & N_4 & 0 \\ 0 & N_1 & 0 & N_2 & 0 & N_3 & 0 & N_4 \end{bmatrix} \tag{5.9}$$

The functions of form are given by:

$$\begin{aligned} N_1 &= \frac{1}{4}(1-\xi)(1-\eta) \quad ; \quad N_2 = \frac{1}{4}(1+\xi)(1-\eta) \\ N_3 &= \frac{1}{4}(1+\xi)(1+\eta) \quad ; \quad N_4 = \frac{1}{4}(1-\xi)(1+\eta) \end{aligned} \tag{5.10}$$

By introducing the strains using the matrix:

$$\{\varepsilon\} = [B]\{q\} \tag{5.11}$$

With:

$[B]$: is the strains-displacements matrix.
$\{\varepsilon\}^t = \{\varepsilon_{11}, \varepsilon_{22}, \varepsilon_{12}\}$

$$[B] = \begin{bmatrix} \frac{\partial N_1}{\partial x} & 0 & \frac{\partial N_2}{\partial x} & 0 & \frac{\partial N_3}{\partial x} & 0 & \frac{\partial N_4}{\partial x} & 0 \\ 0 & \frac{\partial N_1}{\partial y} & 0 & \frac{\partial N_2}{\partial y} & 0 & \frac{\partial N_3}{\partial y} & 0 & \frac{\partial N_4}{\partial y} \\ \frac{\partial N_1}{\partial y} & \frac{\partial N_1}{\partial x} & \frac{\partial N_2}{\partial y} & \frac{\partial N_2}{\partial x} & \frac{\partial N_3}{\partial y} & \frac{\partial N_3}{\partial x} & \frac{\partial N_4}{\partial y} & \frac{\partial N_4}{\partial x} \end{bmatrix} \tag{5.12}$$

As the matrix $[N]$ is a function of the variables (ξ, η), we use the Jacobian $[J]^{-1}$ of the inverse geometric transformation to be able to express the derivatives concerning (x, y) as a function of (ξ, η).
The Jacobian matrix $[J]$ is defined by:

$$[J] = \begin{bmatrix} \frac{\partial x}{\partial \xi} & \frac{\partial y}{\partial \xi} \\ \frac{\partial x}{\partial \eta} & \frac{\partial y}{\partial \eta} \end{bmatrix} \tag{5.13}$$

there is:

$$\begin{cases} x = \sum_{i=1}^{4} N_i x_i \\ y = \sum_{i=1}^{4} N_i y_i \end{cases} \tag{5.14}$$

So the terms of the Jacobian matrix can be calculated by:

$$\begin{aligned} \frac{\partial x}{\partial \xi} = \sum_{i=1}^{4} \frac{\partial N_i}{\partial \xi} x_i \quad ; \quad \frac{\partial x}{\partial \eta} = \sum_{i=1}^{4} \frac{\partial N_i}{\partial \eta} x_i \\ \frac{\partial y}{\partial \xi} = \sum_{i=1}^{4} \frac{\partial N_i}{\partial \xi} y_i \quad ; \quad \frac{\partial y}{\partial \eta} = \sum_{i=1}^{4} \frac{\partial N_i}{\partial \eta} y_i \end{aligned} \tag{5.15}$$

When the Jacobian matrix $[J]$ is not singular, and it written as:

$$\begin{Bmatrix} \frac{\partial N_i}{\partial x} \\ \frac{\partial N_i}{\partial y} \end{Bmatrix} = [J]^{-1} \begin{Bmatrix} \frac{\partial N_i}{\partial \xi} \\ \frac{\partial N_i}{\partial \eta} \end{Bmatrix} \tag{5.16}$$

The nodal estimation of the kinematic and static fields is written as:

$$\begin{Bmatrix} \{\sigma\} \\ \{\varepsilon\} \end{Bmatrix} = \begin{bmatrix} [M] & [0] \\ [0] & [B] \end{bmatrix} \begin{Bmatrix} \{\tau\} \\ \{q\} \end{Bmatrix} \tag{5.17}$$

replacement of the last expression in the Reissner functional (5-4) gives to the discretized form of (R) [250]:

$$R = \frac{1}{2} \begin{Bmatrix} \{\tau\} \\ \{q\} \end{Bmatrix}^t [K_e] \begin{Bmatrix} \{\tau\} \\ \{q\} \end{Bmatrix} - \begin{Bmatrix} \{\tau\} \\ \{q\} \end{Bmatrix}^t \begin{Bmatrix} \{F_\sigma^e\} \\ \{F_u^e\} \end{Bmatrix} \tag{5.18}$$

Where

$[K_e]$: The elementary stiffness-flexibility matrix defined by :

$$[K_e] = \begin{bmatrix} [K_{\sigma\sigma}] & [K_{\sigma u}] \\ [K_{\sigma u}]^t & [0] \end{bmatrix} \tag{5.19}$$

With

$$[K_{\sigma\sigma}] = -e \int_{A^e} [M]^t [S][M] dA^e \tag{5.20}$$

$$[K_{\sigma u}] = e \int_{A^e} [M]^t [B] dA^e \tag{5.21}$$

The vector of equivalent elementary forces is composed of two vectors: the displacements vector $\{F_u^e\}$ and the stresses vector $\{F_\sigma^e\}$. This latter is null in the absence of initial strains. The vectors $\{F_u^e\}$ and $\{F_\sigma^e\}$ are given by:

$$\{F_u^e\} = e \int_{L_\sigma} [N]^t \{\bar{T}^e\} dL_\sigma \tag{5.22}$$

$$\{F_\sigma^e\} = 0 \tag{5.23}$$

Where:

L_σ: The part of the contour where the stresses are imposed.

$[N]$: The shape functions matrix of displacements.

$\{\bar{T}^e\}$:The imposed traction L_σ.

5.2.1.2 Parent element RMQ-5

The RMQ-5 [2] is a mixed element with five nodes and 22 degrees of freedom (see figure 5 .2). This element is made by adding a displacement node to the four nodes of Rissners's element. It has a side (associated with the interface) presenting three nodes. The bottom side of the RMQ-5 related to the interface presented three nodes. The displacement middle node is associated with the bottom of the crack.

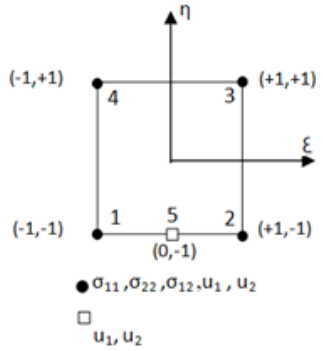

Figure 5.2: The RMQ-5 element.

The number and the position of stress nodes are not changed. The RMQ-5 and Reissner element have the same static behavior. The stress field is written with the same shape functions M_i for (i=1,4).
The field of displacement is written:

$$\{u\} = [N]\{q\} \tag{5.24}$$

With

$$\{q\}^t = \{u_1^1, u_2^1, u_1^2, u_2^2, u_1^3, u_2^3, u_1^4, u_2^4, u_1^5, u_2^5\}$$

$$[N] = \begin{bmatrix} N_1 & 0 & N_2 & 0 & N_3 & 0 & N_4 & 0 & N_5 & 0 \\ 0 & N_1 & 0 & N_2 & 0 & N_3 & 0 & N_4 & 0 & N_5 \end{bmatrix} \tag{5.25}$$

The shape functions are written:

$$\begin{aligned} N_1 &= -\frac{1}{4}(1-\xi)(1-\eta)\xi; \quad N_2 = \frac{1}{4}(1+\xi)(1-\eta)\xi; \quad N_3 = \frac{1}{4}(1+\xi)(1+\eta) \\ N_4 &= \frac{1}{4}(1-\xi)(1+\eta); \qquad N_5 = \frac{1}{2}(1-\xi^2)(1-\eta) \end{aligned} \tag{5.26}$$

The matrix $[B]$ linking the strain to displacements is defined by:

$$[B] = \begin{bmatrix} \frac{\partial N_1}{\partial x} & 0 & \frac{\partial N_2}{\partial x} & 0 & \frac{\partial N_3}{\partial x} & 0 & \frac{\partial N_4}{\partial x} & 0 & \frac{\partial N_5}{\partial x} & 0 \\ 0 & \frac{\partial N_1}{\partial y} & 0 & \frac{\partial N_2}{\partial y} & 0 & \frac{\partial N_3}{\partial y} & 0 & \frac{\partial N_4}{\partial y} & 0 & \frac{\partial N_5}{\partial y} \\ \frac{\partial N_1}{\partial y} & \frac{\partial N_1}{\partial x} & \frac{\partial N_2}{\partial y} & \frac{\partial N_2}{\partial x} & \frac{\partial N_3}{\partial y} & \frac{\partial N_3}{\partial x} & \frac{\partial N_4}{\partial y} & \frac{\partial N_4}{\partial x} & \frac{\partial N_5}{\partial y} & \frac{\partial N_5}{\partial x} \end{bmatrix} \tag{5.27}$$

In the case of element RMQ-5, the terms of the Jacobian matrix are given by:

$$\frac{\partial x}{\partial \xi} = \sum_{i=1}^{5} \frac{\partial N_i}{\partial \xi} x_i \quad ; \quad \frac{\partial x}{\partial \eta} = \sum_{i=1}^{5} \frac{\partial N_i}{\partial \eta} x_i$$
$$\frac{\partial y}{\partial \xi} = \sum_{i=1}^{5} \frac{\partial N_i}{\partial \xi} y_i \quad ; \quad \frac{\partial y}{\partial \eta} = \sum_{i=1}^{5} \frac{\partial N_i}{\partial \eta} y_i \tag{5.28}$$

The kinematic and static fields are expressed by:

$$\begin{Bmatrix} \{\sigma\} \\ \{\varepsilon\} \end{Bmatrix} = \begin{bmatrix} [M] & [0] \\ [0] & [B] \end{bmatrix} \begin{Bmatrix} \{\tau\} \\ \{q\} \end{Bmatrix} \tag{5.29}$$

The elementary stiffness-flexibility matrix is calculated using the formulas (5 – 19), (5 – 20), and (5 – 21).

5.2.1.3 Construction of the RMQ-11 element

The RMQ-11 element is an element with 11-node and 22-degree-of-freedom (see figure 5-3). The relocation technique [253] avoids excessive continuity at the interface. This latter is used to obtain the RMQ-11 from the RMQ-5 parent element by relocating certain variables inside the RMQ-5 and moving static nodal unknowns from the ends to the side itself.

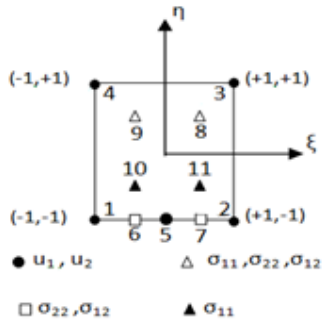

Figure 5.3: The RMQ-11 element.

The number and the position of stress nodes are not changed. The elements RMQ-5 and RMQ-11 have similar kinematic behavior. The displacement field is expressed with the same shape functions.
The generalized approximation of the stress field in the element RMQ-11 according to the nodal variables $\{\tau\}$ is:

$$\sigma(\xi,\eta) = \{P(\xi,\eta)\}[P_n]^{-1}\{\tau\} = [M]\{\tau\} \tag{5.30}$$

Where:
$\{P(\xi,\eta)\} = \{1\ \xi\ \eta\ \xi\eta\}$: The polynomial basis of the element.
$[P_n]$: The nodal matrix.
The stress σ_{11} in the element is expressed by:

$$\sigma_{11}(\xi,\eta) = \{P(\xi,\eta)\}[P_{n11}]^{-1} \begin{Bmatrix} \sigma_{11}^{8} \\ \sigma_{11}^{9} \\ \sigma_{11}^{10} \\ \sigma_{11}^{11} \end{Bmatrix} = [M_{11}] \begin{Bmatrix} \sigma_{11}^{8} \\ \sigma_{11}^{9} \\ \sigma_{11}^{10} \\ \sigma_{11}^{11} \end{Bmatrix} \tag{5.31}$$

With

$$[P_{n11}] = \begin{bmatrix} 1 & \xi_8 & \eta_8 & \xi_8\eta_8 \\ 1 & \xi_9 & \eta_9 & \xi_9\eta_9 \\ 1 & \xi_{10} & \eta_{10} & \xi_{10}\eta_{10} \\ 1 & \xi_{11} & \eta_{11} & \xi_{11}\eta_{11} \end{bmatrix} \tag{5.32}$$

And

$$[P_{n11}] = \begin{bmatrix} 1 & +0,5 & +0,5 & +0,25 \\ 1 & -0,5 & +0,5 & -0,25 \\ 1 & -0,5 & -0,5 & +0,25 \\ 1 & +0,5 & -0,5 & -0,25 \end{bmatrix}$$

And

$$[M_{11}] = \{1\ \xi\ \eta\ \xi\eta\}[P_{n11}]^{-1} \tag{5.33}$$

The shape functions are given by:

$$\begin{aligned} M_{11}^8 &= \frac{1}{4}(1+2\xi)(1+2\eta) \quad ; \quad M_{11}^9 = \frac{1}{4}(1-2\xi)(1+2\eta) \\ M_{11}^{10} &= \frac{1}{4}(1-2\xi)(1-2\eta) \quad ; \quad M_{11}^{11} = \frac{1}{4}(1+2\xi)(1-2\eta) \end{aligned} \tag{5.34}$$

The stresses σ_{22} and σ_{12} reevaluated by:

$$\sigma_{i2}(\xi,\eta) = \{P(\xi,\eta)\}[P_{ni2}]^{-1} \begin{Bmatrix} \sigma_{i2}^6 \\ \sigma_{i2}^7 \\ \sigma_{i2}^8 \\ \sigma_{i2}^9 \end{Bmatrix} = [M_{i2}] \begin{Bmatrix} \sigma_{i2}^6 \\ \sigma_{i2}^7 \\ \sigma_{i2}^8 \\ \sigma_{i2}^9 \end{Bmatrix} \quad \text{for}(i=1,2). \tag{5.35}$$

With

$$[P_{n11}] = \begin{bmatrix} 1 & \xi_6 & \eta_6 & \xi_6\eta_6 \\ 1 & \xi_7 & \eta_7 & \xi_7\eta_7 \\ 1 & \xi_8 & \eta_8 & \xi_8\eta_8 \\ 1 & \xi_9 & \eta_9 & \xi_9\eta_9 \end{bmatrix} \tag{5.36}$$

And

$$[P_{ni2}] = \begin{bmatrix} 1 & -0,5 & -1 & +0,5 \\ 1 & +0,5 & -1 & -0,5 \\ 1 & +0,5 & +0,5 & +0,25 \\ 1 & -0,5 & +0,5 & -0,25 \end{bmatrix}$$

And

$$[M_{i2}] = \{1\ \xi\ \eta\ \xi\eta\}[P_{ni2}]^{-1} \quad \text{for}(i=1,2) \tag{5.37}$$

The shape functions are given by:

$$\begin{aligned} M_{i2}^6 &= \frac{1}{6}(1-2\xi)(1-2\eta) \quad ; \quad M_{i2}^7 = \frac{1}{6}(1+2\xi)(1-2\eta) \\ M_{i2}^8 &= \frac{1}{3}(1+2\xi)(1+\eta) \quad ; \quad M_{i2}^9 = \frac{1}{3}(1-2\xi)(1+\eta) \end{aligned} \tag{5.38}$$

The stress field is given by:

$$\sigma(\xi,\eta) = \begin{Bmatrix} \sigma_{11} \\ \sigma_{22} \\ \sigma_{12} \end{Bmatrix} = [M]\{\tau\} \tag{5.39}$$

With

$$[M] = \begin{bmatrix} \{M_{11}\} & \{0\} & \{0\}\} \\ \{0\} & \{M_{22}\} & \{0\} \\ \{0\} & \{0\} & \{M_{12}\} \end{bmatrix}$$

And

$$\{\tau\}^t = \{\sigma_{11}^8, \sigma_{11}^9, \sigma_{11}^{10}, \sigma_{11}^{11}, \sigma_{22}^6, \sigma_{22}^7, \sigma_{22}^8, \sigma_{22}^9, \sigma_{12}^6, \sigma_{12}^7, \sigma_{12}^8, \sigma_{12}^9\} \tag{5.40}$$

The elementary stiffness-flexibility matrix is given by :

$$[K_e] = \begin{bmatrix} [K_{\sigma\sigma}] & [K_{\sigma u}] \\ [K_{\sigma u}]^t & [0] \end{bmatrix} \tag{5.41}$$

And

$$[K_{\sigma\sigma}] = -e \int_{A^e} [M]^t [S][M] dA^e \tag{5.42}$$

$$[K_{\sigma u}] = e \int_{A^e} [M]^t [B] dA^e \tag{5.43}$$

The calculation of the elementary matrix is carried out by numerical integration according to the method of Gauss. The passage of the integration of the natural element to that of reference involves the Jacobian geometrical transformation.
In the reference configuration, the integration is written:

$$[K^e] = -e \int_{-1}^{+1} d\xi \int_{-1}^{+1} [k^e(\xi, \eta)] detJ(\xi, \eta) d\eta \tag{5.44}$$

4 point integration formula (2 points in each direction ($p = 2$)) were used in the calculation of the elementary matrix .
There is :

$$[K^e] = \sum_{i=1}^{2} \sum_{j=1}^{2} w_i w_j [k^e(\xi_i, \eta_j)] detJ(\xi_i, \eta_j) \tag{5.45}$$

Where:

ξ_i, η_j: The coordinates of the integration points.
w_i, w_j: The coefficients of weight.

5.2.1.4 Construction of the RMQ-7 element

The static condensation was used to obtain element RMQ-7 from element RMQ-11 by eliminating the internal variables of RMQ-11. (see figure 5. 4)

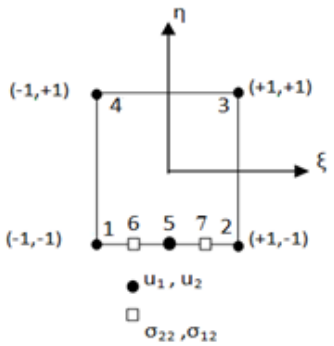

Figure 5.4: The RMQ-7 element.

The internal nodes of the RMQ-11 element do not participate in the matrix assembly and complicate the data setting operation. The size of the half-bandwidth increased during assembly, which will increase the computing time.
The condensation of internal variables to the contour is related to the reduction concept of the system size of equations (the elimination of some number of degrees of freedom). In structural analysis, this type of procedure is called analysis by substructures [267].
The discretized form of the Reissner functional:

$$R = \frac{1}{2}\sum_{e=1}^{N}\begin{Bmatrix}\{\tau^e\}\\ \{q^e\}\end{Bmatrix}^t [K_e]\begin{Bmatrix}\{\tau^e\}\\ \{q^e\}\end{Bmatrix} - \sum_{e=1}^{N}\begin{Bmatrix}\{\tau^e\}\\ \{q^e\}\end{Bmatrix}^t \begin{Bmatrix}\{0\}\\ \{F_u^e\}\end{Bmatrix} \tag{5.46}$$

The operation of condensation calculation is done by breaking up the stress degrees of freedom at the elementary level into two groups:

$\{\tau_c\}$: stresses on the contours of the element.

$\{\tau_i\}$: stresses inside of the finite element.

The decomposition of the elementary matrix $[K_e]$ relative to the groups of degrees of freedom $\{q\}$,τ_c and τ_i is written:

$$[K_e] = \begin{bmatrix}[K_{\sigma\sigma}]_i & [K_{\sigma\sigma}]_{ci} & [K_{\sigma u}]_i\\ [K_{\sigma\sigma}]_{ci}^t & [K_{\sigma\sigma}]_c & [K_{\sigma u}]_c\\ [K_{\sigma u}]_i^t & [K_{\sigma u}]_c^t & [0]\end{bmatrix} \tag{5.47}$$

The stress variables $\{\tau_i\}$ are not assembled. Consequently, the relating equations only involve the degrees of freedom $\{q\}$ $\{\tau_c\}$.
We can then find a relation between these different types of degree of freedom by translating the condition of stationary of (R) concerning $\{\tau_i\}$:

$$\frac{\delta R}{\delta \tau_i} = 0 \tag{5.48}$$

which gives as a relation:

$$[K_{\sigma\sigma}]_i\{\tau_i\} + [K_{\sigma\sigma}]_{ci}\{\tau_c\} + [K_{\sigma u}]_i\{q\} = 0 \tag{5.49}$$

And

$$\{\tau_i\} = -[K_{\sigma\sigma}]_i^{-1}[K_{\sigma\sigma}]_{ci}\{\tau_c\} - [K_{\sigma\sigma}]_i^{-1}[K_{\sigma u}]_i\{q\} \tag{5.50}$$

The matrix $[K_{\sigma\sigma}]_i$ is always invertible because it is a diagonal sub-block of a negative definite symmetric matrix.
From the relation $(5-50)$, the transformation matrix of the degree of freedom $[\Gamma]$ is defined. This latter defined the reduced stiffness matrix relating to the variables $\{q\}\{\tau_c\}$.
there is

$$\begin{Bmatrix}\{\tau_i\}\\ \{\tau_c\}\\ \{q\}\end{Bmatrix} = \Gamma\begin{Bmatrix}\{\tau_c\}\\ \{q\}\end{Bmatrix} \tag{5.51}$$

With

$$[\Gamma] = \begin{bmatrix}[-K_{\sigma\sigma}]_i^{-1}[K_{\sigma\sigma}]_{ci} & -K_{\sigma\sigma}]_i^{-1}[K_{\sigma u}]_i\\ [I] & [0]\\ [0] & [I]\end{bmatrix} \tag{5.52}$$

Where:

$[I]$: The unit matrix.
By substituting the relation (5-52) in the R functional (5-46), to obtain the reduced R functional R^* depending only on the contour variables $\{q\}$ and $\{\tau_c\}$:

$$R^* = \frac{1}{2}\sum_{e=1}^{N}\begin{Bmatrix}\{\tau_c^e\}\\ \{q^e\}\end{Bmatrix}^t [K_e]^* \begin{Bmatrix}\{\tau_c^e\}\\ \{q^e\}\end{Bmatrix} - \sum_{e=1}^{N}\begin{Bmatrix}\{\tau_c^e\}\\ \{q^e\}\end{Bmatrix}^t \begin{Bmatrix}\{0\}\\ \{F_u^e\}\end{Bmatrix} \tag{5.53}$$

Where the reduced elementary matrix defined by:

$$[K_e]^* = [\Gamma]^t [K_e][\Gamma] \tag{5.54}$$

The matrix $[K_e]^*$ is written:

$$[K_e]^* = \begin{bmatrix}[K_{\sigma\sigma}]^* & [K_{\sigma u}]^*\\ [K_{u\sigma}]^* & [K_{uu}]^*\end{bmatrix} \tag{5.55}$$

With

$$[K_{\sigma\sigma}]^* = [K_{\sigma\sigma}]_c - [K_{\sigma\sigma}]_{ci}[K_{\sigma\sigma}]_i^{-1}[K_{\sigma\sigma}]_{ci}^t \tag{5.56}$$

$$[K_{\sigma u}]^* = [K_{\sigma u}]_c - [K_{\sigma u}]_i[K_{\sigma u}]_i^{-1}[K_{\sigma u}]_i^t \tag{5.57}$$

$$[K_{u\sigma}]^* = [K_{\sigma u}]_i^{*t} \tag{5.58}$$

$$[K_{uu}]^* = -[K_{\sigma u}]_i[K_{\sigma\sigma}]_i^{-1}[K_{\sigma u}]_i^t \tag{5.59}$$

The reduced stiffness matrix has a positive semi-definite block $[K_{uu}]^*$, unlike the unreduced form where this block is always zero. The condensation of the internal variables is used to reduce the time of computation during an analysis.

The practical construction does not modify the vector of the second member. The construction simplicity came through the assumption concerning the static nodes without loads. The static condensation technique allows us to construct the RMQ-7 element owning only seven nodes with 2 degrees of freedom per node (nodes 6 and 7 are in pure stress and the rest of the nodes are in pure displacement).

5.3 Formulation of special mixed finite element for FGMs

FGMs are not like previously known materials. Modeling the change of properties in these materials constituted a problem for researchers. The researchers model it in two ways, either by using homogenous finite elements or using graded finite elements.
The conventional finite element formulation interpolates displacements and coordinates from the nodal element values. Likewise, material properties can also be interpolated from the element nodal values using shape functions. The general approach interpolates material properties at each Gaussian integration point from the nodal material properties of this element using isoparametric formulation. The shape functions are the same for spatial coordinates and displacements.
The graded element computes different properties in each node of the element. Li et al. [268] simulated the variations of the material properties by using an isoparametric finite element formulation. Santare and Lambros [155] used graded elements to analyze FGM plate under traction loading perpendicular to the graded material direction. The numerical result proves the outperformance of the graded element from the conventional one. Kim and Paulino [157] used isoparametric graded elements to analyze orthotropic and isotropic plates. The plate has infinite length and finite width subject to fixed grip, tension, and bending conditions. The linear $Q4$ and quadratic $Q8$ quadrilateral elements are more performance than the classical elements and have given a good argument with analytical solutions.

Paulino and Kim [168] used graded finite elements to analyze the consistency and stability of FGM by weak patch test and using graded quadrature elements $Q4$, $Q8$, and $Q9$ for axisymmetric problems. The study discussed the effect of these elements on the analysis.
In this section, the necessary modification into RMQ-7 to handle isotropic FGMs is presented.

The displacement component of the element is estimated by:

$$\{u\} = [N]\{q\} \tag{5.60}$$

Where $[N]$ is the interpolation functions matrix of stresses and $\{q\}$ is the nodal displacements vector.
The shape functions N_i used to estimated u_1, u_2 [3] are given as follows:

$$\begin{aligned} &N_1 = -\frac{1}{4}(1-\xi)(1-\eta)\xi; \quad N_2 = \frac{1}{4}(1+\xi)(1-\eta)\xi; \quad N_3 = \frac{1}{4}(1+\xi)(1+\eta) \\ &N_4 = \frac{1}{4}(1-\xi)(1+\eta); \qquad N_5 = \frac{1}{2}(1-\xi^2)(1-\eta) \end{aligned} \tag{5.61}$$

The stress component of the element is estimated by:

$$\{\sigma\} = [M]\{\tau\} \tag{5.62}$$

Where $[M]$ is the matrix of interpolation functions for stresses and $\{\tau\}$ is the nodal stresses vector.

For the RMQ-7 element, the shape functions M_{i2}, used to evaluate σ_{12} and σ_{22} [3] for nodes 6, 7 are given by:

$$\begin{aligned} M_{i2}^6 &= \frac{1}{6}(1-2\xi)(1-2\eta) \\ M_{i2}^7 &= \frac{1}{6}(1+2\xi)(1-2\eta) \qquad \text{for}(i=1,2) \end{aligned} \tag{5.63}$$

The nodal displacement and stress fields were approximated by the expression:

$$\begin{Bmatrix} \{\sigma\} \\ \{\varepsilon\} \end{Bmatrix} = \begin{bmatrix} [M] & [0] \\ [0] & [B] \end{bmatrix} \begin{Bmatrix} \{\tau\} \\ \{q\} \end{Bmatrix} \tag{5.64}$$

Where $[B]$ strain-displacement transformation matrix.
The element matrix $[K_e]$ is given by:

$$[K_e] = \begin{bmatrix} [K_{\sigma\sigma}] & [K_{\sigma u}] \\ [K_{\sigma u}]^t & [0] \end{bmatrix} \tag{5.65}$$

The sub-matrix $[K_{\sigma\sigma}]$ is approximated by:

$$[K_{\sigma\sigma}] = -t \int_{A^e} [M]^T [S(z)][M] dA^e \tag{5.66}$$

and the sub-matrix $[K_{\sigma u}]$ is given by:

$$[K_{\sigma u}] = t \int_{A^e} [M]^T [B] \partial dA^e \tag{5.67}$$

Where $[S(z)]$ is the compliance matrix, A^e is the element area, t is the thickness, and T indicates the matrix transpose.
Taking into consideration a FGM their properties (Poisson's ratio ν and Young's modulus E) change in the thickness direction (z-axis direction), the compliance matrix $[S(z)]$ for isotropic material with functionally graded properties is written as follows:

$$[S(z)] = \begin{bmatrix} \frac{1}{E(z)} & \frac{-\nu(z)}{E(z)} & 0 \\ \frac{-\nu(z)}{E(z)} & \frac{1}{E(z)} & 0 \\ 0 & 0 & \frac{1}{\mu(z)} \end{bmatrix} \tag{5.68}$$

5.3.1 Modeling of FGMs

A FGM beam made from different phases of material, ceramic, and metal is considered for example (see figure 5-5).

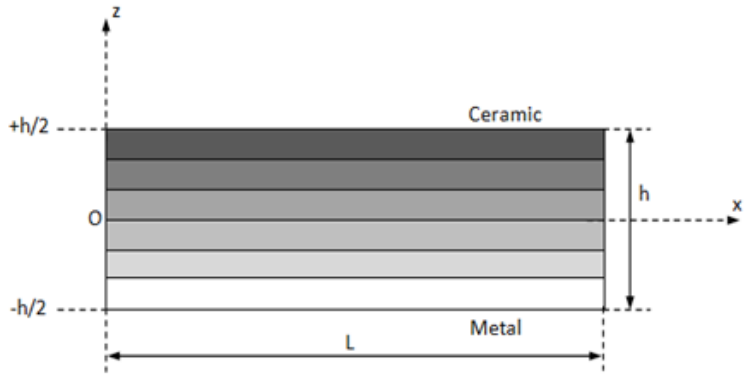

Figure 5.5: The geometry of multi-layered FGM beams.

In this study, the material with functionally graded properties is modeled as numerous homogeneous layers. Each layer has constant material properties. The homogeneous layer is composed of multiple homogeneous elements (see figure 5-6). The elastic properties of elements are related to the property located at the centroid element.

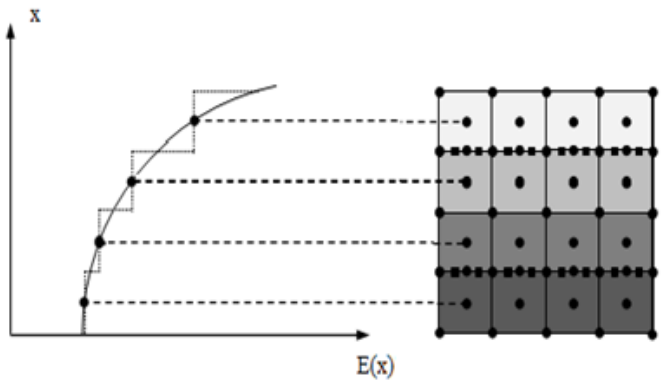

Figure 5.6: Modeling functionally graded properties.

In this work, the material properties of the FGM change according to different distribution. This section is devoted to the presentation of the power law, the exponential and linear variation laws.

5.3.1.1 Power-law

The changing of the mechanical properties in composite materials by the relative amounts of the constituents and their self-properties are approximated by a mathematical relationship, as shown below:

$$\begin{aligned} E(z) &= (E_m - E_c)\left(\frac{z}{h}+\frac{1}{2}\right)^k + E_c \\ \nu(z) &= (\nu_m - \nu_c)\left(\frac{z}{h}+\frac{1}{2}\right)^k + \nu_c \end{aligned} \tag{5.69}$$

Where :

k: The power-law index (positive variable parameter).

The subscripts m and c indicated the metal and ceramic constituents of the FGM.

5.3.1.2 Exponential law

This model is applied in order to model the continuous changing in FGM in various researches especially in fracture mechanics and it is expressed by this relation:

$$\begin{aligned} E(x) &= E^0 e^{\beta_E x} \\ \nu(x) &= \nu^0 e^{\beta_\nu x} \end{aligned} \tag{5.70}$$

where $E^0 = E(x=0)$ and $\nu^0 = \nu(0)$, and the coefficients β_E, β_ν are the nonhomogeneity parameters given by:

$$\begin{aligned} \beta_E &= \frac{1}{W} log\left[\frac{E(W)}{E(0)}\right] \\ \beta_\nu &= \frac{1}{W} log\left[\frac{\nu(W)}{\nu(0)}\right] \end{aligned} \tag{5.71}$$

where W is the width of the FGM and $E(W) = E(x = W)$.

5.3.1.3 Linear law

The linear variation of the material properties of an FGM plate is expressed by:

$$\begin{aligned} E(x) &= E^0 + \gamma_E x \\ \nu(x) &= \nu^0 + \gamma_\nu x \end{aligned} \tag{5.72}$$

where $E^0 = E(x=0)$ and $\nu^0 = \nu(0)$.
The nonhomogeneity parameters γ_E, γ_ν are characterized by:

$$\begin{aligned} \gamma_E &= \frac{E(W) - E(0)}{W} \\ \gamma_\nu &= \frac{\nu(W) - \nu(0)}{W} \end{aligned} \tag{5.73}$$

5.4 Evaluation of the energy release rate

The virtual extension method [269] [270] coupled with element RMQ-7 is used to calculate the rate of energy release G, in the case of a collinear crack extension [2]. Bouzerd [271] showed that a single discretization is sufficient to calculate the energy release rate . Kinking crack is analyzed in homogenous materials by one-step finite element analysis [272] (see figure 5-7-b). Bouziane et al. [273] formulate it to model kinking crack in homogenous and bi-materials. Bouziane et al. [274] used it to compute the energy release rate in dissimilar isotropic materials crack. The interface crack in orthotropic bi-materials was studied by the previous computation [275].
Recently, Mohamed Ben Ali et al. [276] use $2D$ mixed finite element with virtual crack extension technique to evaluate strain energy release rate of interfacial crack in sandwich beams delamination. Derouiche et al. [277] implemented virtual crack closure-integral technique and stiffness derivative procedure to a mixed finite element, to evaluate the energy release rate of cracked anisotropic materials.
The kinking crack was represented by considering an extension (Δa) of the first crack according to the direction to forming an angle θ with the initial direction (a) (see figure 5-7-a and 5-7-b). The situation can be represented by an oblique segment arising at the medium node of the upper crack tip element and passing through the new position of the crack tip after extension as shown in (see figure 5-7-c).
This approximation is acceptable as (Δa) is small. Theoretically, the Δa must be chosen as small as possible to represent numerically [260].
This geometric approximation requires a rearrangement of the mesh around the crack tip dealing with only four elements, the two elements containing the crack tip and the two elements linked to them in the crack direction. While the rest of the mesh is unchanged (see figure 5-7-c).
Bouzerd [2] evaluated the energy release rate of G from the analysis of the ($a+\Delta a$) configuration with inclination (kinking). In this analysis, the configuration (a) is computed implicitly in the first processing by canceling (a) and storing the corresponding elementary matrices of the respective elements.

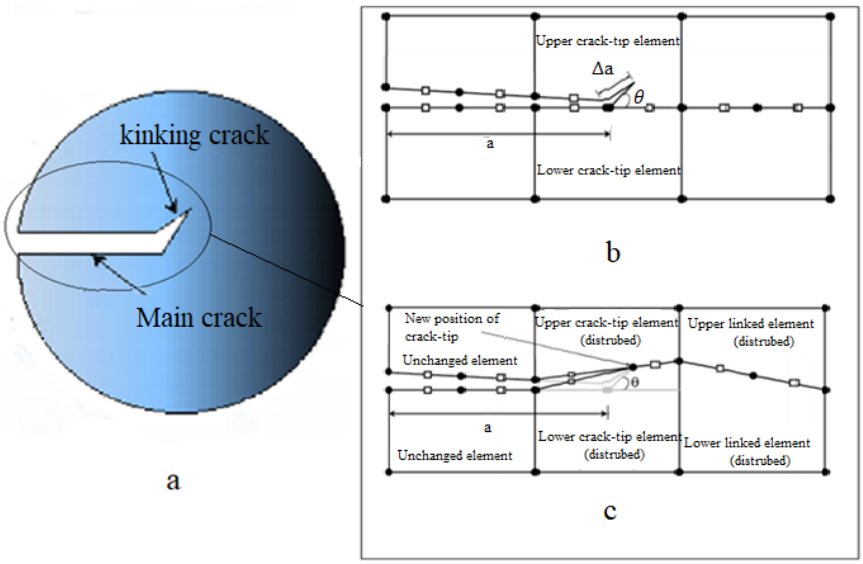

Figure 5.7: Infinitesimal extension of kinking crack [272].

The solutions $u(a)$ and $u(a+\Delta a)$ were obtained by the assumptions of the linear elastic behavior in small displacements and the crack length (a) and crack length ($a+\Delta a$) is closer,

as the disturbance Δa is smaller than dimensions of the element of crack. Therefore the approximation is written:

$$u(a) \backsimeq u(a + \Delta a) \tag{5.74}$$

The energy release rate is calculated by considering a constant applied loading during the enlarging of Δa, as follows:

$$G = -\frac{W_{(\varepsilon)}}{\Delta a} = \frac{W_{(\varepsilon)}(a) - W_{(\varepsilon)}(a + \Delta)}{\Delta a} \tag{5.75}$$

Where:

$W_{(\varepsilon)}(a)$ is the strain energy of cracked material in the configurations (a).

$W_{(\varepsilon)}(a + \Delta a)$ is the strain energy of cracked material in the configurations $(a + \Delta a)$.

In this discretized the strain energy is written:

$$W(\varepsilon) = \frac{1}{2} \sum_{i=1}^{n_e} \{u\}_i^t [K]_i \{u\}_i \tag{5.76}$$

Where:

n_e : The total number of elements in the discretized structure.

$[K]_i$: The elementary matrix of the element.

$\{u\}_i$: The column vector containing the nodal values of element i, and the exponent t indicates the transposed vector.

By substituting (5-76) into (5-75) and taking into account (5-74), the expression of the energy release rate G is given by the relation :

$$G = -\frac{1}{2\Delta a} \sum_{f=1}^{n_f} \{u(a + \Delta a)\}_f^t \Big[[K(a + \Delta a)]_f - [K(a)]_f \Big] \{u(a + \Delta a)\}_f \tag{5.77}$$

Where:

n_f: The number of elements concerned by the disturbance Δa due to the inclined extension of the crack.

5.5 Conclusion

In the above chapter the formulation steps of mixed finite element with seven nodes based on the Reissner formulation is presented. In addition, the reformulation of this element to the natural coordinate is presented. The special mixed finite element was adapted with necessary modification to handle with isotropic FGMs with different material distribution.

Chapter 6

Numerical examples

6.1 Introduction

The interest of this chapter is to present the numerical results to validate the proposed model and verify the accuracy of this special mixed finite element in the analysis of isotropic functionally graded materials (FGMs). In this study, a mixed finite element was developed to analyze materials that have functionally graded properties. The construction of the element has been employing an isoparametric formulation in the natural plane coordinate (ξ, η).
Firstly the mixed finite element has been extended for bending analysis of beams which has functionally graded properties. Two numerical examples are treated cantilever and simply supported isotropic beams with functionally graded properties under uniform distributed loads. The parameters of beams like Poisson's ratio and Young's modulus are changing through the thickness direction as a power-law distribution. The third example treated a cantilever isotropic functionally graded beam, Where the material properties are changing quadratically through the thickness.
Secondly, the special mixed finite element has been prolonged to analyze kinking crack in FGMs. Two numerical examples are treated. Quasi-static crack propagation simulation in mode1 and the mixed-mode is performed for the homogenous and functionally graded plate under uniform axial tension.
The results presented by the present mixed finite element are satisfied after the comparison with numerical, analytical solutions, and experimental results published in the literature.

6.2 Bending of functionally graded beam

A beam with functionally graded properties was analyzed using the proposed mixed finite element. In this work, two examples are treated: cantilever beam and simply supported beam with functionally graded properties under static load as shown in figure 6-1 and figure 6-4 respectively. The graded beams are composed of ceramic and metal, the material properties vary through the thickness as a power-law distribution given by the equation:

$$\begin{aligned} E(z) &= (E_m - E_c)\left(\frac{z}{h} + \frac{1}{2}\right)^k + E_c \\ \nu(z) &= (\nu_m - \nu_c)\left(\frac{z}{h} + \frac{1}{2}\right)^k + \nu_c \end{aligned} \tag{6.1}$$

Where:

k: The power-law index (positive variable parameter).
The subscripts m and c indicated the metal and ceramic constituents of the FGM.

The two graded beams are composed of aluminium ($E_m = 70GPa$, $\nu_m = 0,3$) and zirconia ($E_c = 200GPa$, $\nu_c = 0,3$). The width of the graded beam $b = 0,1m$. The thickness of the graded beam $h = 0,1m$. The length of the beam $L = 0.4m$ where the load applied on the top beam has the value is $q = 5000N/m^2$.
The used mesh contained 10 layers. Figures 6-1 and 6-4 illustrate the boundary conditions. The present element presents results which compared to those presented by numerical simulation based on Timoshenko beam theory (TBT) [75], Classical beam theory (CBT) [75], Timoshenko beam theory (TBT) [278], and the computational results found by Alexraja et al. [279], this latter study used also 10 layers for the two examples in the ANSYS code.

6.2.1 Graded cantilever beam under uniform static load

Consider a cantilever beam with functionally graded properties as shown in figure 6-1.

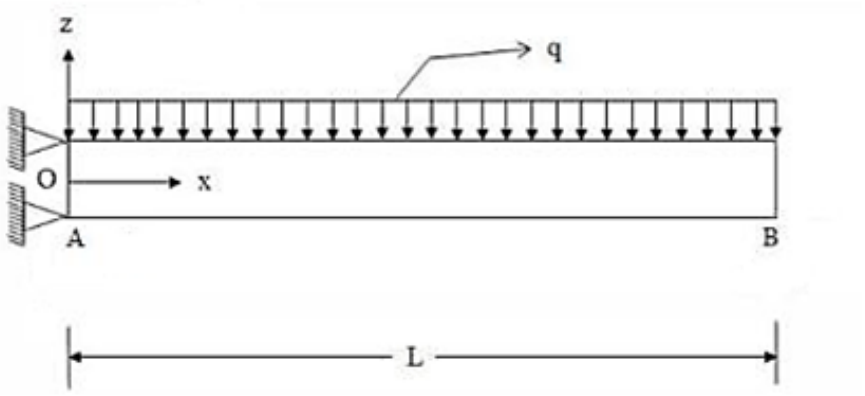

Figure 6.1: FGM cantilever beam.

In the first analysis, the graded cantilever beam is considered with one fixed end. The upper side of the graded beam (zirconia side) is loaded with a uniform distributed load. The effect of the power-law index on the bending behavior of FGM is presented in this numerical example.
The case of the graded cantilever beam, with different power-law index k, is modeled and analyzed. There is a good correlation between the numerical and analytical values (see table 6-1) for the situation of homogeneous materials pure Aluminium $k = 0$ (full metal) and pure Zirconia and $k = 100$ (full-ceramic) and the other values of k.
The non dimensional displacement is written as:

$$\overline{w} = 100\frac{E_m h^3}{qL^4}w \tag{6.2}$$

Where:
w: The maximum displacement.
$\overline{w}$: The non dimensional displacement.

Power-law index	Non Dimensional Deflection [279]	Non Dimensional Deflection Present element
$k = 0$ (full metal)	1.05110	1.05110
$k = 0.2$	0.79562	0.71168
$k = 0.5$	0.66788	0.65693
$k = 1$	0.58759	0.59854
$k = 2$	0.52190	0.54745
$k = 5$	0.45620	0.49270
$k = 100$ (full ceramic)	0.36861	0.36861

Table 6.1: Maximum non dimensional deflections for FGM cantilever beam.

Table 6-1 summarized the maximum nondimensional displacements for different values of the power-law index k. Through the comparison of the values obtained by the present mixed finite element and those published by Alexraj et al. [279] using the ANSYS code. There is practically a similar behavior of the graded beam under the applied load for the different values of k. For $k = 0$ there 1.05110 was obtained by ANSYS code and 1.05110 using the present mixed finite element. While for $k = 100$ the vertical non-dimensional displacements 0.36861 for ANSYS code and 0.36861 using the present mixed finite element. There is a good agreement between the results obtained. It is noted that when the power-law index increases, the maximum nondimensional deflection decreased.

The results of the variation of the vertical nondimensional displacements along the cantilever beam with functionally graded properties for different values of the power-law index presented by the present mixed finite element and by Alexraj et al. [279] are dressed in figure 6-2.

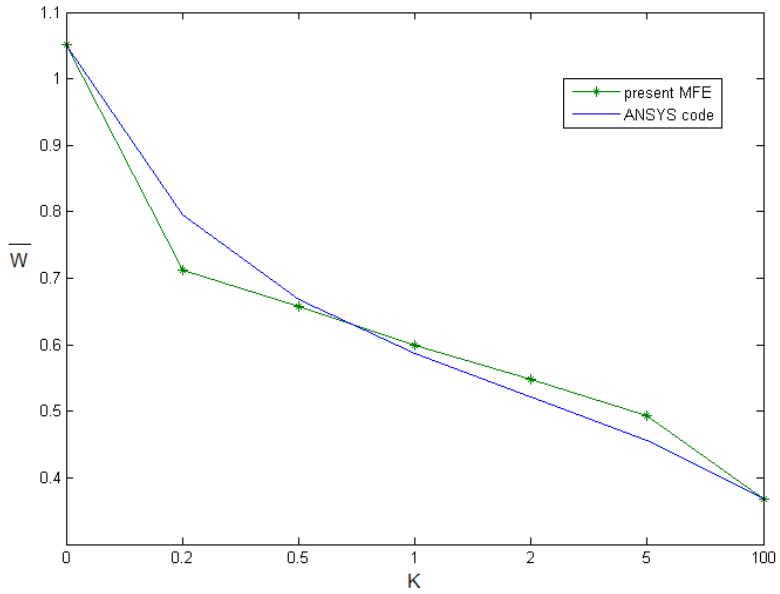

Figure 6.2: Non dimensional displacement of cantilever beam.

The comparison of the displacement along the cantilever beam between the present mixed finite element and the ANSYS code [279] is dressed in figure 6-3. An excellent agreement can be observed. The displacements given using the present mixed element models are dressed in figure 6-4. The results confirmed a similar behavior of the graded beam for many

values of the power index. This latter describes the variation of the material properties of this graded beam.

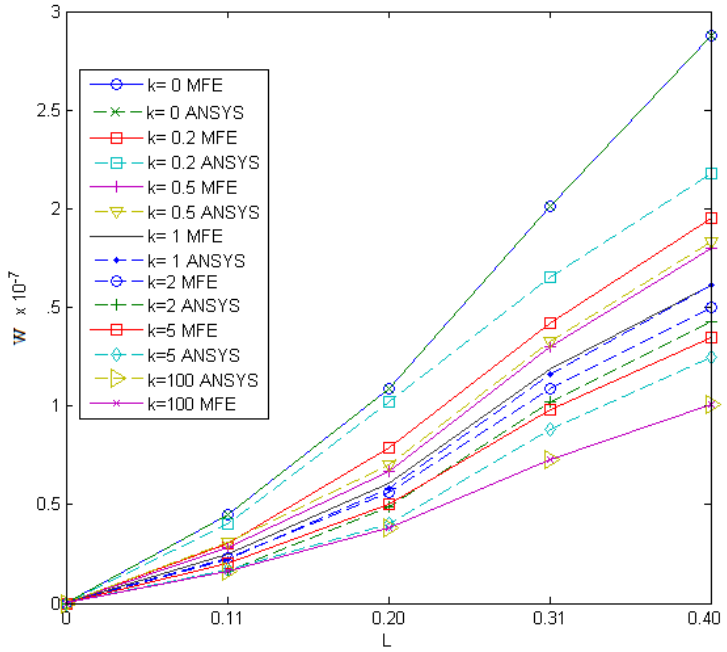

Figure 6.3: The displacement along cantilever beam by MFE.

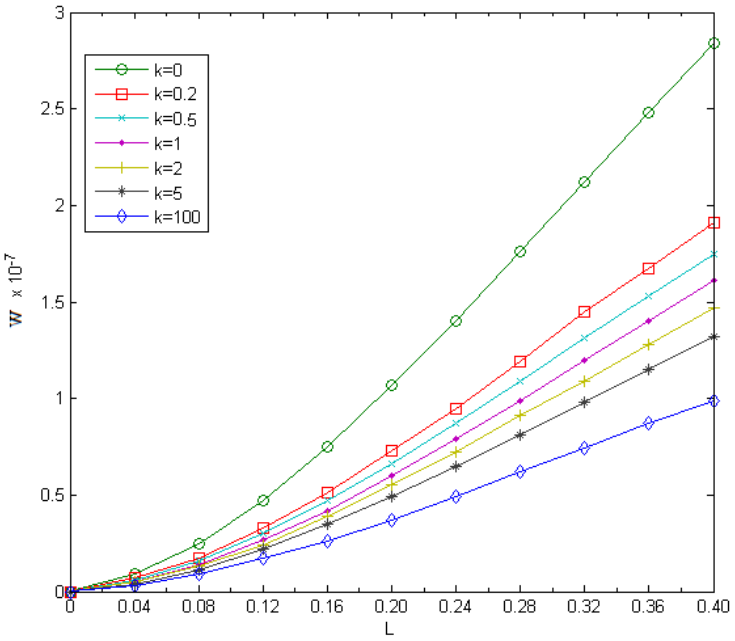

Figure 6.4: The displacement along cantilever beam by MFE and ANSYS.

6.2.2 Graded simple supported beam under uniform static load

Let be a simply supported beam with functionally graded subject to a uniform distributed static load as shown in figure 6-5. The lower side of the graded beam is fabricated of Alu-

minum (metal) and the upper side of Zirconia (ceramic).

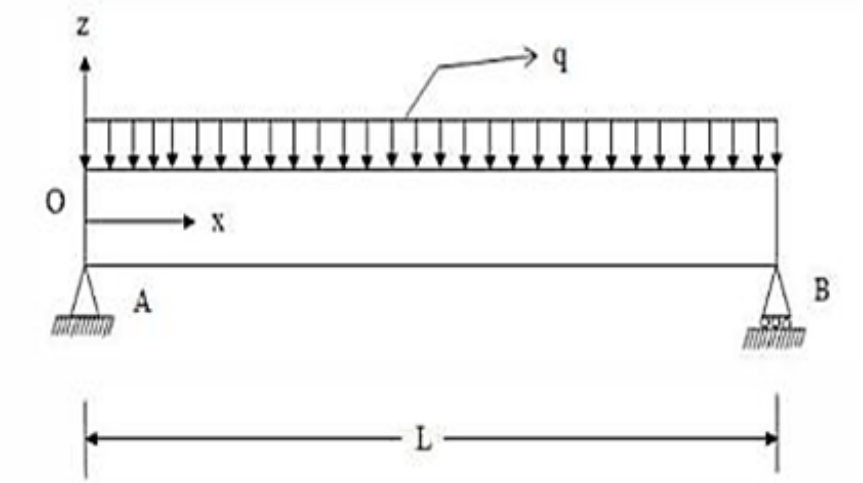

Figure 6.5: FGM simply supported beam.

The second numerical analysis has been performed for a simple supported FGM beam under mechanical load. First, the cases where $k = 0$ and $k = 100$. There is a good correlation between numerical and analytical values for homogeneous materials and for the other values of k (see table 6-2).

Power-law index	Non Dimensional Deflection [278]	Non Dimensional Deflection [279]	Non Dimensional Deflection Present element
$k = 0$ (full metal)	1.13002	1.11888	1.14685
$k = 0.2$	0.84906	0.84965	0.76573
$k = 0.5$	0.71482	0.71329	0.68881
$k = 1$	0.62936	0.62238	0.62588
$k = 2$	0.56165	0.55245	0.56644
$k = 5$	0.49176	0.48252	0.51049
$k = 100$ (full ceramic)	0.39550	0.39161	0.40210

Table 6.2: Maximum non dimensional deflections for FGM simply supported beam.

Table 6-2 is summarized the maximum non-dimensional deflections at the center of the beam obtained using the two numerical models (ANSYS code [279] and the present mixed finite element) and the analytical solution (TBT) [278] for various values of the power-law index. The maximum non-dimensional obtained using the present mixed finite element is 1.14685.While the maximum value using the ANSYS code [279] is 1.11888. The minimum value of the non-dimensional displacement obtained using the ANSYS code is 0.39161, while the present mixed element is 0.40210. It appears an excellent agreement between the results obtained using the two models.
The comparison between the non displacement values of the simply supported graded beams for the present mixed finite element and the numerical solution of Sismek[278], the TBT and CBT of ziou [75]is dressed in figure 6-6.

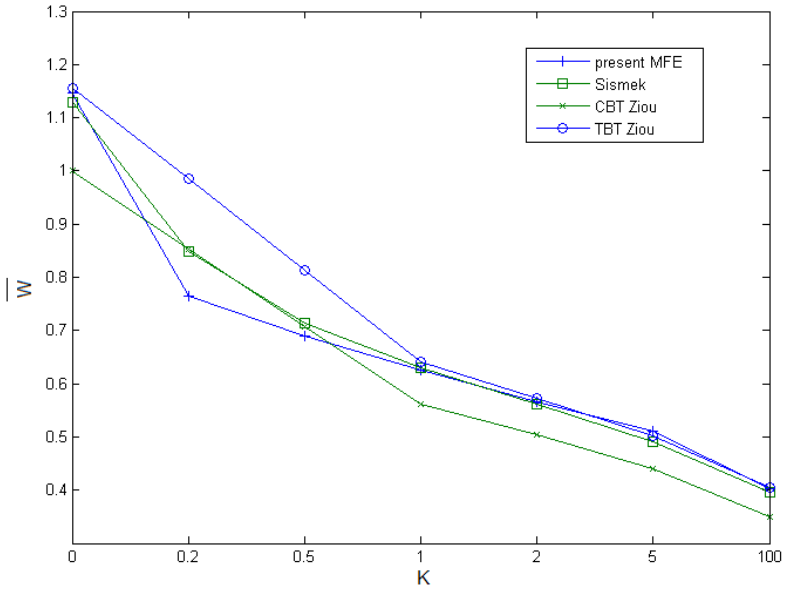

Figure 6.6: Non dimensional displacement of FGM simply supported beam.

The comparison between the displacement along the simply supported beam for the present mixed finite element and the numerical solution of Alexraj [279] obtained by ANSYS code is presented in figure 6-7. An excellent accord of the results is observed between the values given by the two models.

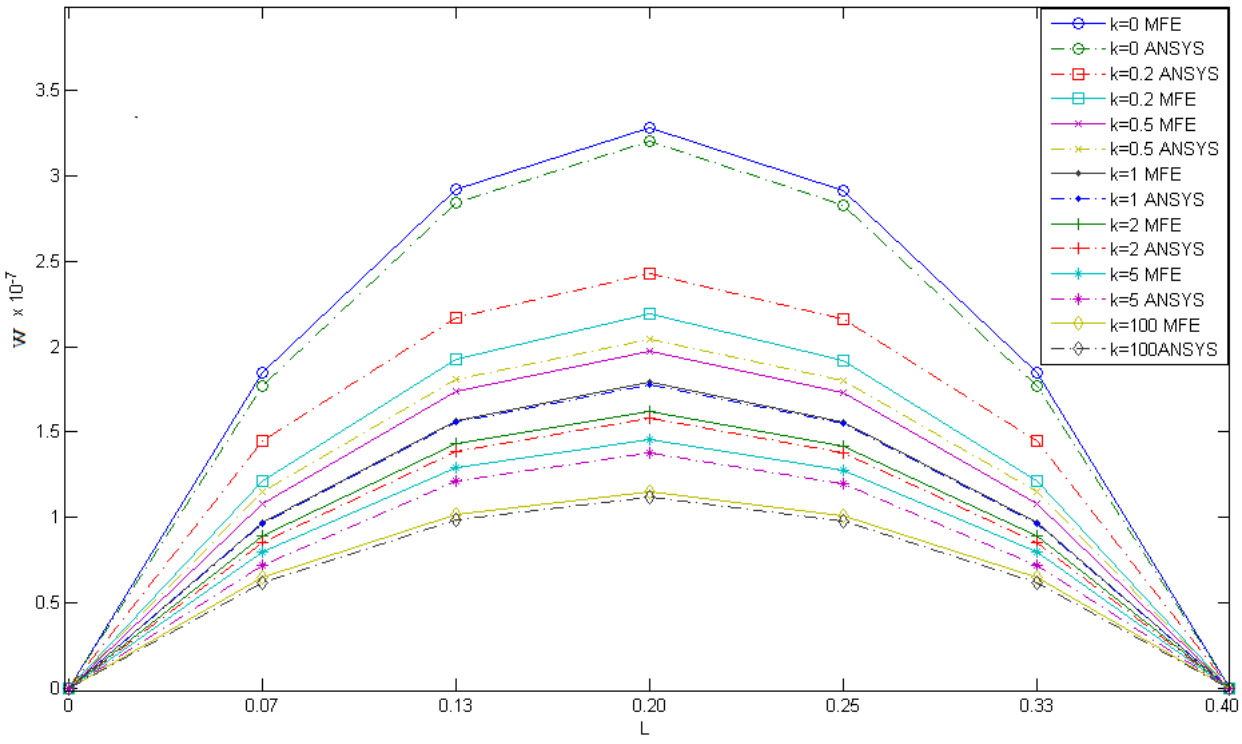

Figure 6.7: The displacement of FGM simple supported beam

The changing of the vertical displacements along the simple supported graded beam for different values of the power-law index k presented by MFE is shown in figure 6-8. It observed a similar behavior of the graded beam under the applied load, in addition to the

same remark made for the case of graded cantilever beams. The maximum displacement is related to the power-law index k changing. The increases in the value of power-law index k are followed by decreasing in the displacements values.

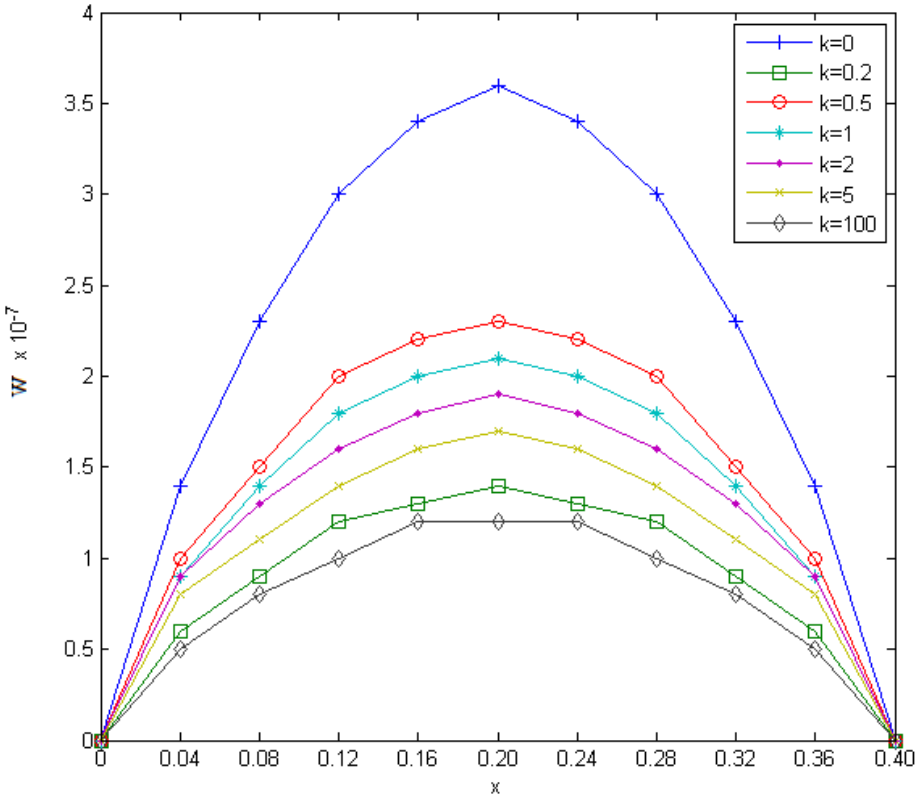

Figure 6.8: The displacement along with simple supported FGM beam By MFE.

The figure 6-8 illustrated the results presented by the present mixed finite element for different indexes of a power k. It is observed from the comparison of the different displacements that the center deflection of the graded beam reaches the highest values when there is a lower index of a power law.

6.2.3 Graded cantilever beam under uniform static load

An elastic cantilever beam is treated in this example (see figure 6-9), the FGM made of a two-phase. The material properties are varied quadratically through the thickness, according to this equation:

$$E(x_2) = 2.5\alpha_0(1 + \beta x_2)^2 \tag{6.3}$$

Where:

The graded parameters are $\alpha_0 = 28Gpa$. $\beta = 0.49mm^{-1}$.

In the analysis with the proposed mixed finite element, the graded beam with functionally properties divided into 10 layers along the graded direction and modeled by 250 mixed finite element.

Wang and Qin [280] modeled the FGM beam with 8 and 12 hybrid elements and divided the beam into 12 and 20 layers along the graded direction by ABAQUS with 300 HFS-FEM. The mesh configuration used in the present MFE and HFS-FEM is shown in figure 6-10.

The displacement distributions in the right and the top facade of the functionally graded beam are dressed in figures. 6-11 and 6-12 respectively.

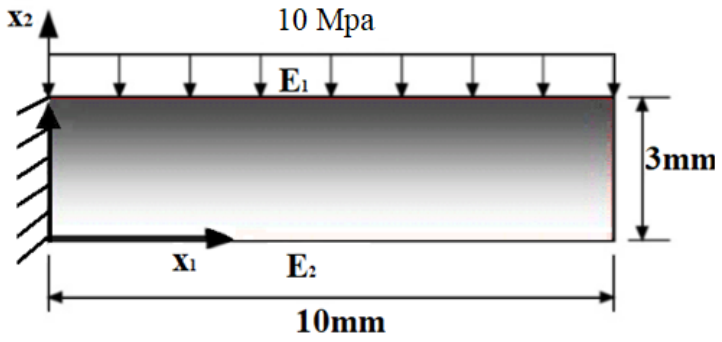

Figure 6.9: functionally graded cantilever beam.

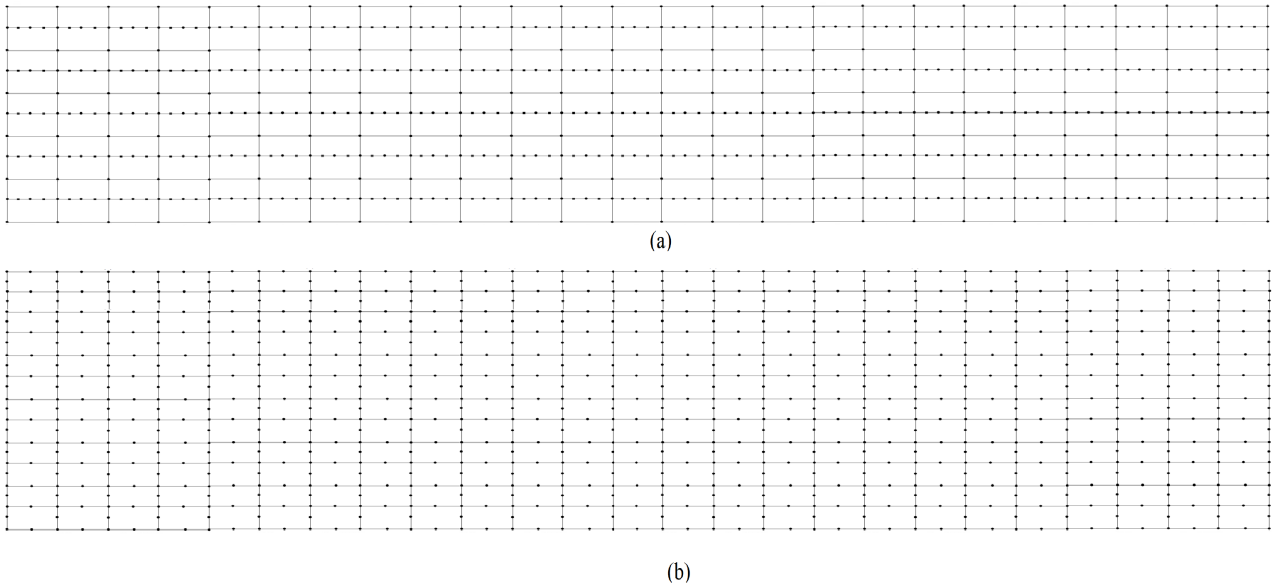

Figure 6.10: Mesh configuration of the FGM beam (a) by the MFE (b) by the HFS-FEM.

The numerical results of the present MFE with seven nodes are in accord with those from HFS-FEM with eight nodes. The two homogenous models results are also presented in figures 6-11 and 6-12 to illustrate the power of graded beams over traditional homogenous materials.
The two homogeneous beam results are similar to the upper and lower bounds of functionally graded beam deformation. Moreover, it can see from figure 6-11 that there is a similar deformation center ($u_1 = 0$) for the two homogeneous beams, and the location of the deformation center is the geometric center of the cross-section. The effect of FGM could move this latter upwards because the upper half of the beam is stiffer than the lower half in FGM.

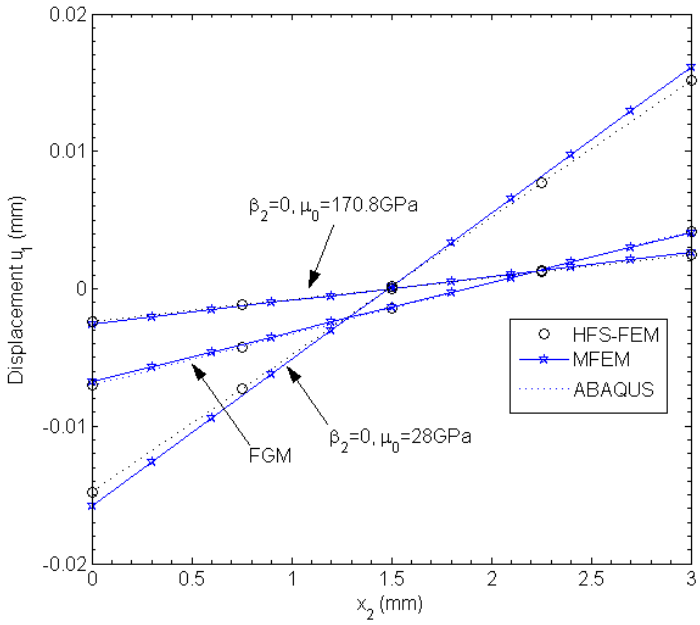

Figure 6.11: The displacement distributions in the right facade of the functionally graded and homogenous beam.

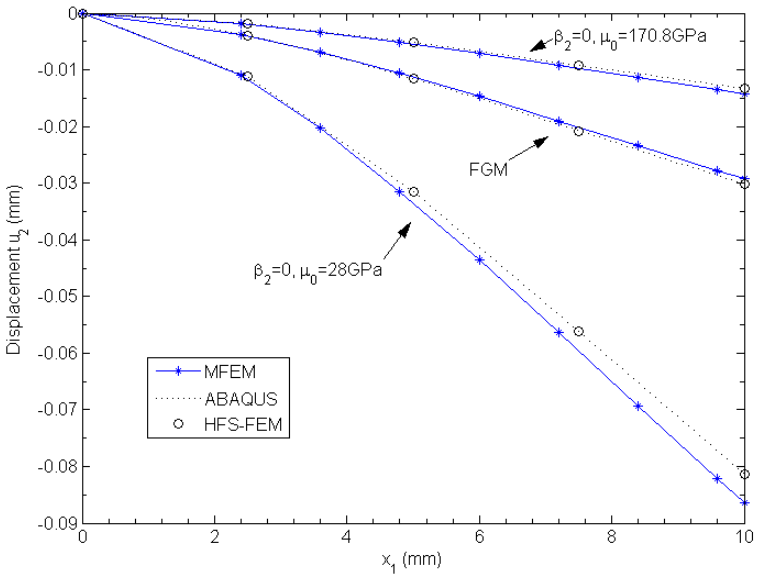

Figure 6.12: The displacement distributions in the top facade of the functionally graded and homogenous beam.

6.3 Kinking crack in FGMs

Quasi-static crack propagation in homogenous and FGM plates under uniaxial tension is simulated. In this study, the problem was treated with 2380 mixed elements and 6145 nodes.

The mixed finite element results were compared to the finite element results obtained using the maximum hoop stress [181] and the maximum strain energy release rate [176]. In addition, to the experimental results [181].

6.3.1 Kinking crack in homogenous materials

A sheet of irradiated ECO (poly-ethylene carbon monoxide) is studied as a homogeneous material. Where the elastic properties are $E = 280MPa, \nu = 0.45$. An inclined edge cracked specimen, dimensions and geometry are shown in Table 6-3. The boundary conditions and mixed mode fracture specimen configuration are dressed in figure 6-13-a. Where v_0, a and Φ are the applied displacement, initial crack length and crack orientation to the applied displacement respectively. The geometry under consideration is an edge cracked plate subjected to uniaxial tension [181].
The two specimens with $\pi/3$ and $\pi/6$ crack inclination angles are studied.

	H	W	h	a	$\Phi(rad)$
Homegenous 1	90	70	45	33	$\pi/3$
Homegenous 2	90	70	45	40	$\pi/6$

Table 6.3: Geometry of homogeneous plate and crack direction.

The simulation results tabulated in table 6-4 and table 6-5 for kinking direction (see figure 13-b) in the homogeneous plate with initial crack angle $\pi/6$ and kinking direction in the homogeneous plate with initial crack angle $\pi/3$, respectively.
The present mixed element predicted the crack direction with high accuracy to the experimental and numerical results for different initial crack directions.

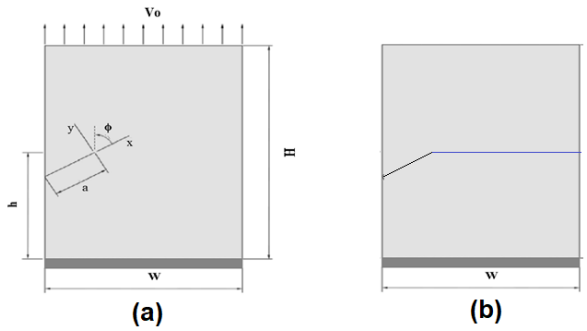

Figure 6.13: (a) Geometry and boundary conditions of the homogeneous plate under uniaxial tension. (b) Crack path prediction.

HOMGENOUSE $\pi/6$			
Expérimental [181]	Finite element [181]	Finite element [176]	Present MFE
-52±1.5	-47.9	-49	-53.13

Table 6.4: Kinking direction in homogeneous plate with initial crack angle $\pi/6$.

HOMGENOUSE $\pi/3$			
Expérimental [181]	Finite element [181]	Finite element [176]	Present MFE
-28±1.5	-26.9	-27	-27.53

Table 6.5: Kinking direction in homogeneous plate with initial crack angle $\pi/3$.

6.3.2 Kinking crack in FGM

A sheet of FGM (graded eco) specimen was produced by Abanto-Bueno and Lambros [181]. The geometry and boundary condition are shown in figure 6-14-a. v_0, a and Φ are the applied displacement, initial crack length and crack orientation to the applied displacement respectively. The crack path predicted for this case is shown in figure 6-14-b.
The material properties like Poisson ration is constant $\nu = 0.45$. While the Young modulus changes in the X direction as:

$$E(X) = -9.2x10^{-7}X^4 + 4.1x10^{-4}X^3 - 5.010^{-2}X^2 - 0.2X + 437.2 \tag{6.4}$$

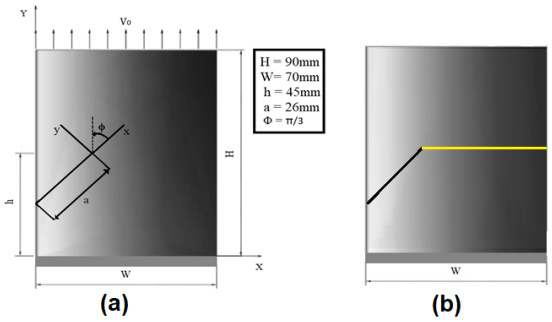

Figure 6.14: (a) Geometry and boundary conditions of FGM plate under uniaxial tension. (b) Crack path prediction.

The results of crack simulation in FGM plates are tabulated in Table 6-6. The present finite element predicted good results compared to the experimental using and numerical results for different crack directions.

FGM $\pi/3$			
Expérimental [181]	Finite element [181]	Finite element [176]	Present MFE
-28±1.5	-24.20	-24	-28.70

Table 6.6: Kinking direction in FGM plate with initial crack angle $\pi/3$.

6.4 Conclusion

The mixed-finite element has shown its performance with few degrees of freedom at the bending analysis of the beam with functionally graded properties with different boundary conditions like simply supported and cantilever beam. the present element compute the displacement and represent the behavior of the FGM for different power law index.
The mixed-finite element extended for the crack analysis in the functionally graded plate for different material distribution. The mixed finite element has proven its performance in crack path predicting with high accuracy and similar to the experimental results, unlike the other numerical results.

General conclusion

In this study, a mixed finite element is proposed to analyze the static behavior of beams that have functionally graded properties under mechanical loads. The present mixed finite element, formulated in the natural plane, has been extended to study the bending and cracking of FGMs.
In this work, the beam with functionally graded properties is treated as several homogeneous layers. The material properties are considered constant for each layer. The properties of the homogeneous element correspond to the property at its center.
The first part of the study deals with the bending behavior of isotropic FGMs. Three examples were treated in this study, a cantilever and simple supported isotropic beams have functionally graded properties under uniform static load. From the results obtained and the comparisons made, the proposed mixed finite element gives accurate results compared to those found by analytical solution (TBT) and other numerical models in the literature. The performance of the present mixed finite element has shown few degrees of freedom in the bending analysis of FGM beams.
In the second part, the study deals with kinking crack behavior of FGMs. The presented mixed finite element present satisfies numerical simulation results compared to numerical and experimental results with fewer elements and lower computational effort. The energy release rate in cracked FGMs is evaluated using a formulation based on the requirement of a lower number of nodal points discretization grid. The graded material is modeled as several homogeneous layers, and the proprieties are situated at the center of the homogenous element. The mixed finite element predicts the direction of kinking crack and accurate results for numerical examples and experiments in the literature.
The numerical results of this study motivated us to use the present mixed finite element in bending and crack analysis of orthotropic FGMs in future studies. To further motivate use the graded element by reformulate the special mixed element to compute the material properties (in each Gaussian integration point) within the present element by using the generalization isoparametric shape functions. The material properties will be interpolated using the same isoparametric shape functions which used for the natural coordinates formulation.

Bibliography

[1] Matthew T Tilbrook, Robert J Moon, and Mark Hoffman. Crack propagation in graded composites. *Composites science and technology*, 65(2):201–220, 2005.

[2] Hamoudi Bouzerd. *Mixed finite element for coherent or cracked interface*. PhD thesis, Lyon 1, 1992.

[3] Salah Bouziane, Hamoudi Bouzerd, and Mohamed Guenfoud. Mixed finite element for modelling interfaces. *European Journal of Computational Mechanics/Revue Européenne de Mécanique Numérique*, 18(2):155–175, 2009.

[4] Chun Deng, Hyeongwon Kim, and Hyungson Ki. Fabrication of functionally-graded yttria-stabilized zirconia coatings by 355 nm picosecond dual-beam pulsed laser deposition. *Composites Part B: Engineering*, 160:498–504, 2019.

[5] Islam M El-Galy, Bassiouny I Saleh, and Mahmoud H Ahmed. Functionally graded materials classifications and development trends from industrial point of view. *SN Applied Sciences*, 1(11):1–23, 2019.

[6] Motoaki Kawase, Teruoki Tago, Michihiro Kurosawa, Hisashi Utsumi, and Kenji Hashimoto. Chemical vapor infiltration and deposition to produce a silicon carbide–carbon functionally gradient material. *Chemical engineering science*, 54(15-16):3327–3334, 1999.

[7] Youyun Lian, Xiang Liu, Zengyu Xu, Jiupeng Song, and Yang Yu. Preparation and properties of cvd-w coated w/cu fgm mock-ups. *Fusion Engineering and Design*, 88(9-10):1694–1698, 2013.

[8] Bassiouny Saleh, Jinghua Jiang, Reham Fathi, Tareq Al-hababi, Qiong Xu, Lisha Wang, Dan Song, and Aibin Ma. 30 years of functionally graded materials: An overview of manufacturing methods, applications and future challenges. *Composites Part B: Engineering*, page 108376, 2020.

[9] Sheila Shahidi, Bahareh Moazzenchi, and Mahmood Ghoranneviss. A review-application of physical vapor deposition (pvd) and related methods in the textile industry. *The European Physical Journal Applied Physics*, 71(3):31302, 2015.

[10] Olayinka Oluwatosin Abegunde, Esther Titilayo Akinlabi, Oluseyi Philip Oladijo, Stephen Akinlabi, and Albert Uchenna Ude. Overview of thin film deposition techniques. *AIMS Materials Science*, 6(2):174–199, 2019.

[11] Dipen Kumar Rajak, Pratiksha H Wagh, Pradeep L Menezes, Anisha Chaudhary, and Ravinder Kumar. Critical overview of coatings technology for metal matrix composites. *Journal of Bio-and Tribo-Corrosion*, 6(1):1–18, 2020.

[12] Kang Hyun Choi, Hyun-Su Kim, Chang Hyun Park, Gon-Ho Kim, Kyoung Ho Baik, Sung Ho Lee, Taehyung Kim, and Hyoung Seop Kim. High-temperature thermomechanical behavior of functionally graded materials produced by plasma sprayed coating: experimental and modeling results. *Metals and Materials International*, 22(5):817–824, 2016.

[13] Omer Van der Biest, Luc Vandeperre, Stijn Put, Guy Anné, and Jef Vleugels. Laminated and functionally graded ceramics by electrophoretic deposition. In *Key Engineering Materials*, volume 333, pages 49–58. Trans Tech Publ, 2007.

[14] Lei Yan, Yitao Chen, and Frank Liou. Additive manufacturing of functionally graded metallic materials using laser metal deposition. *Additive Manufacturing*, 31:100901, 2020.

[15] Chi Zhang, Fei Chen, Zhifeng Huang, Mingyong Jia, Guiyi Chen, Yongqiang Ye, Yaojun Lin, Wei Liu, Bingqing Chen, Qiang Shen, et al. Additive manufacturing of functionally graded materials: A review. *Materials Science and Engineering: A*, 764:138209, 2019.

[16] Michael Gasik, Akira Kawasaki, and Sei Ueda. Design and powder metallurgy processing of functionally graded materials. *Materials Development and Processing-Bulk Amorphous Materials, Undercooling and Powder Metallurgy*, 8:258–264, 2000.

[17] Mahmoud M Nemat-Alla, Moataz H Ata, Mohamed R Bayoumi, Wael Khair-Eldeen, et al. Powder metallurgical fabrication and microstructural investigations of aluminum/steel functionally graded material. *Materials Sciences and Applications*, 2(12):1708, 2011.

[18] Yoshimi Watanabe and Hisashi Sato. Review fabrication of functionally graded materials under a centrifugal force. *Nanocomposites with unique properties and applications in medicine and industry*, pages 133–150, 2011.

[19] Saad Mahmood Ali. Optimization of centrifugal casting parameters of alsi alloy by using the response surface methodology. *International Journal of Engineering*, 32(11):1516–1526, 2019.

[20] TPD Rajan, E Jayakumar, and BC Pai. Developments in solidification processing of functionally graded aluminium alloys and composites by centrifugal casting technique. *Transactions of the Indian Institute of Metals*, 65(6):531–537, 2012.

[21] Saifulnizan Jamian, Yoshimi Watanabe, and Hisashi Sato. Formation of compositional gradient in al/sic fgms fabricated under huge centrifugal forces using solid-particle and mixed-powder methods. *Ceramics International*, 45(7):9444–9453, 2019.

[22] Mohammad Reza Rahimipour and Manoochehr Sobhani. Evaluation of centrifugal casting process parameters for in situ fabricated functionally gradient fe-tic composite. *Metallurgical and Materials Transactions B*, 44(5):1120–1123, 2013.

[23] Justyna Zygmuntowicz, Joanna Szymańska, Marcin Wachowski, Michał Gloc, and Waldemar Kaszuwara. New al2o3–cu–ni functionally graded composites manufactured using the centrifugal slip casting. *International Journal of Applied Ceramic Technology*, 17(6):2580–2590, 2020.

[24] K Morinaga, H Masuda, and K Hayashi. Fabrication of metal/oxide ceramic functionally graded materials by slip casting. In *Interfacial Science in Ceramic Joining*, pages 383–398. Springer, 1998.

[25] Rafael Kenji Nishihora, Priscila Lemes Rachadel, Mara Gabriela Novy Quadri, and Dachamir Hotza. Manufacturing porous ceramic materials by tape casting—a review. *Journal of the European Ceramic Society*, 38(4):988–1001, 2018.

[26] Regina Bulatova, Christian Bahl, Kjeld Andersen, Luise Theil Kuhn, and Nini Pryds. Functionally graded ceramics fabricated with side-by-side tape casting for use in magnetic refrigeration. *International Journal of Applied Ceramic Technology*, 12(4):891–898, 2015.

[27] KM Sree Manu, VG Resmi, M Brahmakumar, P Narayanasamy, TPD Rajan, C Pavithran, and BC Pai. Squeeze infiltration processing of functionally graded aluminum–sic metal ceramic composites. *Transactions of the Indian Institute of Metals*, 65(6):747–751, 2012.

[28] D Janković Ilić, J Fiscina, CJR Gonzalez-Oliver, and F Mücklich. Properties of cu-w functionally graded materials produced by segregation and infiltration. In *Materials Science Forum*, volume 492, pages 123–128. Trans Tech Publ, 2005.

[29] RM Mahamood and ET Akinlabi. Functionally graded materials, topics in mining. *Metallurgy and Materials Engineering. Springer International Publishing, Cham*, 2017.

[30] Emilio Carlos Nelli Silva, Matthew C Walters, and Glaucio H Paulino. Modeling bamboo as a functionally graded material. In *AIP conference proceedings*, volume 973, pages 754–759. American Institute of Physics, 2008.

[31] Sergey V Dorozhkin. Calcium orthophosphate (capo4) scaffolds for bone tissue engineering applications. *Journal of Biotechnology and Biomedical Science*, 1(3):25–93, 2018.

[32] G. Criscenti C. Mota C. van Blitterswijk A. Di Luca, A. Longoni and L. Moroni. Toward mimicking the bone structure: design of novel hierarchical scaffolds with a tailored radial porosity gradient. *Biofabrication,*, 8(4):045007, 2016.

[33] Sandeep S Ahankari and Kamal K Kar. Functionally graded composites: processing and applications. In *Composite Materials*, pages 119–168. Springer, 2017.

[34] Laurent Weiss, Yaël Nessler, Marc Novelli, Pascal Laheurte, and Thierry Grosdidier. On the use of functionally graded materials to differentiate the effects of surface severe plastic deformation, roughness and chemical composition on cell proliferation. *Metals*, 9(12):1344, 2019.

[35] Michael Herrmann and Werner Sobek. Functionally graded concrete: Numerical design methods and experimental tests of mass-optimized structural components. *Structural Concrete*, 18(1):54–66, 2017.

[36] Arif Hidayat, Johan Puspowardojo, Farisi Abdul Aziz, et al. The influence of graded concrete strength on concrete element. *Procedia Engineering*, 125:1023–1029, 2015.

[37] Buntara Sthenly Gan, Han Aylie, and M Mirza Abdillah Pratama. The behavior of graded concrete, an experimental study. *Procedia Engineering*, 125:885–891, 2015.

[38] Gururaja Udupa, S Shrikantha Rao, and KV Gangadharan. Functionally graded composite materials: an overview. *Procedia Materials Science*, 5:1291–1299, 2014.

[39] W Pompe, H Worch, M Epple, W Friess, M Gelinsky, P Greil, U Hempel, D Scharnweber, and KJMS Schulte. Functionally graded materials for biomedical applications. *Materials Science and Engineering: A*, 362(1-2):40–60, 2003.

[40] Eckhard Mueller, Č Drašar, J Schilz, and WA Kaysser. Functionally graded materials for sensor and energy applications. *Materials Science and Engineering: A*, 362(1-2):17–39, 2003.

[41] Woo-Young Jung and Sung-Cheon Han. Analysis of sigmoid functionally graded material (s-fgm) nanoscale plates using the nonlocal elasticity theory. *Mathematical Problems in Engineering*, 2013, 2013.

[42] Ankur Gupta, NK Jain, and R Salhotra. Effect of crack orientation on vibration characteristics of partially cracked fgm plate: an analytical approach. *Materials Today: Proceedings*, 4(9):10179–10183, 2017.

[43] VN Burlayenko, H Altenbach, T Sadowski, and SD Dimitrova. Computational simulations of thermal shock cracking by the virtual crack closure technique in a functionally graded plate. *Computational Materials Science*, 116:11–21, 2016.

[44] Hamid Zabihi Ferezqi, Masoud Tahani, and Hamid Ekhteraei Toussi. Analytical approach to free vibrations of cracked timoshenko beams made of functionally graded materials. *Mechanics of Advanced Materials and Structures*, 17(5):353–365, 2010.

[45] MK Kassir. A note on the twisting deformation of a non-homogeneous shaft containing a circular crack. *International Journal of Fracture Mechanics*, 8(3):325–334, 1972.

[46] Xiao-Jian Xu and Jun-Miao Meng. A model for functionally graded materials. *Composites Part B: Engineering*, 145:70–80, 2018.

[47] RC Batra et al. Some basic fracture mechanics concepts in functionally graded materials. *J. Mech. Phys. Solids*, 44:1221–1235, 1996.

[48] F Erdogon. Fracture mechanics of functionally graded material. *J Comp Eng*, 5:753–770, 1995.

[49] Rolf Mahnken. Material forces for crack analysis of functionally graded materials in adaptively refined fe-meshes. *International journal of fracture*, 147(1):269–283, 2007.

[50] N Knoda and F Erdogan. The mixed mode crack problem in a nonhomogeneous elastic plane. *Eng Fract Mech*, 47:533–545, 1994.

[51] F Delale and F Erdogan. The crack problem for a nonhomogeneous plane. *J Appl Mech*, 50(3):609–614, 1983.

[52] Shyang-ho Chi and Yen-Ling Chung. Cracking in coating–substrate composites with multi-layered and fgm coatings. *Engineering Fracture Mechanics*, 70(10):1227–1243, 2003.

[53] MFGM Koizumi. Fgm activities in japan. *Composites Part B: Engineering*, 28(1-2):1–4, 1997.

[54] Yoshihisa Uchidat. Properties of functionally graded materials manufactured by progressive lamination method for application. *Aichi Institute of Technology Research Report .B*, 39-B:53–57, 2004.

[55] Isaac Elishakoff. Who developed the so-called timoshenko beam theory? *Mathematics and Mechanics of Solids*, 25(1):97–116, 2020.

[56] Tahar Hassaine Daouadji, Abdelaziz Hadj Henni, Abdelouahed Tounsi, and Adda Bedia El Abbes. Elasticity solution of a cantilever functionally graded beam. *Applied Composite Materials*, 20(1):1–15, 2013.

[57] Zheng Zhong and Tao Yu. Analytical solution of a cantilever functionally graded beam. *Composites Science and Technology*, 67(3-4):481–488, 2007.

[58] P Chu, X-F Li, J-X Wu, and KY Lee. Two-dimensional elasticity solution of elastic strips and beams made of functionally graded materials under tension and bending. *Acta Mechanica*, 226(7):2235–2253, 2015.

[59] Yepeng Xu, Tiantang Yu, and Ding Zhou. Two-dimensional elasticity solution for bending of functionally graded beams with variable thickness. *Meccanica*, 49(10):2479–2489, 2014.

[60] DeJin Huang, HaoJiang Ding, and WeiQiu Chen. Analytical solution and semi-analytical solution for anisotropic functionally graded beam subject to arbitrary loading. *Science in China Series G: Physics, Mechanics and Astronomy*, 52(8):1244–1256, 2009.

[61] Qing Yang, Bailin Zheng, Kai Zhang, and Jianxin Zhu. Analytical solution of a bi-layer functionally graded cantilever beam with concentrated loads. *Archive of Applied Mechanics*, 83(3):455–466, 2013.

[62] Trung-Kien Nguyen, Thuc P Vo, and Huu-Tai Thai. Static and free vibration of axially loaded functionally graded beams based on the first-order shear deformation theory. *Composites Part B: Engineering*, 55:147–157, 2013.

[63] MA Benatta, I Mechab, A Tounsi, and EA Adda Bedia. Static analysis of functionally graded short beams including warping and shear deformation effects. *Computational Materials Science*, 44(2):765–773, 2008.

[64] MA Benatta, Abdelouahed Tounsi, I Mechab, and M Bachir Bouiadjra. Mathematical solution for bending of short hybrid composite beams with variable fibers spacing. *Applied Mathematics and Computation*, 212(2):337–348, 2009.

[65] Sallai Ben-Oumrane, Tounsi Abedlouahed, Mechab Ismail, Bachir Bouiadjra Mohamed, Meradjah Mustapha, and Adda Bedia El Abbas. A theoretical analysis of flexional bending of al/al2o3 s-fgm thick beams. *Computational Materials Science*, 44(4):1344–1350, 2009.

[66] Huu-Tai Thai and Thuc P Vo. Bending and free vibration of functionally graded beams using various higher-order shear deformation beam theories. *International Journal of Mechanical Sciences*, 62(1):57–66, 2012.

[67] Lazreg Hadji, Zoubida Khelifa, and Adda Bedia El Abbes. A new higher order shear deformation model for functionally graded beams. *KSCE Journal of Civil Engineering*, 20(5):1835–1841, 2016.

[68] Hassen Ait Atmane, Abdelouahed Tounsi, and Fabrice Bernard. Effect of thickness stretching and porosity on mechanical response of a functionally graded beams resting on elastic foundations. *International Journal of Mechanics and Materials in Design*, 13(1):71–84, 2017.

[69] Shi-Rong Li, Da-Fu Cao, and Ze-Qing Wan. Bending solutions of fgm timoshenko beams from those of the homogenous euler–bernoulli beams. *Applied Mathematical Modelling*, 37(10-11):7077–7085, 2013.

[70] Şeref Doğuşcan Akbaş. Free vibration and bending of functionally graded beams resting on elastic foundation. *Research on Engineering Structures and Materials*, 1(1):25–37, 2015.

[71] Gaetano Giunta, Salim Belouettar, and Erasmo Carrera. Analysis of fgm beams by means of classical and advanced theories. *Mechanics of Advanced Materials and Structures*, 17(8):622–635, 2010.

[72] X-F Li. A unified approach for analyzing static and dynamic behaviors of functionally graded timoshenko and euler–bernoulli beams. *Journal of Sound and vibration*, 318(4-5):1210–1229, 2008.

[73] Shirong Li, Zeqing Wan, and Xuan Wang. Homogenized and classical expressions for static bending solutions for functionally graded material levinson beams. *Applied Mathematics and Mechanics*, 36(7):895–910, 2015.

[74] Ahmed Frikha, Abdessalem Hajlaoui, Mondher Wali, and Fakhreddine Dammak. A new higher order c0 mixed beam element for fgm beams analysis. *Composites Part B: Engineering*, 106:181–189, 2016.

[75] Hassina. Ziou. *Contribution to the modeling of structures in Functional Gradient Materials*. PhD thesis, university of Mohamed Khider biskra, 2017.

[76] Hamza. Guenfoud. *Special finite element modeling of structures in functional gradient materials*. PhD thesis, university of mai 8,1945 Guelma, 2019.

[77] Thuc P Vo, Huu-Tai Thai, Trung-Kien Nguyen, and Fawad Inam. Static and vibration analysis of functionally graded beams using refined shear deformation theory. *Meccanica*, 49(1):155–168, 2014.

[78] S Kapuria, M Bhattacharyya, and AN Kumar. Bending and free vibration response of layered functionally graded beams: a theoretical model and its experimental validation. *Composite Structures*, 82(3):390–402, 2008.

[79] Li-Long Jing, Ping-Jian Ming, Wen-Ping Zhang, Li-Rong Fu, and Yi-Peng Cao. Static and free vibration analysis of functionally graded beams by combination timoshenko theory and finite volume method. *Composite structures*, 138:192–213, 2016.

[80] M Filippi, E Carrera, and AM Zenkour. Static analyses of fgm beams by various theories and finite elements. *Composites Part B: Engineering*, 72:1–9, 2015.

[81] SM Aldousari. Bending analysis of different material distributions of functionally graded beam. *Applied Physics A*, 123(4):296, 2017.

[82] Farshad Rahmani, Reza Kamgar, and Reza Rahgozar. Finite element analysis of functionally graded beams using different beam theories. *Civil Engineering Journal*, 6(11):2086–2102, 2020.

[83] Junuthula Narasimha Reddy. *Mechanics of laminated composite plates and shells: theory and analysis*. CRC press, 2003.

[84] LS Ma and TJ Wang. Nonlinear bending and post-buckling of a functionally graded circular plate under mechanical and thermal loadings. *International Journal of Solids and Structures*, 40(13-14):3311–3330, 2003.

[85] AR Damanpack, MAHDI Bodaghi, HASSAN Ghassemi, and MESBAH Sayehbani. Boundary element method applied to the bending analysis of thin functionally graded plates. *Latin American Journal of Solids and Structures*, 10:549–570, 2013.

[86] Raymond D Mindlin. Influence of rotatory inertia and shear on flexural motions of isotropic, elastic plates. 18:31–38, 1951.

[87] Lucia Della Croce and Paolo Venini. Finite elements for functionally graded reissner–mindlin plates. *Computer Methods in Applied Mechanics and Engineering*, 193(9-11):705–725, 2004.

[88] M Memar Ardestani, B Soltani, and Sh Shams. Analysis of functionally graded stiffened plates based on fsdt utilizing reproducing kernel particle method. *Composite Structures*, 112:231–240, 2014.

[89] JN Reddy, CM Wang, and S Kitipornchai. Axisymmetric bending of functionally graded circular and annular plates. *European Journal of Mechanics-A/Solids*, 18(2):185–199, 1999.

[90] Junuthula N Reddy. A simple higher-order theory for laminated composite plates. *J Appl Mech*, 51(4):745–752, 1984.

[91] JN Reddy. Analysis of functionally graded plates. *International Journal for numerical methods in engineering*, 47(1-3):663–684, 2000.

[92] MNA Gulshan Taj, Anupam Chakrabarti, and Abdul Hamid Sheikh. Analysis of functionally graded plates using higher order shear deformation theory. *Applied Mathematical Modelling*, 37(18-19):8484–8494, 2013.

[93] T Kant et al. A critical review and some results of recently developed refined theories of fiber-reinforced laminated composites and sandwiches. *Composite structures*, 23(4):293–312, 1993.

[94] Abdeldjalil. Benbakhti. *Modeling of the thermomechanical behavior of FGM plates(Functionally Graded Materials)*. PhD thesis, Universty of Abdelhamid Ibn Badis Mosteghanem, 2017.

[95] JN Reddy. A general nonlinear third-order theory of functionally graded plates. *International Journal of Aerospace and Lightweight Structures (IJALS)*, 1(1), 2011.

[96] T Kant, DK Jha, and RK Singh. A higher-order shear and normal deformation functionally graded plate model: some recent results. *Acta Mechanica*, 225(10):2865–2876, 2014.

[97] DK Jha, Tarun Kant, and RK Singh. Stress analysis of transversely loaded functionally graded plates with a higher order shear and normal deformation theory. *Journal of Engineering Mechanics*, 139(12):1663–1680, 2013.

[98] DK Jha, Tarun Kant, K Srinivas, and RK Singh. An accurate higher order displacement model with shear and normal deformations effects for functionally graded plates. *Fusion Engineering and Design*, 88(12):3199–3204, 2013.

[99] Rafik Meksi, Samir Benyoucef, Abdelkader Mahmoudi, Abdelouahed Tounsi, El Abbas Adda Bedia, and SR Mahmoud. An analytical solution for bending, buckling and vibration responses of fgm sandwich plates. *Journal of Sandwich Structures & Materials*, 21(2):727–757, 2019.

[100] Loc V Tran, AJM Ferreira, and Hung Nguyen-Xuan. Isogeometric analysis of functionally graded plates using higher-order shear deformation theory. *Composites Part B: Engineering*, 51:368–383, 2013.

[101] H Jari, HR Atri, and S Shojaee. Nonlinear thermal analysis of functionally graded material plates using a nurbs based isogeometric approach. *Composite Structures*, 119:333–345, 2015.

[102] AS Oktem, JL Mantari, and C Guedes Soares. Static response of functionally graded plates and doubly-curved shells based on a higher order shear deformation theory. *European Journal of Mechanics-A/Solids*, 36:163–172, 2012.

[103] M Touratier. An efficient standard plate theory. *International journal of engineering science*, 29(8):901–916, 1991.

[104] M Karama, KS Afaq, and S Mistou. Mechanical behaviour of laminated composite beam by the new multi-layered laminated composite structures model with transverse shear stress continuity. *International Journal of solids and structures*, 40(6):1525–1546, 2003.

[105] Hassen Ait Atmane, Abdelouahed Tounsi, Ismail Mechab, et al. Free vibration analysis of functionally graded plates resting on winkler–pasternak elastic foundations using a new shear deformation theory. *International Journal of Mechanics and Materials in Design*, 6(2):113–121, 2010.

[106] Emilio Martínez-Pañeda. On the finite element implementation of functionally graded materials. *Materials*, 12(2):287, 2019.

[107] Engin Orakdöğen, Semih Küçükarslan, A Sofiyev, and MH Omurtag. Finite element analysis of functionally graded plates for coupling effect of extension and bending. *Meccanica*, 45(1):63–72, 2010.

[108] S Brischetto and E Carrera. Advanced mixed theories for bending analysis of functionally graded plates. *Computers & Structures*, 88(23-24):1474–1483, 2010.

[109] Nguyen Van Long, Tran Huu Quoc, and Tran Minh Tu. Bending and free vibration analysis of functionally graded plates using new eight-unknown shear deformation theory by finite-element method. *International Journal of Advanced Structural Engineering*, 8(4):391–399, 2016.

[110] Trung Thanh Tran, Quoc-Hoa Pham, and Trung Nguyen-Thoi. Static and free vibration analyses of functionally graded porous variable-thickness plates using an edge-based smoothed finite element method. *Defence Technology*, 17(3):971–986, 2021.

[111] JN Reddy. A generalization of two-dimensional theories of laminated composite plates. *Communications in applied numerical methods*, 3(3):173–180, 1987.

[112] M Shakeri and R Mirzaeifar. Static and dynamic analysis of thick functionally graded plates with piezoelectric layers using layerwise finite element model. *Mechanics of Advanced Materials and Structures*, 16(8):561–575, 2009.

[113] Erasmo Carrera, S Brischetto, M Cinefra, and M Soave. Refined and advanced models for multilayered plates and shells embedding functionally graded material layers. *Mechanics of Advanced Materials and Structures*, 17(8):603–621, 2010.

[114] Erasmo Carrera. Theories and finite elements for multilayered, anisotropic, composite plates and shells. *Archives of Computational Methods in Engineering*, 9(2):87–140, 2002.

[115] Alexander Tessler, Marco Di Sciuva, and Marco Gherlone. A refined zigzag beam theory for composite and sandwich beams. *Journal of Composite Materials*, 43(9):1051–1081, 2009.

[116] M Di Sciuva and M Sorrenti. Bending, free vibration and buckling of functionally graded carbon nanotube-reinforced sandwich plates, using the extended refined zigzag theory. *Composite Structures*, 227:111324, 2019.

[117] Mehmet Dorduncu. Stress analysis of sandwich plates with functionally graded cores using peridynamic differential operator and refined zigzag theory. *Thin-Walled Structures*, 146:106468, 2020.

[118] Huu-Tai Thai and Seung-Eock Kim. A review of theories for the modeling and analysis of functionally graded plates and shells. *Composite Structures*, 128:70–86, 2015.

[119] Tahir Khan, Ning Zhang, and Abdullah Akram. State of the art review of functionally graded materials. In *2019 2nd International Conference on Computing, Mathematics and Engineering Technologies (iCoMET)*, pages 1–9. IEEE, 2019.

[120] George R Irwin. Analysis of stresses and strains near the end of a crack traversing a plate. *Trans AIME J Appl Mech*, 6:361–364, 1957.

[121] Nikolaĭ Ivanovich Muskhelishvili. *Some basic problems of the mathematical theory of elasticity*. Springer Science & Business Media, 2013.

[122] Harold M Westergaard. Bearing pressures and cracks: Bearing pressures through a slightly waved surface or through a nearly flat part of a cylinder, and related problems of cracks. *Trans AIME J Appl Mech*, 6:49–53, 1939.

[123] Alan Arnold Griffith. Vi. the phenomena of rupture and flow in solids. *Philosophical transactions of the royal society of london. Series A, containing papers of a mathematical or physical character*, 221(582-593):163–198, 1921.

[124] F Erdogan and BH Wu. The surface crack problem for a plate with functionally graded properties. *J Appl Mech*, 64(3):449–456, 1997.

[125] Naotake Noda and Jin Zhi-He. Thermal stress intensity factors for a crack in a strip of a functionally gradient material. *International Journal of Solids and structures*, 30(8):1039–1056, 1993.

[126] XW Gao, Ch Zhang, J Sladek, and V Sladek. Fracture analysis of functionally graded materials by a bem. *Composites Science and Technology*, 68(5):1209–1215, 2008.

[127] SERKAN Dag, BORA Yildirim, and FAZIL Erdogan. Interface crack problems in graded orthotropic media: Analytical and computational approaches. *International Journal of Fracture*, 130(1):471–496, 2004.

[128] Mojtaba Mahmoudi Monfared. Mode iii sifs for interface cracks in an fgm coating-substrate system. *Structural engineering and mechanics: An international journal*, 64(1):71–79, 2017.

[129] Jeong-Ho Kim and Glaucio H Paulino. T-stress in orthotropic functionally graded materials: Lekhnitskii and stroh formalisms. *International Journal of Fracture*, 126(4):345–384, 2004.

[130] T Fujimoto and N Noda. Crack propagation in a functionally graded plate under thermal shock. *Archive of Applied Mechanics*, 70(6):377–386, 2000.

[131] Ted Belytschko, Lei Gu, and YY Lu. Fracture and crack growth by element free galerkin methods. *Modelling and Simulation in Materials Science and Engineering*, 2(3A):519, 1994.

[132] Sheng-Hu Ding and Xing Li. Mode-i crack problem for functionally graded layered structures. *International journal of fracture*, 168(2):209–226, 2011.

[133] Li-Cheng Guo, Lin-Zhi Wu, Li Ma, and Tao Zeng. Fracture analysis of a functionally graded coating-substrate structure with a crack perpendicular to the interface-part i: Static problem. *International Journal of fracture*, 127(1):21–38, 2004.

[134] Max L Williams. On the stress distribution at the base of a stationary crack. *Journal of Applied Mechanics*, 24(1), 1957.

[135] Jeffrey Warren Eischen. Fracture of nonhomogeneous materials. *International Journal of Fracture*, 34(1):3–22, 1987.

[136] Zhi-He Jin and Naotake Noda. Crack-tip singular fields in nonhomogeneous materials. *J Appl Mech*, 61(3):738–740, 1994.

[137] Jeong-Ho Kim and Glaucio H Paulino. Finite element evaluation of mixed mode stress intensity factors in functionally graded materials. *International Journal for Numerical Methods in Engineering*, 53(8):1903–1935, 2002.

[138] Jeong-Ho Kim and Glaucio H Paulino. On fracture criteria for mixed-mode crack propagation in functionally graded materials. *Mechanics of Advanced Materials and Structures*, 14(4):227–244, 2007.

[139] CF Shih, HG De Lorenzi, and MD German. Crack extension modeling with singular quadratic isoparametric elements. *International Journal of Fracture*, 12(4):647–651, 1976.

[140] Edmund F Rybicki and Melvin F Kanninen. A finite element calculation of stress intensity factors by a modified crack closure integral. *Engineering fracture mechanics*, 9(4):931–938, 1977.

[141] IS Raju. Calculation of strain-energy release rates with higher order and singular finite elements. *Engineering Fracture Mechanics*, 28(3):251–274, 1987.

[142] James R Rice. A path independent integral and the approximate analysis of strain concentration by notches and cracks. *J Appl Mech*, 35(2):379–386, 1968.

[143] Tony Honein and George Herrmann. Conservation laws in nonhomogeneous plane elastostatics. *Journal of the Mechanics and Physics of Solids*, 45(5):789–805, 1997.

[144] MA Hussain, SL Pu, and J Underwood. Strain energy release rate for a crack under combined mode i and mode ii. In *Fracture analysis: Proceedings of the 1973 national symposium on fracture mechanics, part II*. ASTM International, 1974.

[145] F Erdogen and GC Shi. On the crack extension in plates under loading and transverse shear. *Journal of Basic*, 85(4):519–525, 1963.

[146] BL Wang, Yiu-Wing Mai, and Naotake Noda. Fracture mechanics analysis model for functionally graded materials with arbitrarily distributed properties. *International Journal of Fracture*, 116(2):161–177, 2002.

[147] Jian-Ping Zhao, Wen-Long Huang, and Shu-Ho Dai. The application of 2d elastic stochastic finite element method in the field of fracture mechanics. *International journal of pressure vessels and piping*, 71(2):169–173, 1997.

[148] Matthew T Tilbrook, Robert J Moon, and Mark Hoffman. Finite element simulations of crack propagation in functionally graded materials under flexural loading. *Engineering Fracture Mechanics*, 72(16):2444–2467, 2005.

[149] Ahmed Hassan Ahmed Hassan and İbrahim Keleş. Fgm modelling using dummy thermal loads. *Journal of Selcuk International Science and Technology*, 1(10-16), 2017.

[150] Meriem Chafi and Abdelkader Boulenouar. A numerical modelling of mixed mode crack initiation and growth in functionally graded materials. *Materials Research*, 22, 2019.

[151] Imène Hebbar, Abdelkader Boulenouar, and Yazid Ait Ferhat. Two-dimensional fracture analysis of fgm under mechanical loading. *Journal of Materials and Engineering Structures «JMES»*, 7(2):241–252, 2020.

[152] Y Ait Ferhat, A Boulenouar, N Benamara, and L Benabou. Generalized displacement correlation method for mechanical and thermal fracture of fgm. *International Journal of Computational Materials Science and Engineering*, 9(01):2050004, 2020.

[153] Yazid Ait Ferhat and Abdelkader Boulenouar. Computation of sifs for cracks in fgms and tbc under mechanical and thermal loadings. *International Journal on Interactive Design and Manufacturing (IJIDeM)*, 14(4):1347–1356, 2020.

[154] Chunyu Li, Zhenzhu Zou, and Zhuping Duan. Multiple isoparametric finite element method for nonhomogeneous media. *Mechanics Research Communications*, 27(2):137–142, 2000.

[155] MH Santare and J Lambros. Use of graded finite elements to model the behavior of nonhomogeneous materials. *J. Appl. Mech.*, 67(4):819–822, 2000.

[156] A Ajdari, P Canavan, H Nayeb-Hashemi, and G Warner. Mechanical properties of functionally graded 2-d cellular structures: A finite element simulation. *Materials Science and Engineering: A*, 499(1-2):434–439, 2009.

[157] Jeong-Ho Kim and GH Paulino. Isoparametric graded finite elements for nonhomogeneous isotropic and orthotropic materials. *J. Appl. Mech.*, 69(4):502–514, 2002.

[158] Alpay Oral, John Lambros, and Gunay Anlas. Crack initiation in functionally graded materials under mixed mode loading: experiments and simulations. *Journal of Applied Mechanics*, 75(5), 2008.

[159] Jeong-Ho Kim and Glaucio H Paulino. Mixed-mode fracture of orthotropic functionally graded materials using finite elements and the modified crack closure method. *Engineering Fracture Mechanics*, 69(14-16):1557–1586, 2002.

[160] De Xie, Anthony M Waas, Khaled W Shahwan, Jessica A Schroeder, and Raymond G Boeman. Computation of energy release rates for kinking cracks based on virtual crack closure technique. *Computer Modeling in Engineering & Sciences*, 6(6):515–524, 2004.

[161] A Boulenouar, N Benamara, and M Merzoug. Prediction of mixed-mode crack propagation paths in fgms. *2nd CIMDD, University M'hamed Bougara Boumerdes, Algeria*, 2015.

[162] C-E Rousseau and HV Tippur. Compositionally graded materials with cracks normal to the elastic gradient. *Acta Materialia*, 48(16):4021–4033, 2000.

[163] J Sladek, V Sladek, M Repka, and Choon-Lai Tan. Evaluation of the t-stress for cracks in functionally graded materials by the fem. *Theoretical and Applied Fracture Mechanics*, 86:332–341, 2016.

[164] Yongdong Li, Hongcai Zhang, and Wei Tan. Fracture analysis of functionally gradient weak/micro-discontinuous interface with finite element method. *Computational materials science*, 38(2):454–458, 2006.

[165] S El-Borgi, F Erdogan, and F Ben Hatira. Stress intensity factors for an interface crack between a functionally graded coating and a homogeneous substrate. *International Journal of Fracture*, 123(3):139–162, 2003.

[166] MS Kirugulige, R Kitey, and HV Tippur. Dynamic fracture behavior of model sandwich structures with functionally graded core: a feasibility study. *Composites Science and Technology*, 65(7-8):1052–1068, 2005.

[167] RC Batra and BM Love. Crack propagation due to brittle and ductile failures in microporous thermoelastoviscoplastic functionally graded materials. *Engineering fracture mechanics*, 72(12):1954–1979, 2005.

[168] Glaucio H Paulino and Jeong-Ho Kim. The weak patch test for nonhomogeneous materials modeled with graded finite elements. *Journal of the Brazilian Society of Mechanical Sciences and Engineering*, 29:63–81, 2007.

[169] Alpay Oral, Jorge L Abanto-Bueno, John Lambros, and Gunay Anlas. Crack initiation angles in functionally graded materials under mixed mode loading. In *AIP Conference Proceedings*, volume 973, pages 248–253. American Institute of Physics, 2008.

[170] Bora Yıldırım, Suphi Yılmaz, and Suat Kadıoğlu. Delamination of compressively stressed orthotropic functionally graded material coatings under thermal loading. *Journal of applied mechanics*, 75(5), 2008.

[171] Jui-Hung Chang and Geo-Jih Liao. Nonhomogenized displacement discontinuity method for calculation of stress intensity factors for cracks in anisotropic fgms. *Journal of Engineering Mechanics*, 140(12):04014093, 2014.

[172] Mohamad Molavi Nojumi and Xiaodong Wang. A new graded singular finite element for crack problems in functionally graded materials. *International Journal of Fracture*, 205(2):203–220, 2017.

[173] Li Ming Zhou, Guang Wei Meng, Xiao Lin Li, and Feng Li. Analysis of dynamic fracture parameters in functionally graded material plates with cracks by graded finite element method and virtual crack closure technique. *Advances in Materials Science and Engineering*, 2016, 2016.

[174] Pei Gu and RJ Asaro. Crack deflection in functionally graded materials. *International Journal of Solids and Structures*, 34(24):3085–3098, 1997.

[175] B Cotterell and JR Rice. Slightly kinked or curved cracks. *lnternat, or. Fracture*, 16:155, 1980.

[176] TL Becker Jr, RM Cannon, and RO Ritchie. Finite crack kinking and t-stresses in functionally graded materials. *International Journal of Solids and Structures*, 38(32-33):5545–5563, 2001.

[177] K Hayashi and S Nemat-Nasser. Energy-release rate and crack kinking under combined loading. *J Appl Mech*, 48(3):520–524, 1981.

[178] K Hayashi and S Nemat-Nasser. Energy release rate and crack kinking. *International Journal of Solids and Structures*, 17(1):107–114, 1981.

[179] Y Shindo, S Ueda. Crack kinking in functionally graded materials due to an initial strain resulting from stress relaxation. *Journal of thermal stresses*, 23(3):285–290, 2000.

[180] BL Karihaloo, LM Keer, and S Nemat-Nasser. Crack kinking under nonsymmetric loading. *Engineering Fracture Mechanics*, 13(4):879–888, 1980.

[181] J Abanto-Bueno and J Lambros. An experimental study of mixed mode crack initiation and growth in functionally graded materials. *Experimental Mechanics*, 46(2):179–196, 2006.

[182] J Chapa-Cabrera and IE Reimanis. Effects of residual stress and geometry on crack kink angles in graded composites. *Engineering fracture mechanics*, 69(14-16):1667–1678, 2002.

[183] De Xie, Anthony M Waas, Khaled W Shahwan, Jessica A Schroeder, and Raymond G Boeman. Fracture criterion for kinking cracks in a tri-material adhesively bonded joint under mixed mode loading. *Engineering Fracture Mechanics*, 72(16):2487–2504, 2005.

[184] Dominique Leguillon and Sébastien Murer. A criterion for crack kinking out of an interface. In *Key Engineering Materials*, volume 385, pages 9–12. Trans Tech Publ, 2008.

[185] KS Ravi Chandran and I Barsoum. Determination of stress intensity factor solutions for cracks in finite-width functionally graded materials. *International Journal of Fracture*, 121(3):183–203, 2003.

[186] Britta Schramm, Hans Albert Richard, and Gunter Kullmer. Theoretical, experimental and numerical investigations on crack growth in fracture mechanical graded structures. *Engineering Fracture Mechanics*, 167:188–200, 2016.

[187] Amit Banerjee, Brajesh Panigrahi, and G Pohit. Crack modelling and detection in timoshenko fgm beam under transverse vibration using frequency contour and response surface model with ga. *Nondestructive Testing and Evaluation*, 31(2):142–164, 2016.

[188] Brajesh Panigrahi and Goutam Pohit. Nonlinear modelling and dynamic analysis of cracked timoshenko functionally graded beams based on neutral surface approach. *Proceedings of the Institution of Mechanical Engineers, Part C: Journal of Mechanical Engineering Science*, 230(9):1486–1497, 2016.

[189] Guillaume Gautier, Jean-Mathieu Mencik, and Roger Serra. 2d localization of a crack on a beam by subspace fitting. In *Congrès français de mécanique*. AFM, Association Française de Mécanique, 2015.

[190] F Erdogan et al. Interface cracking of fgm coatings under steady-state heat flow. *Engineering Fracture Mechanics*, 59(3):361–380, 1998.

[191] Vera Petrova and Siegfried Schmauder. Fgm/homogeneous bimaterials with systems of cracks under thermo-mechanical loading: Analysis by fracture criteria. *Engineering Fracture Mechanics*, 130:12–20, 2014.

[192] TL Becker Jr, RM Cannon, and RO Ritchie. Statistical fracture modeling: crack path and fracture criteria with application to homogeneous and functionally graded materials. *Engineering Fracture Mechanics*, 69(14-16):1521–1555, 2002.

[193] H-A Bahr, H Balke, T Fett, I Hofinger, G Kirchhoff, D Munz, A Neubrand, AS Semenov, H-J Weiss, and YY Yang. Cracks in functionally graded materials. *Materials Science and Engineering: A*, 362(1-2):2–16, 2003.

[194] Licheng Guo and Naotake Noda. Investigation methods for thermal shock crack problems of functionally graded materials–part i: analytical method. *Journal of Thermal Stresses*, 37(3):292–324, 2014.

[195] Victor Rizov. Fracture analysis of a three-dimensional functionally graded beam. *International Journal of Structural Integrity*, 2018.

[196] Victor Rizov. Delamination in a two-dimensional functionally graded beam. *Journal of Applied Mechanics & Technical Physics*, 59(1), 2018.

[197] Zhanqi Cheng and Zheng Zhong. Analysis of a moving crack in a functionally graded strip between two homogeneous layers. *International Journal of Mechanical Sciences*, 49(9):1038–1046, 2007.

[198] Li-Cheng Guo, Lin-Zhi Wu, Tao Zeng, and Li Ma. The dynamic fracture behavior of a functionally graded coating–substrate system. *Composite Structures*, 64(3-4):433–441, 2004.

[199] X-F Li and S-H Guo. Effects of nonhomogeneity on dynamic stress intensity factors for an antiplane interface crack in a functionally graded material bonded to an elastic semi-strip. *Computational materials science*, 38(2):432–441, 2006.

[200] Yong dong Li, Jia Bin, Zhang Nan, Li qiang Tang, and Dai Yao. Dynamic stress intensity factor of the weak/micro-discontinuous interface crack of a fgm coating. *International Journal of Solids and Structures*, 43(16):4795–4809, 2006.

[201] Yong-Dong Li, Kang Yong Lee, and Yao Dai. Dynamic stress intensity factors of two collinear mode-iii cracks perpendicular to and on the two sides of a bi-fgm weak-discontinuous interface. *European Journal of Mechanics-A/Solids*, 27(5):808–823, 2008.

[202] Jeong Woo Shin and Young-Shin Lee. Dynamic propagation of a weak-discontinuous interface crack between two dissimilar functionally graded layers under anti-plane shear. *Journal of mechanical science and technology*, 25(10):2551, 2011.

[203] Glaucio H Paulino and Zheng Yu Zhang. Dynamic fracture of functionally graded composites using an intrinsic cohesive zone model. In *Materials Science Forum*, volume 492, pages 447–452. Trans Tech Publ, 2005.

[204] Tinh Quoc Bui, Nha Thanh Nguyen, Minh Ngoc Nguyen, Thien Tich Truong, et al. Analysis of transient dynamic fracture parameters of cracked functionally graded composites by improved meshfree methods. *Theoretical and Applied Fracture Mechanics*, 96:642–657, 2018.

[205] Zhanqi Cheng, Yingkai Liu, Jun Zhao, Hu Feng, and Yizhang Wu. Numerical simulation of crack propagation and branching in functionally graded materials using peridynamic modeling. *Engineering Fracture Mechanics*, 191:13–32, 2018.

[206] DH Li, X Yang, RL Qian, and D Xu. Static and dynamic response analysis of functionally graded material plates with damage. *Mechanics of Advanced Materials and Structures*, 27(2):94–107, 2020.

[207] Mohamad Molavi Nojumi and Xiaodong Wang. Dynamic analysis of crack problems in functionally graded materials using a new graded singular finite element. *Theoretical and Applied Fracture Mechanics*, 93:183–194, 2018.

[208] Baojing Zheng, Yang Yang, Xiaowei Gao, and Ch Zhang. Dynamic fracture analysis of functionally graded materials under thermal shock loading by using the radial integration boundary element method. *Composite Structures*, 201:468–476, 2018.

[209] J Chapa-Cabrera and IE Reimanis. Crack deflection in compositionally graded cu-w composites. *Philosophical Magazine A*, 82(17-18):3393–3403, 2002.

[210] Emilio Martínez-Pañeda and Rafael Gallego. Numerical analysis of quasi-static fracture in functionally graded materials. *International Journal of Mechanics and Materials in Design*, 11(4):405–424, 2015.

[211] Li Yongdong, Tan Wei, and Zhang Hongcai. Anti-plane transient fracture analysis of the functionally gradient elastic bi-material weak/infinitesimal-discontinuous interface. *International Journal of fracture*, 142(1):163–171, 2006.

[212] Li-Cheng Guo, Lin-Zhi Wu, Tao Zeng, and Li Ma. Fracture analysis of a functionally graded coating-substrate structure with a crack perpendicular to the interface-part ii: Transient problem. *International Journal of Fracture*, 127(1):39–59, 2004.

[213] Kwang Ho Lee. Analysis of a transiently propagating crack in functionally graded materials under mode i and ii. *International journal of engineering science*, 47(9):852–865, 2009.

[214] Yang Liao, Lisheng Liu, Qiwen Liu, Xin Lai, Migbar Assefa, and Jingang Liu. Peridynamic simulation of transient heat conduction problems in functionally gradient materials with cracks. *Journal of Thermal Stresses*, 40(12):1484–1501, 2017.

[215] Wenzhi Yang and Zengtao Chen. Thermo-viscoelastic response of a cracked, functionally graded half-plane under a thermal shock. *Engineering Fracture Mechanics*, 206:267–277, 2019.

[216] Akira Kawasaki and Ryuzo Watanabe. Cyclic thermal fracture behavior and spallation life of psz/nicraly functionally graded thermal barrier coatings. In *Materials science forum*, volume 308, pages 402–409. Trans Tech Publ, 1999.

[217] B Siber, Markus Rettenmayr, C Müller, and Hans Eckart Exner. Concentration gradients in aluminium alloys generated by directional solidification and their effects on fatigue crack propagation. In *Materials science forum*, volume 308, pages 211–218. Trans Tech Publ, 1999.

[218] A Sveinbjörnsson and Lothar Wagner. Near-surface gradient microstructures in metastable beta-titanium alloys for improved fatigue performance. In *Materials Science Forum*, volume 308, pages 307–312. Trans Tech Publ, 1999.

[219] José F Bartolomé, José S Moya, Joaquín Requena, Javier LLorca, and Marc Anglada. Fatigue crack growth behavior in mullite/alumina functionally graded ceramics. *Journal of the American Ceramic Society*, 81(6):1502–1508, 1998.

[220] Somnath Bhattacharya, Kamal Sharma, and Vaibhav Sonkar. Numerical simulation of elastic plastic fatigue crack growth in functionally graded material using the extended finite element method. *Mechanics of Advanced Materials and Structures*, 24(16):1367–1380, 2017.

[221] S Bhattacharya, IV Singh, BK Mishra, and TQ Bui. Fatigue crack growth simulations of interfacial cracks in bi-layered fgms using xfem. *Computational Mechanics*, 52(4):799–814, 2013.

[222] Mohit Pant and Somnath Bhattacharya. Fatigue crack growth analysis of functionally graded materials by efgm and xfem. *International Journal of Computational Methods*, 14(01):1750004, 2017.

[223] Hyung Jip Choi, Tae Eun Jin, and Kang Yong Lee. Collinear cracks in a layered half–plane with a graded nonhomogeneous interfacial zone–part ii: Thermal shock response. *International Journal of Fracture*, 94(2):123–135, 1998.

[224] Zhi-He Jin and Naotake Noda. Edge crack in a nonhomogeneous half plane under thermal loading. *Journal of thermal stresses*, 17(4):591–599, 1994.

[225] Naotake Noda. Thermal stresses in functionally graded materials. *Journal of Thermal Stresses*, 22(4-5):477–512, 1999.

[226] Zhi-He Jin and RC Batra. Stress intensity relaxation at the tip of an edge crack in a functionally graded material subjected to a thermal shock. *Journal of Thermal Stresses*, 19(4):317–339, 1996.

[227] M Nemat-Alla and N Noda. Edge crack problem in a semi-infinite fgm plate with a bi-directional coefficient of thermal expansion under two-dimensional thermal loading. *Acta Mechanica*, 144(3):211–229, 2000.

[228] Z-H Jin and Glaucio H Paulino. Transient thermal stress analysis of an edge crack in a functionally graded material. *International Journal of Fracture*, 107(1):73–98, 2001.

[229] Z-H Jin. An asymptotic solution of temperature field in a strip a functionally graded material. *International communications in heat and mass transfer*, 29(7):887–895, 2002.

[230] Iman Eshraghi, Nasser Soltani, and Serkan Dag. Hyperbolic heat conduction based weight function method for thermal fracture of functionally graded hollow cylinders. *International Journal of Pressure Vessels and Piping*, 165:249–262, 2018.

[231] Yoshinobu Tanigawa. Some basic thermoelastic problems for nonhomogeneous structural materials. *Appl Mech Rev*, 48(6):287–300, 1995.

[232] Yoshinobu Tanigawa, Takehisa Muraki, and Ryuusuke Kawamura. Evaluation of axisymmetric steady thermal stress and thermal stress intensity factor in kassir's nonhomogeneous infinite body with a penny-shaped crack. *JSME international journal. Ser. A, Mechanics and material engineering*, 39(4):540–547, 1996.

[233] Y Tanigawa, T Akai, R Kawamura, and N Oka. Transient heat conduction and thermal stress problems of a nonhomogeneous plate with temperature-dependent material properties. *Journal of Thermal Stresses*, 19(1):77–102, 1996.

[234] S Ueda. Thermal shock fracture in a w-cu divertor plate with a functionally graded nonhomogeneous interface. *Journal of thermal stresses*, 24(11):1021–1041, 2001.

[235] Sei Ueda. Transient thermal singular stresses of multiple cracking in a w-cu functionally graded divertor plate. *Journal of thermal stresses*, 25(1):83–95, 2002.

[236] Takao Fujimoto and Naotake Noda. Two crack growths in a functionally graded plate under thermal shock. *Journal of thermal stresses*, 24(9):847–862, 2001.

[237] Naotake Noda. Thermal stresses intensity factor for functionally gradient plate with an edge crack. *Journal of Thermal Stresses*, 20(3-4):373–387, 1997.

[238] Matthew C Walters, Glaucio H Paulino, and Robert H Dodds Jr. Stress-intensity factors for surface cracks in functionally graded materials under mode-i thermomechanical loading. *International Journal of Solids and Structures*, 41(3-4):1081–1118, 2004.

[239] Naotake Noda and Zhi-He Jin. Crack-tip singularity fields in nonhomogeneous body under thermal stress fields. *JSME international journal. Ser. A, Mechanics and material engineering*, 38(3):364–369, 1995.

[240] Klod Kokini and Michael Case. Initiation of surface and interface edge cracks in functionally graded ceramic thermal barrier coatings. *J Eng Mater Technol*, 119(2):148–152, 1997.

[241] Vera Petrova and Tomasz Sadowski. Theoretical modeling and analysis of thermal fracture of semi-infinite functionally graded materials with edge cracks. *Meccanica*, 49(11):2603–2615, 2014.

[242] Farzin Tavakkoli and Rahmatollah Ghajar. The effect of nonhomogeneous parameter on stress intensity factor in a cracked layer in functionally graded material under thermal stresses. 15(11):275–283, 2016.

[243] Somnath Bhattacharya and Kamal Sharma. Fatigue crack growth simulations of fgm plate under cyclic thermal load by xfem. *Procedia Engineering*, 86:727–731, 2014.

[244] Himanshu Pathak, Akhilendra Singh, IV Singh, and SK Yadav. Fatigue crack growth simulations of 3-d linear elastic cracks under thermal load by xfem. *Frontiers of Structural and Civil Engineering*, 9(4):359–382, 2015.

[245] Ali Shaghaghi Moghaddam and Marco Alfano. Determination of stress intensity factors of 3d curved non-planar cracks in fgms subjected to thermal loading. *Engineering Fracture Mechanics*, 146:172–184, 2015.

[246] HH Zhang, SM Liu, SY Han, and LF Fan. Modeling of 2d cracked fgms under thermomechanical loadings with the numerical manifold method. *International Journal of Mechanical Sciences*, 148:103–117, 2018.

[247] VE Petrova and S Schmauder. Fracture of functionally graded thermal barrier coating on a homogeneous substrate: models, methods, analysis. In *Journal of Physics: Conference Series*, volume 973, page 012017. IOP Publishing, 2018.

[248] Tiantang Yu, Tinh Quoc Bui, Shuohui Yin, Duc Hong Doan, CT Wu, Thom Van Do, and Satoyuki Tanaka. On the thermal buckling analysis of functionally graded plates with internal defects using extended isogeometric analysis. *Composite Structures*, 136:684–695, 2016.

[249] V Parameswaran and A Shukla. Crack-tip stress fields for dynamic fracture in functionally gradient materials. *Mechanics of materials*, 31(9):579–596, 1999.

[250] Eric Reissner. On a variational theorem in elasticity. *Journal of Mathematics and Physics*, 29(1-4):90–95, 1950.

[251] R. M. Courtade. *Vibrational elastostatic methods*. PhD thesis, INSA, lyon, 1983.

[252] Sharam Aivaz-Zadeh Mokari, Yvon Gilibert, and Georges Verchery. Interface finite elements. application to glued assemblies and laminated structures. In *in Third conference Current trends in structural design*, volume 1, pages 265–281, 1985.

[253] G Verchery. Numerical methods of calculating stress fields in heterogeneous materials. *Calculation of Structures and Artificial Intelligence, Fouet JM, Ladeveze P., Ohayon R*, 1:7–21, 1974.

[254] M Habib. *Axisymmetric finite elements of interface for the analysis of layered structures and glued assemblies*. 1989.

[255] A Sarhan-Bajbouj. *Finite elements of interface for the calculation of heterogeneous structures*. PhD thesis, Lyon 1, 1989.

[256] Salima Bouchemella, Hamoudi Bouzerd, and Nacira Khaldi. Modeling of cracked interfaces of orthotropic bi materials.

[257] Abdelfatah Boufelloussa. Study of cracked interfaces in anistropic media by mixed finite element of interfaces. Master's thesis, University of Augst ,20 ,1955, Skikda, 2004.

[258] Salah Bouziane. *Mixed finite element for fissured interfaces of anisotropic bimaterials*. PhD thesis, University of Augst ,20 ,1955, Skikda, 2009.

[259] Salah Bouziane, Hamoudi Bouzerd, and Mohamed Guenfoud. Application of a mixed finite element to the analysis of laminated composite. page 6, 2009.

[260] Noureddine Boularas. Kinking study with the isoparametric form of the rmq-7 element. Master's thesis, University of Augst ,20 ,1955, Skikda, 2011.

[261] Mahira Mouats. Modeling of failure in plane sliding mode in composite materials. Master's thesis, University of Augst ,20 ,1955, Skikda, 2012.

[262] Larbi Djoudi. Numerical modeling of interlaminar fracture in laminates. Master's thesis, University of Augst ,20 ,1955, Skikda, 2012.

[263] Abdelkrim Remmach. Numerical study by mixed finite elements of the non-coplanar propagation of a crack (kinking) in a composite material. Master's thesis, University of Augst ,20 ,1955, Skikda, 2012.

[264] Salah Bouziane, Hamoudi Bouzerd, and Mohamed Guenfoud. Analysis of sandwich beams using mixed finite element. page 5, 2013.

[265] Salah Bouziane, Hamoudi Bouzerd, and Mohamed Guenfoud. Mixed interface finite element for sandwich beams. page 13, 2013.

[266] G.Dhatt and G. Touzot. *A presentation of the finite element method*. Maloine. paris, 1981.

[267] R.H . Gallagher. *Introduction to finite elements*. Pluralis. paris, 1976.

[268] Xiang-yu Li, Hao-jiang Ding, and Wei-qiu Chen. Pure bending of simply supported circular plate of transversely isotropic functionally graded material. *Journal of Zhejiang University-SCIENCE A*, 7(8):1324–1328, 2006.

[269] TK Hellen. On the method of virtual crack extensions. *International Journal for numerical methods in engineering*, 9(1):187–207, 1975.

[270] David Moore Parks. A stiffness derivative finite element technique for determination of crack tip stress intensity factors. *International Journal of fracture*, 10(4):487–502, 1974.

[271] Hamoudi Bouzerd and R. M. Courtade. Plasticity around a circular hole. theoretical and numerical analysis. *10ème Congrès Français de mécanique*, 2(6):197–200, 1991.

[272] Hamoudi Bouzerd, Noureddine Boulares, and Abdelhamid Bouchair. A mixed finite element for the calculation of the rate of energy return of the bending (kinking) of a crack. 2011.

[273] Bouziane Salah, Bouzerd Hamoudi, Boulares Noureddine, and Guenfoud Mohamed. Energy release rate for kinking crack using mixed finite element. *Structural Engineering and Mechanics*, 50(5):665–677, 2014.

[274] Salah Bouziane, Hamoudi Bouzerd, and Mohamed Guenfoud. Computation of energy release rate for interfacial crack between dissimilar isotropic materials using mixed finite element. In *Congrès français de mécanique*. AFM, Maison de la Mécanique, 39/41 rue Louis Blanc, 92400 Courbevoie, France ..., 2011.

[275] Salah Bouziane and Hamoudi Bouzerd. Computation of energy release rate for interfacial crack in orthotropic bimaterials. 2020.

[276] Amina Mohamed Ben Ali, Salah Bouziane, and Hamoudi Bouzerd. Computation of mode i strain energy release rate of symmetrical and asymmetrical sandwich structures using mixed finite element. *FratturaedIntegrità Strutturale*, 15(56):229–239, 2021.

[277] Sami Derouiche, Salah Bouziane, and Hamoudi Bouzerd. Mixed finite element computation of energy release rate in anisotropic materials based on virtual crack closure-integral method. *FratturaedIntegrità Strutturale*, 15(57):359–372, 2021.

[278] M Şimşek. Static analysis of a functionally graded beam under a uniformly distributed load by ritz method. *International Journal of Engineering and Applied Sciences*, 1(3):1–11, 2009.

[279] S Alexraj, N Vasiraja, and P Nagaraj. Static behaviour of functionally graded material beam using finite element method. In *2013 International Conference on Energy Efficient Technologies for Sustainability*, pages 267–273. IEEE, 2013.

[280] Hui Wang and Qing-Hua Qin. Boundary integral based graded element for elastic analysis of 2d functionally graded plates. *European Journal of Mechanics-A/Solids*, 33:12–23, 2012.